Microfluidic Solvent Extraction of Medical Radionuclides

Trapp, S.

DOI
10.4233/uuid:0ffd1744-ca01-48e1-b1ce-ab0ae0b6d800

Publication date
2025

Document Version
Final published version

Citation (APA)
Trapp, S. (2025). *Microfluidic Solvent Extraction of Medical Radionuclides*. [Dissertation (TU Delft), Delft University of Technology]. https://doi.org/10.4233/uuid:0ffd1744-ca01-48e1-b1ce-ab0ae0b6d800

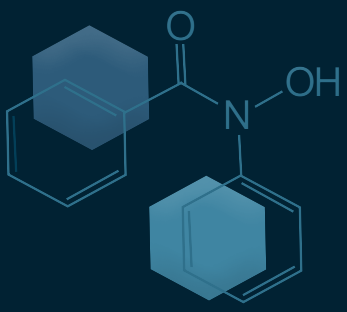

Microfluidic Solvent Extraction of Medical Radionuclides

Svenja Trapp

Microfluidic Solvent Extraction of Medical Radionuclides

Svenja TRAPP

Microfluidic Solvent Extraction of Medical Radionuclides

Dissertation

for the purpose of obtaining the degree of doctor
at Delft University of Technology
by the authority of the Rector Magnificus Prof. Dr. ir T.H.J.J. van der Hagen
chair of the board for Doctorates
to be defended publicly on Friday 28th of March, 2025 at 10:00 o'clock

by

Svenja TRAPP

Master of Science in Geosciences, University of Bonn, Germany
born in Viersen, Germany

This dissertation has been approved by the promotor and copromotors.

Composition of doctoral committee:

Rector Magnificus,	Chair
Dr. ir. A.G. Denkova	Delft University of Technology, promotor
Dr. ir. R.M. de Kruijff	Delft University of Technology, copromotor
Dr. E. Paulßen	Delft University of Technology, copromotor

Independent members:

Prof.dr. E.A. Pidko	Delft University of Technology
Prof.dr. S. Heskamp	Radboud University Medical Center
Prof.dr. D. Vugts	Amsterdam University Medical Center
Dr. V. Radchenko	University of British Columbia / TRIUMF, Canada
Prof.dr.ir. J.R. van Ommen	Delft University of Technology, reserve member

The research presented in this thesis was performed at the Applied Radiation and Isotopes section of the Department of Radiation Science and Technology, Faculty of Applied Sciences, Delft University of Technology, the Netherlands.

This research was funded by the Dutch Research Council (NWO) under project number 16913.

Cover design by: Svenja Trapp and Eva Nießen

Printed by: Ridderprint

ISBN 978-94-6518-008-3

Printed in the Netherlands

Contents

Summary

In nuclear medicine, radionuclides are used to image and treat several diseases, including cancer. Either freely or coupled to a tumor-targeting molecule, γ and β^+ emitting radionuclides are successfully used for SPECT (single-photon emission computed tomography) and PET (positron emission tomography) imaging, while β^-, α and Auger emitters are applied in radionuclide therapy. All radionuclides used in nuclear medicine have comparably short half-lives in the range of minutes to days. Therefore, these radionuclides don't occur naturally, but are generally produced by irradiation of a target material with e.g. neutrons or protons. These irradiations cause nuclear transformation of a stable isotope into a short-lived radioisotope of either the same or a different element than the target material. After the production of the radionuclides, they need to be chemically separated from their target material, but this is only possible if a different element was produced. One example of this process is the proton irradiation of enriched Zn-68, causing the following reaction:

$$^{68}Zn(p,n)^{68}Ga$$

in which a neutron in the nucleus of Zn-68 is replaced by a proton, resulting in the radionuclide Ga-68. The main goal of this thesis is to develop chemical separation methods based on solvent extraction (or liquid-liquid extraction) to separate medical radionuclides from their respective irradiated targets. During solvent extraction, two immiscible solutions, an aqueous radionuclide-containing solution and an organic chelator-containing solution, are brought in contact with each other. At the interface of these two solutions a complex between the radionuclide and the chelator is formed, which is subsequently extracted into the organic solution due to its hydrophobic nature. As a second step, the chelator-radionuclide complex is broken by adding a different acidic or basic aqueous solution, which releases the radionuclide back into an aqueous solution. Because irradiated targets are highly radioactive and need to be handled in hot cells, automation of the separation method is preferred, or even necessary. However, automation of solvent extraction is difficult to achieve. Therefore, microfluidic devices are currently of high interest for the automation of solvent extraction. Multiple different devices including membrane-separators and microfluidic chips were studied in this thesis and tested for their applicability to separate radionuclides.

In Chapter 2, a method was developed for the above-mentioned separation of Ga-68 from Zn-68, using a membrane-separator. By applying the chelator N-benzoyl-N-phenylhydroxilamine (BPHA) a very high extraction efficiency of Ga-68 from $Zn(NO_3)_2$ was achieved. Back-extraction was successful in 6 M HCl using the same method. It was also found that the total amount of Zn contamination in the final Ga-68 containing solution is below 3 ppm. However, when applying this method to an irradiated $Zn(NO_3)_2$ liquid target, the membrane degraded due to the high radiolysis in the solutions, proving the necessity of microfluidic devices without membranes or further research on improvements of radiation stability of organic/aqueous-separation membranes.

Next, a step was made towards microfluidic chips. In Chapter 3 a commercial glass microfluidic chip was used for the separation of Cu-isotopes from a $Zn(NO_3)_2$ target. From all tested chelators, dithizone has shown the highest potential for the extraction of Cu from acidic solutions, achieving extraction efficiencies of over 90 % with the Zn co-extraction remaining below 3 %. Next it was found that back-extraction of Cu into dilute HCl solution is only successful for higher Cu concentrations. When only a Cu-64 radiotracer was used, back-extraction fails, showing the stability of this Cu-dithizone complex. When the extraction was moved from a batch approach to a glass microfluidic chip, it became clear, that the current commercially available glass microfluidic YY-chips fail to achieve a sufficient phase separation of the aqueous and organic phases used for the solvent extraction. This phase separation is crucial for the successful application of microfluidic solvent extraction for the separation of medical radionuclides.

Next, PDMS microfluidic chips were utilized for the extraction of Ac-225 from Ra, as well as the chemically similar separations of La from Ba, Y from Sr and Sc from Ca (Chapter 4). The chelator D2EHPA proved very successful in the separation of these elements within extremely short contact times of under 2 seconds. This was the first time reaching maximum extraction efficiencies (as determined by batch experiments) in a microfluidic chip. Additionally, because of the unique geometry of the self-made PDMS chips with metal oxide nano-layer coating of the microchannel, a near perfectly organic/aqueous phase separation was achieved. This study provides a proof-of-concept for the future application of microfluidic chips for the automation of solvent extraction for the separation of medical radionuclides.

To better understand the chemical processes that occur during microfluidic solvent extraction and to optimize future experiments, numerical models can be designed. However, these models need to be fed with certain information, including diffusion coefficients of the radionuclide, but this data is often lacking, also due to the difficulty of precise diffusion measurement. Therefore, Chapter 5 deals with the application of microflu-

idic chips for the determination of diffusion coefficients. It was found that microfluidic devices are useful in estimating diffusion coefficients, even of compounds with very low concentrations in the pico-molar range (such as Ga-68 radiotracer). However, varying flow rates show large differences in diffusion coefficients. An exponential trend was observed when plotting the measured apparent diffusion coefficients against the contact time, making it necessary to determine the diffusion coefficient over a larger range of flowrates, to observe the plateau from which the actual diffusion coefficient can be determined.

In the following Chapter 6 it was found that solvent extraction can lead to contaminations of the used chelator in the aqueous solutions that are obtained after the back-extraction. Apart from potential toxicity, prohibiting the use of these solutions for patients, chelator contaminations can potentially interfere with the labelling of radionuclides to pharmaceuticals, and therefore prevent their use. In this chapter, after confirmation of the presence of chelator contamination, a microfluidic ion-exchange column (containing AG 1-X8 resin) was studied for the clean-up of collected solutions after microfluidic solvent extraction of Ga-68 (as done in Chapter 2). This ion-exchange microcolumn was able to eliminate organic contamination, as well as reduce the acidity and volume of the final solution.

The final Chapter 7 explores an alternative application of chelators, in the form of a chelator-impregnated resin. While chelator-impregnated resins are easy to produce and have been studied extensively in the literature, their common issue of low chemical stability has prevented their use in the separation of medical radionuclides. A case study was conducted using the chelator D2EHPA for the separation of Ac-225 from Ra, as was studied before in chapter 4 by microfluidic solvent extraction. Using PDMS as the solid support resulted in a high chemical stability, as well as a very fast adsorption of Ac-225, proving the potential of PDMS-based chelator-impregnated resins.

Overall, in this thesis, tremendous improvements were achieved towards the automation of solvent extraction for future application in the separation of medical radionuclides from their targets. Using nano-layer coated PDMS microfluidic chips has the ability to achieve perfect phase separation. Multiple solvent extraction methods were developed, showing the versatility of this approach. Further improvements in combining all necessary steps into a single microfluidic device will enable the use of solvent extraction for the separation of medical radionuclide, even under the stringent purity requirements of radiopharmaceutical production.

Samenvatting

In de nucleaire geneeskunde worden radionucliden gebruikt om verschillende ziekten, waaronder kanker, in beeld te brengen en te behandelen. Hiervoor worden, onder andere, tumor specifieke moleculen gebruikt, die gekoppeld worden aan diagnostische radionucliden (welke vervallen onder uitzending van γ^- en β^+-straling) voor medische beeldvorming middels SPECT (single-photon emission computed tomography) en PET (positron emission tomography), of aan β^-, α en Auger -elektron emitterende radionucliden welke worden toegepast voor radionuclidentherapie. Alle radionucliden die in de nucleaire geneeskunde worden gebruikt, hebben vergelijkbaar korte halfwaardetijden van minuten tot dagen. Daar deze radionucliden niet voorkomen in de natuur, moeten ze specifiek geproduceerd worden door een targetmateriaal te bestralen met bijvoorbeeld neutronen of protonen. Deze bestralingen veroorzaken nucleaire transformaties van stabiel isotopen naar radio-isotopen van hetzelfde of een ander element als het targetmateriaal. Na de productie moeten de radionucliden chemisch gescheiden worden van hun targetmateriaal. Dit is echter alleen mogelijk wanneer er een ander element is geproduceerd. Een voorbeeld van dit proces is de protonenbestraling van verrijkt Zn-68, via de volgende reactie:

$$^{68}Zn(p,n)^{68}Ga$$

Hierbij wordt een neutron in de kern van Zn-68 vervangen door een proton, wat resulteert in het radionuclide Ga-68. Het voornaamste doel van dit proefschrift is het ontwikkelen van chemische scheidingsmethoden gebaseerd op vloeistof-vloeistof extractie om medische radionucliden te scheiden van hun respectievelijke bestraalde targets. Tijdens vloeistof-vloeistof extractie worden twee niet-mengbare oplossingen, een waterige oplossing die radionucliden bevat en een organische oplossing die chelators bevat, met elkaar in contact gebracht. Op het grensvlak van deze twee oplossingen wordt een complex gevormd tussen het radionuclide en de chelator, dat door zijn hydrofobe aard in de organische oplossing wordt geëxtraheerd. Als tweede stap wordt het chelator-radionuclidecomplex verbroken door een andere zure of basische waterige oplossing toe te voegen, waardoor de radionuclide vrijkomt in de waterige oplossing. Omdat bestraalde targets zeer radioactief zijn en scheidingsprocedures zodoende in een hotcel moeten plaatsvinden, heeft automatisering van de scheidingsmethode de voorkeur, en is vaak zelfs noodzakelijk. Automatisering van de vloeistof-vloeistof extractie is echter moeilijk te realiseren,daarom is er momenteel grote belangstelling voor de mogelijkheden die microfluïdische apparaten hier bieden. In dit proefschrift worden verschillende

apparaten, waaronder membraanscheiders en microfluïdische chips, onderzocht en getest op hun toepasbaarheid voor het scheiden van radionucliden.

In Hoofdstuk 2 is een methode ontwikkeld voor de bovengenoemde scheiding van Ga-68 van Zn-68 targets met behulp van een membraan-scheider. Door gebruik te maken van de chelator N-benzoyl-N-fenylhydroxilamine (BPHA) werd een zeer hoge scheidingsefficientie (%) tussen Ga-68 en $Zn(NO_3)_2$ bereikt. Terugextractie van het Ga-68 in een waterige oplossing was succesvol in 6 M HCl met dezelfde methode. Er is ook aangetoond dat de totale hoeveelheid Zn-verontreiniging in de uiteindelijke Ga-68-bevattende oplossing minder dan 3 ppm bedraagt. Wanneer deze methode echter werd toegepast op een bestraald $Zn(NO_3)_2$ vloeistoftarget ging het membraan achteruit als gevolg van de hoge radiolysegraad in de oplossing, wat de noodzaak aantoont van microfluïdische apparaten zonder membranen danwel verder onderzoek naar verbeteringen van de stralingsstabiliteit van dergelijke scheidingsmembranen.

Na het membraanscheideronderzoek werd de eerste stap gezet richting microfluïdische chips. In Hoofdstuk 3 werden commerciele glazen microfluïdische chips gebruikt voor de scheiding van Cu-isotopen van $Zn(NO_3)_2$ targetoplossingen. Van alle geteste chelators heeft dithizone de hoogste extractie efficiëntie laten zien voor Cu uit zure oplossingen, waarbij een efficientie van meer dan 90 % werd bereikt. De co-extractie van Zn bleef ook hier onder de 3 %. Vervolgens werd gevonden dat de terugextractie van Cu in een verdunde HCl-oplossing alleen succesvol is bij hogere Cu-concentraties. Wanneer enkel een Cu-64 radiotracer werd gebruikt mislukte de terugextractie, wat de hoge chemische stabiliteit van dit Cu-dithizone complex aantoont. Toen de extractie van een batchbenadering naar een glazen microfluïdische chip overging, werd duidelijk dat de huidige commercieel verkrijgbare glazen microfluïdische YY-chips er niet in slagen om voldoende scheiding te bereiken van de waterige en organische fasen. Deze fasescheiding is cruciaal voor de succesvolle toepassing van microfluïdische vloeistof-vloeistof extractie voor de scheiding van medische radionucliden.

Vervolgens werden PDMS microfluïdische chips gebruikt voor de extractie van Ac-225 uit Ra targets, evenals voor de chemisch vergelijkbare scheidingen van La van Ba targets, Y van Sr targets en Sc van Ca targets (Hoofdstuk 4). De chelator D2EHPA bleek zeer succesvol in het scheiden van deze elementen binnen extreem korte contacttijden van minder dan 2 seconden. Dit was de eerste keer dat de maximale extractie efficiëntie (zoals bepaald tijdens de batchexperimenten) werd bereikt in een microfluïdische chip. Bovendien werd vanwege de unieke geometrie van de zelfgemaakte PDMS-chips met metaaloxide-nanolaagcoating van het microkanaal een vrijwel perfect organische/waterige fasescheiding bereikt. Deze studie is een proof-of-concept voor de toe-

komstige toepassing van microfluïdische chips voor de automatisering van oplosmiddelextractie voor de scheiding van medische radionucliden.

Numerieke modellen kunnen van grote waarde zijn om de chemische processen die plaatsvinden tijdens de extractie van microfluïdische oplosmiddelen beter te begrijpen en toekomstige experimenten te optimaliseren. Deze modellen hebben echter bepaalde experimentele informatie nodig, waaronder diffusiecoefficienten van de radionucliden. Dergelijke gegevens ontbreken vaak, onder andere vanwege de moeilijkheid van nauwkeurige diffusiemetingen. Daarom behandelt Hoofdstuk 5 de mogelijke toepassingen van microfluïdische chips voor de bepaling van diffusiecoefficienten. Er werd gevonden dat microfluïdische apparaten nuttig zijn bij het bepalen van diffusiecoefficienten, zelfs van verbindingen met zeer lage concentraties in het pico-molaire bereik (zoals de Ga-68 radiotracer). Varierende stroomsnelheden in de chips lieten echter grote verschillen in diffusiecoefficienten zien. Er werd een exponentiele trend waargenomen bij het uitzetten van de gemeten schijnbare diffusiecoefficienten tegen de contact tijd. Hierdoor werd het noodzakelijk om de diffusiecoefficient over een groter bereik aan stroomsnelheden te bepalen, om zodoende het plateau te observeren waarvan de werkelijke diffusiecoefficient kon worden bepaald.

In het volgende Hoofdstuk 6 werd gevonden dat vloeistof-vloeistof extractie kan leiden tot verontreinigingen van de gebruikte chelator in de waterige oplossingen die resulteren uit de terugextractie. Afgezien van de potentiele toxiciteit, waardoor de radionucliden in deze oplossingen niet kunnen worden toegepast bij patienten, kunnen deze chelator verontreinigingen mogelijk ook de binding van de radionuclide aan het farmaceutische molecuul verstoren. In dit hoofdstuk werd, na bevestiging van de aanwezigheid van chelatorverontreinigingen, een microfluïdische ionenuitwisselingskolom bestudeerd voor het schoonmaken van de oplossingen geproduceerd na microfluïdische vloeistof-vloeistof extractie van Ga-68 (zoals gedaan in Hoofdstuk 2). Deze microkolom kon niet alleen de aanwezige organische verontreiniging elimineren, maar ook de zuurgraad en het volume van de uiteindelijke oplossing verminderen.

Het laatste hoofdstuk 7 onderzoekt een alternatieve toepassing van chelators, in de vorm van een met chelator geïmpregneerde hars . Hoewel harsen geïmpregneerd met chelators relatief gemakkelijk te produceren zijn en uitgebreid in de literatuur zijn bestudeerd, is hun toepassing voor de scheiding van medische radionucliden tot nu toe gelimiteerd door hun zeer slechte chemische stabiliteit. We hebben een case study uitgevoerd met behulp van de chelator D2EHPA voor de scheiding van Ac-225 van Ra targets, zoals eerder in hoofdstuk 4 werd onderzocht door middel van microfluïdische vloeistof-vloeistof extractie. Door PDMS als te impregnerende hars te gebruiken, konden een hoge

chemische stabiliteit en zeer snelle adsorptie van Ac-225 worden bereikt. Deze studie heeft de mogelijkheden van het gebruik van PDMS als chelator geïmpregneerde hars bewezen.

Over het geheel genomen heeft dit proefschrift enorme verbeteringen laten zien in de mogelijke automatisering van de vloeistof-vloeistof extractie voor toekomstig gebruik bij de scheiding van medische radionucliden van hun targets. Het gebruik van met nanolagen gecoate PDMS-microfluïdische chips heeft het vermogen om een perfecte fasescheiding te bereiken. Er zijn meerdere vloeistof-vloeistof extractiemethoden ontwikkeld, wat de veelzijdigheid van deze aanpak aantoont. Verdere verbeteringen bij het combineren van alle noodzakelijke stappen in een enkel microfluïdisch apparaat zullen het gebruik van vloeistof-vloeistof extractie voor de scheiding van medische radionucliden mogelijk maken, zelfs onder de strenge zuiverheidseisen van radiofarmaceutische productie.

Zusammenfassung

In der Nuklearmedizin werden Radionuklide zur Bildgebung und Behandlung verschiedener Krankheiten, einschließlich Krebs, eingesetzt. Es werden γ und β^+ emittierende Radionuklide erfolgreich für die SPECT- (Einzelphotonen-Emissions-Computertomographie) und PET-Bildgebung (Positronen-Emissions-Tomographie) eingesetzt, während β^-, α und Auger-emmitierende Nuklide für Radionuklidtherapie eingesetzt werden. Unabhängig davon, welcher Zerfallsmodus für das Verfahren erforderlich ist, haben alle in der Nuklearmedizin verwendeten Radionuklide vergleichsweise kurze Halbwertszeiten im Bereich von Minuten bis Tagen. Daher werden diese Nuklide gezielt durch Bestrahlung eines bestimmten Targets (also eines bestimmten, meist angereicherten Ausgangsmaterials), mit z.B. Neutronen oder Protonen, produziert. Diese Bestrahlungen bewirken eine nukleare Umwandlung eines stabilen Isotops in ein kurzlebiges Radioisotop, entweder desselben oder eines anderen Elementes als das Target. Nach der Produktion der Radionuklide müssen diese chemisch von ihrem Target getrennt werden, was jedoch nur möglich ist, wenn ein anderes Element produziert wurde. Ein Beispiel für diesen Prozess ist die Protonenbestrahlung von angereichertem Zn-68, was die folgende Reaktion hervorruft:

$$^{68}Zn(p,n)^{68}Ga$$

Dabei wird ein Neutron im Kern von Zn-68 durch ein Proton ersetzt, wodurch das Radionuklid Ga-68 entsteht.

Das Hauptziel dieser Doktorarbeit ist die Entwicklung chemischer Trennmethoden auf Basis der flüssig-flüssig Extraktion, um medizinische Radionuklide von ihren jeweiligen bestrahlten Targets zu trennen. Bei der flüssig-flüssig Extraktion werden zwei nichtmischbare Lösungen, eine wässrige radionuklidhaltige Lösung und eine organische Lösung, miteinander in Kontakt gebracht. An der Kontaktzone dieser zwei Lösungen entsteht ein Komplex zwischen dem Radionuklid und einem organischen Molekül (einem Chelator). Aufgrund seines hydrophoben Charakters wird der Komplex daraufhin in die organische Lösung extrahiert. Als nächstes wird der Chelator-Radionuklid-Komplex durch Zugabe einer anderen sauren oder basischen Lösung aufgebrochen, was das Radionuklid wieder in eine wässrige Lösung freisetzt. Da bestrahlte Targets stark radioaktiv sind und in speziellen Einrichtungen (heißen Zellen) gehandhabt werden müssen, ist eine Automatisierung der Trennmethode wünschenswert oder sogar notwendig. Eine Automatisierung der flüssig-flüssig Extraktion ist jedoch schwierig. Für diesen Zweck sind mikrofluidische Verfahren derzeit von großem Interesse. In dieser Arbeit werden

mehrere verschiedene mikrofluidische Instrumente untersucht, darunter Membranseparatoren und mikrofluidische Chips, und auf ihre Anwendbarkeit zur Trennung hochradioaktiver Nuklide getestet.

In Kapitel 2 wurde eine Methode zur oben erwähnten Trennung von Ga-68 von Zn-68 entwickelt. In dieser ersten Studie wurde ein Membranseparator verwendet. Durch die Verwendung des Chelators N-Benzoyl-N-phenylhydroxilamin wurde eine sehr hohe Trennung von Ga-68 und $Zn(NO_3)_2$ erreicht. Die Rückextraktion war mit der gleichen Methode in 6 M HCl erfolgreich. Es wurde außerdem festgestellt, dass die Gesamtmenge der Zink Verunreinigung in der endgültigen Ga-68-haltigen Lösung unter erforderlichen Grenzwerten liegt. Bei der Anwendung dieser Methode auf ein bestrahltes flüssiges $Zn(NO_3)_2$-Target kam es jedoch zu einer Zersetzung der Membran aufgrund der starken Radiolyse in den Lösungen, was die Notwendigkeit mikrofluidischer Geräte ohne Membranen voraussetzt oder weitere Forschung zur Verbesserungen der Strahlungsresistenz von organischen/wässrigen Trennmembranen.

In Kapitel 3 wurden kommerzielle mikrofluidische Glaschips für die Trennung von Cu-Isotopen von $Zn(NO_3)_2$-Targets verwendet. Von allen hierfür getesteten Chelatoren zeigte Dithizon das höchste Potenzial für die Extraktion von Cu aus sauren Lösungen und erreichte Extraktionseffizienzen von über 90 % bei einer Zn-Koextraktion, die unter 3 % blieb. Als nächstes wurde festgestellt, dass die Rückextraktion von Cu in verdünnte HCl-Lösung nur bei höheren Cu-Konzentrationen erfolgreich ist. Wenn nur ein Cu-64-Radiotracer verwendet wurde, schlug die Rückextraktion fehl, was die Stabilität dieses Cu-Dithizon-Komplexes unterstreicht. Nach dem Umstieg von einem "Batch"-Ansatz auf einen mikrofluidischen Glaschip wurde deutlich, dass die derzeit im Handel erhältlichen mikrofluidischen YY-Glaschips keine ausreichende Phasentrennung der für die Lösungsmittelextraktion verwendeten wässrigen und organischen Phasen erreichen. Diese Phasentrennung ist entscheidend für den erfolgreichen Einsatz der mikrofluidischen Lösungsmittelextraktion zur Trennung medizinischer Radionuklide, weshalb kommerzielle Glaschips hierfür nicht geeignet sind.

Als nächstes wurden PDMS-Mikrofluidchips für die Trennung von Ac-225 und Radium sowie für die chemisch ähnlichen Trennungen Lanthan von Barium, Yttrium von Strontium und Scandium von Calcium verwendet (Kapitel 4). Der Chelator D2EHPA erwies sich bei der Trennung dieser Elemente innerhalb extrem kurzer Kontaktzeiten von unter 2 Sekunden als sehr erfolgreich. Dies war das erste Mal, dass maximale Extraktionseffizienzen (wie sie durch Batch-Experimente bestimmt werden konnten) in einem Mikrofluidchip erreicht wurden. Darüber hinaus wurde aufgrund der einzigartigen Geometrie der selbst hergestellten PDMS Chips mit Metalloxid-Nanobeschichtung des

Mikrokanals eine nahezu perfekte organische/wässrige Phasentrennung erreicht. Diese Studie ist ein proof-of-concept für die zukünftige Anwendung von Mikrofluidchips zur Automatisierung der flüssig-flüssig Extraktion zur Trennung medizinischer Radionuklide.

Um die chemischen Prozesse, die bei der mikrofluidischen flüssig-flüssig Extraktion ablaufen, besser zu verstehen und zukünftige Experimente zu optimieren, können numerische Modelle verwendet werden. Allerdings sind für diese Modelle bestimmte Informationen, einschließlich Diffusionskoeffizienten des Radionuklids, notwendig. Diese Daten fehlen jedoch häufig, aufgrund der Schwierigkeit einer präzisen Diffusionsmessung. Daher befasst sich Kapitel 5 mit den möglichen Anwendungen mikrofluidischer Chips zur Bestimmung von Diffusionskoeffizienten. Es wurde festgestellt, dass der mikrofluidische Ansatz zur Bestimmung von Diffusionskoeffizienten nützlich ist, selbst bei Stoffen mit sehr geringen Konzentrationen im pico-molaren Bereich (wie Ga-68-Radiotracer). Unterschiedliche Durchflussraten der Lösungen im mikrofluidischen Chip zeigen jedoch große Variationen in den gemessenen Diffusionskoeffizienten. Beim Plotten der gemessenen scheinbaren Diffusionskoeffizienten gegen die Kontaktzeit wurde ein exponentieller Trend beobachtet. Daher ist es erforderlich, scheinbare Diffusionskoeffizienten über einen größeren Bereich von Durchflussraten zu beobachten, um den tatsächlichen Diffusionskoeffizienten aus den Scheinbaren bestimmen zu können.

Im folgenden Kapitel 6 wurde festgestellt, dass die flüssig-flüssig Extraktion zu Verunreinigungen mit dem verwendeten Chelatoren in den resultierenden wässrigen Lösungen führen kann. Abgesehen von der potenziellen Toxizität der Chelatoren, die die Verwendung der Lösungen bei Patienten verbietet, können diese Chelatorkontaminationen möglicherweise die Komplexierung des Radionuklids mit pharmazeutischen Komponenten beeinträchtigen und daher deren Verwendung verhindern. In diesem Kapitel wurde nach Bestätigung des Vorhandenseins von Chelatorkontaminationen ein mikrofluidisches Ionenaustauschverfahren entwickelt, zur Reinigung der Lösungen nach der mikrofluidischen flüssig-flüssig Extraktion von Ga-68 (wie in Kapitel 2 durchgeführt). Diese Ionenaustausch-Mikrosäule war in der Lage, organische Verunreinigungen zu beseitigen, sowie den Säuregehalt und das Volumen der Endlösung zu reduzieren.

Im letzten Kapitel 7 wird eine alternative Anwendung von Chelatoren in Form eines mit Chelatoren imprägnierten Harzes untersucht. Obwohl mit Chelatoren imprägnierte Harze einfach herzustellen sind und ausführlich in der Literatur untersucht wurden, verhinderte die geringe chemischen Stabilität ihre Verwendung bei der Trennung medizinischer Radionuklide. Es wurde eine Fallstudie mit dem Chelator D2EHPA zur Trennung von Ac-225 von Ra durchgeführt, wie bereits in Kapitel 4 durch mikrofluidische

flüssig-flüssig Extraktion. Durch die Verwendung von PDMS als Basismaterial konnte eine hohe chemische Stabilität des Harzes, sowie eine sehr schnelle Adsorption von Ac-225 erreicht werden, was das Potenzial von mit Chelatoren imprägnierten Harzen auf PDMS-Basis unter Beweis stellt.

Insgesamt wurden in dieser Arbeit enorme Fortschritte bei der Automatisierung der flüssig-flüssig Extraktion erzielt, für den zukünftigen Einsatz bei der Trennung medizinischer Radionuklide von ihren Targets. Durch die Verwendung nanobeschichteter PDMS-Mikrofluidchips kann eine nahezu perfekte Phasentrennung erreicht werden. Es wurden mehrere Methoden zur flüssig-flüssig Extraktion entwickelt, was die Vielseitigkeit dieses Ansatzes zeigt. Weitere Verbesserungen bei der Kombination aller notwendigen Schritte in einem einzigen Mikrofluidgerät werden den Einsatz der flüssig-flüssig Extraktion zur Trennung medizinischer Radionuklide ermöglichen, selbst unter den strengen Reinheitsanforderungen bei der Produktion von Radiopharmazeutika.

1

Introduction

1

Introduction

1

1.1. Nuclear Medicine

Nuclear medicine is a rapidly growing field that uses radioactive substances for the diagnosis or treatment of various diseases, including cancer [1]. Currently, over 50 million nuclear medicine procedures are performed world wide every year with an expected annual market growth rate of 12.8% until 2030 [1], thanks to advances in hybrid imaging systems, targeted radiopharmaceuticals and artificial intelligence in nuclear imaging [2]. Around 90% of the procedures including radionuclides are for diagnostic purposes [1], but a steady increase in therapeutic applications of radionuclides can be observed and is expected to further increase in the future [3]. For nuclear imaging either SPECT (Single Photon Emission Computerized Tomography) or PET (Positron-Emission Tomography) is used [4], currently often combined with CT or MRI to enable better diagnosis of various diseases or visualization of soft tissue [5, 6]. SPECT imaging is the current major scanning technology utilizing γ emitters as the radiotracer (see Fig. 1.1). The most commonly applied radionuclide for this is Tc-99m in 85% of all nuclear imaging procedures [1], thanks to its availability through Mo-99/Tc-99m generators. In comparison, PET imaging uses positron-emitting radionuclides, that can be produced in medical cyclotrons of which over 1300 exist worldwide [7]. After a positron is emitted, it promptly combines with a nearby electron, resulting in the simultaneous emission of two 511 keV γ rays in opposite directions (see Fig. 1.1), a process called annihilation. These are detected by a PET camera and allow for a non-invasive diagnosis. PET's most important radionuclides are F-18 and Ga-68 [8], mostly used for the diagnosis of cancer, but also in cardiac and brain imaging [9]. Therapeutic approaches in nuclear medicine include brachytherapy and targeted radionuclide therapy [1]. Especially targeted radionuclide therapy is rapidly expanding, due to less invasiveness and side effects compared to other traditional therapeutic approaches like surgery or chemotherapy. [10]. In many nuclear diagnostic and therapeutic procedures, the radionuclide is linked to a tumor-type spe-

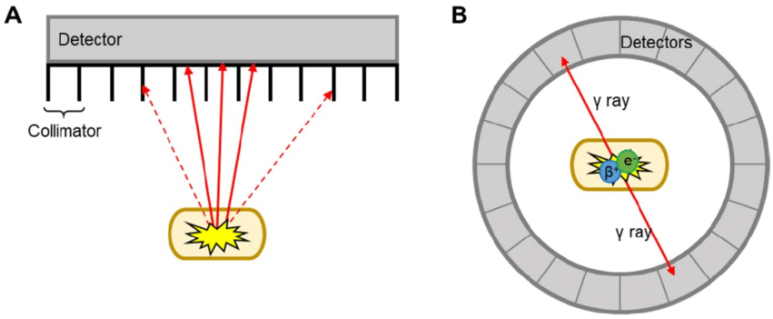

Figure 1.1: Schematic representation of a) SPECT imaging, utilizing collimators that only allow for near perpendicular γ rays to hit the detector, enabling spacial reconstruction, and b) PET imaging with a ring detector, measuring γ rays, produced by positron annihilation (from [11]).

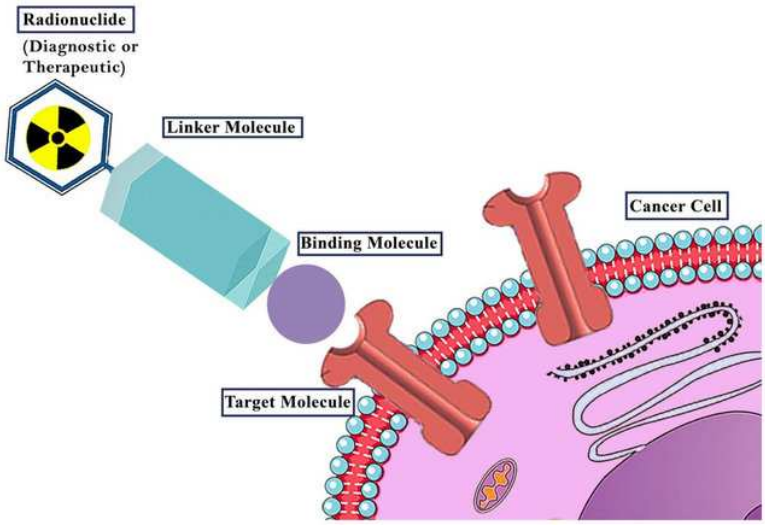

Figure 1.2: Illustration of radiopharmaceuticals, showing the combination of a radionuclide over a linker and a binding molecule with a tumor-type specific targeting vector (or targeting molecule), that specifically binds to a target molecule of a cancer cell (from [14]).

cific targeting vector (which includes antibodies, peptides, and small molecules) [10]. Major improvements in precision medicine, especially for the diagnosis and treatment of cancer, have been achieved since the enhanced development of tumor-type specific targeting vectors [10]. Those targeting vectors, when labelled with e.g. therapeutic β^--emitting radionuclides, can deliver very localized high radiation doses, reducing the radiation dose to healthy surrounding tissue and improving the therapeutic efficacy (see Fig 1.2).

Currently three radiopharmaceuticals for targeted radionuclide therapy have been approved by the Food and Drug Administration (FDA), namely ^{223}Ra-dichloride (Xofigo®) against metastatic castration-resistant prostate cancer with bone metastases, ^{177}Lu-DOTA-TATE (LUTATHERA®) against somatostatin receptor-positive neuroendocrine tumours and ^{131}I-iobguane (AZEDRA®) against metastatic pheochromocytoma or paraganglioma [12]. New developments in the field of targeted radionuclide therapy include the use of α-emitters, such as Bi-213 or Ac-225, thanks to great therapeutic effects of ^{225}Ac-PSMA-617 against metastatic prostate cancer during clinical trials [13].

The combination of imaging and therapy, known as theranostic, is also of increasing interest [15]. Ideally, one radionuclide has both therapeutic β^- as well as diagnostic γ emission, as in the case of Cu-67, which decays with a half-live 2.58 days by β^- (562 keV) and γ-emission (93 keV and 185 keV) [16]. But also a combination of a diagnostic and a therapeutic radionuclide (potentially of the same element or elemental group) is also possible, allowing for personalized precision medicine and the ability to determine

1

radiation doses for the patient from the imaging analogue [17].

1.2. Production of medical radionuclides

Since radionuclides used for medical applications usually have a short half-live in the range of hours to days, they do not occur naturally but have to be produced on-demand. Multiple different production methods have been studied and applied for the production of medical radionuclides, including the direct production in nuclear reactors, cyclotrons and linear accelerators, although some of the most used isotopes in clinical applications are eluted from generators [18]. These generators contain a long-lived mother nuclide on an adsorbent material (mostly produced in nuclear reactors), that decays to the desired medical radionuclide, which can be selectively eluted from the generator (see Fig. 1.3). The most famous and often used generator to date is the Mo-99/Tc-99m generator, followed by the Ge-68/Ga-68 generator [19]. Major advantages of generators are that they can be handled on site in a clinical environment, on demand, without the need for highly expensive and complex equipment [19]. Even though these generators have a shelf-life (the time frame in which a generator can be eluted efficiently until the radioactivity of the mother isotope is too low) of a few weeks to months, and they can be eluted up to several times per day, they still show several disadvantages.

One major issue in the case of Mo-99/Tc-99m generators, is that the production of Mo-99 is limited to currently seven nuclear reactors worldwide, accompanied with the production of large amounts of nuclear waste, and reduced yields due to the proliferation-related reduction of highly enriched uranium (HEU) to low enriched uranium (LEU) [21]. Another disadvantage of generators include the potential breakthrough of the long-lived

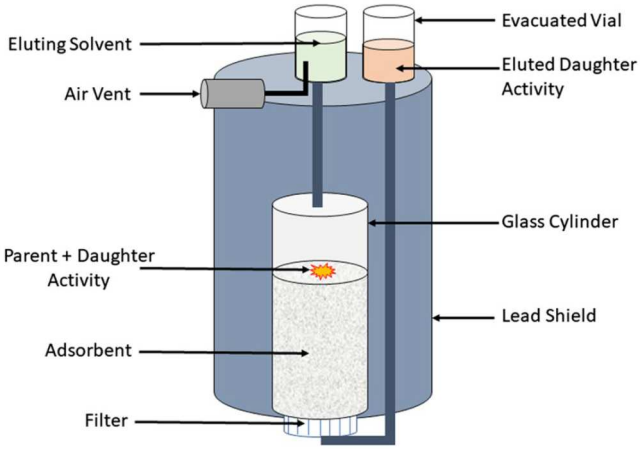

Figure 1.3: Schematic figure of a radionuclide generator, showing how the eluting solvent is passed through the adsorbent-containing column, to elute the daughter activity (from [20]).

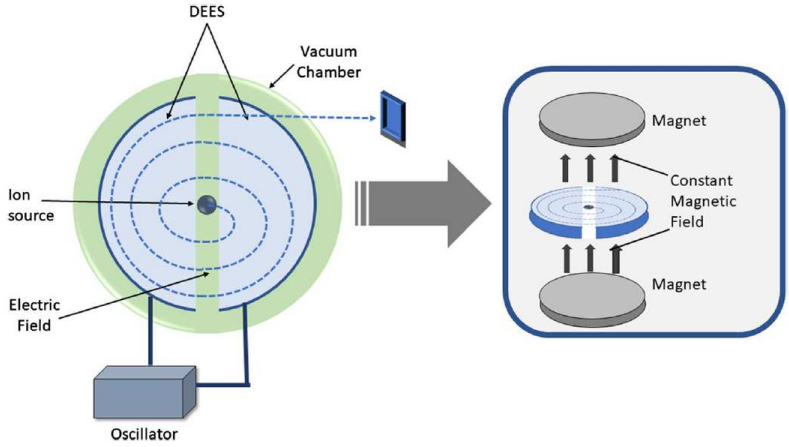

Figure 1.4: Schematic figure of a cyclotron, showing the spiral acceleration of protons between two magnets and a target at the exit beam (from [20]).

mother nuclides in the elution [22].

Nuclear reactors are also used for the direct production of medical radionuclides via neutron activation. Examples include Ho-166, produced by neutron irradiation of Ho-165 microspheres and used for radioembolization therapy against liver cancer [23] and Lu-177 against e.g. neuroendocrine tumors [24], produced either directly by neutron activation of Lu-176 or indirectly by neutron activation of Yb-176, resulting in Yb-177 which decays to Lu-177 [25].

Another possibility to produce radionuclides is using particle accelerators, for example a cyclotron [18, 26, 27]. A cyclotron accelerates charged particles with a strong magnetic field and irradiates a specific target placed at the exit of the beam (see Fig. 1.4). As an example, Ga-68 can be produced by irradiation of Zn-68 with protons, inducing the ^{68}Zn(p,n)^{68}Ga nuclear reaction [28–30] in which a neutron is replaced by a proton in the nucleus of the target. The target material can be either liquid or solid. While irradiation of solid targets is usually preferred due to a significantly higher yield, it is accompanied

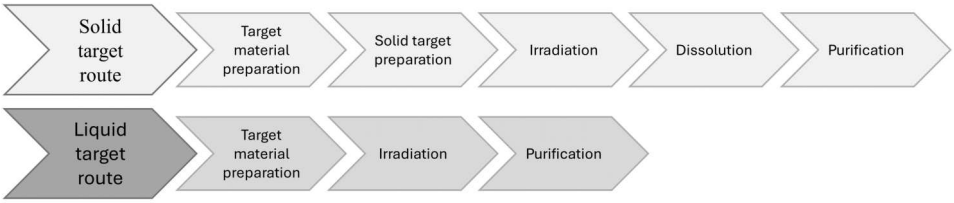

Figure 1.5: Different processing steps of solid and liquid cyclotron targets.

by time-consuming pre- and post-irradiation preparation steps (see Fig. 1.5). The use of liquid targets promises to be a convenient, cost-efficient and fast alternative and is, therefore, of increasing interest [29–31].

1.3. Chemical separation methods

The most frequently used chemical separation method for the purification of medical radionuclides is ion-exchange chromatography. For this, a column is filled with an ion-exchange resin, which separates ions based on their charge. These ion-exchange resins generally consist of a polymer coupled to charged functional groups, either anions or cations (for cation-exchange or anion-exchange, respectively) [32]. This separation technique is well established, but also exhibits several disadvantages when used for medical radionuclides, such as (I) large amounts of resin needed, resulting in large amounts of chemical and solid waste (II) large elution volumes, necessitating further concentration steps, (III) slow processing, significantly reducing the final radioactivity, or (IV) low radiation stability, resulting in radiolysis-related degradation products that require multiple washing steps [33]. As an alternative purification method, solvent extraction is increasingly studied for the processing of medical radionuclides. Due to its significance for this PhD thesis it is described in detail below.

1.3.1. Solvent extraction

During solvent extraction (also called liquid-liquid extraction) two immiscible solutions are brought in contact to each other, and ions are extracted from one phase to the other based on solubility differences. Mostly, the two phases are an aqueous and an organic phase, but also aqueous two-phase systems [34], super critical fluids [35] and ionic liquids [36] are applied. The extraction is often accomplished or enhanced by the use of selective chelators, that form hydrophobic complexes with the desired metal ions, that are then extracted into an organic solution. Chelation describes the complex formation of a metal ion with a ligand via coordinate bonds. Only polydentate ligands, forming a complex by two or more bonds, are described as chelating ligands, chelating agents or simply chelators. They have a higher affinity for the metal ion than a monodentate ligand, with just one bond, and, therefore, also form more stable complexes.

Batch extractions are usually done in separatory funnels for larger amounts, or vials for smaller amounts, as shown in Fig. 1.6. The two phases are mixed by static mixers or vortex mixers. The mixing creates droplets that increase the surface-to-volume ratio of the two phases. With decreasing droplet size, the surface-to-volume ratio increases, leading to increased extraction. After the selective extraction of the radionuclide from the aqueous solution to the organic solution another step is necessary to release the radionuclide from the chelator and to enable radiopharmaceutical labelling. This process is called back-extraction and is typically done with strong acids or bases, depending on

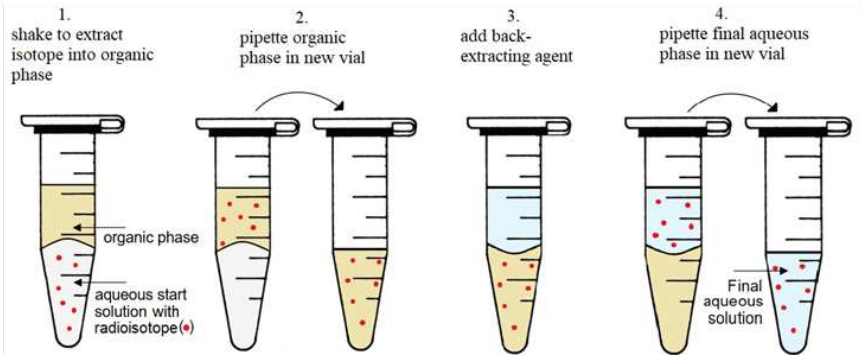

Figure 1.6: Schematic image of the batch solvent extraction and back-extraction process. First the radionuclide is extracted into the organic phase, followed by pipetting of the organic phase into a new vial. For the back-extraction an acidic aqueous solution is added to the organic phase, breaking the chelator-complex and releasing the radionuclide into the aqueous solution, followed again by pipetting of the aqueous solution to a new vial for measurements.

the used extraction system, that are able to break the chelation complex and release the metal ion back into an aqueous solution. Hydrochloric acid (HCl) is usually preferred for medical radionuclides, since most following radiopharmaceutical labelling processes are executed from HCl solutions [19, 37, 38]. Back-extraction is performed in a similar way. The organic phase is pipetted in a new vial together with the back-extracting agent, an acidic or basic aqueous solution. The solutions are then mixed again. After the second mixing step, the radionuclide is back in an aqueous solution and can be pipetted out of the vial separately for further use (see Fig 1.6).

This approach is straight-forward and was already pioneered in 1942 during the Manhattan project and since has large industrial applications in hydro-metallurgy [39] and recycling in the nuclear fuel cycle [40], and also medical applications for e.g. heavy metal detoxification [41]. However, its use for the extraction of medical radionuclides from irradiated target is a novel approach and to date not regularly used, mainly due to the difficulty in automation of the separation of the aqueous and organic solution. For this purpose, microfluidic systems are studied, aiming to enable future use of solvent extraction in medical radionuclide separation.

1.4. Microfluidics

Microfluidics describe the behavior of fluids at sub-millimeter scale, in which surface forces dominate over inertial forces [42]. The Reynolds number (Re), which is the ratio of inertial forces to viscous forces (Eq. 1.1), describes the internal movement of a fluid.

$$Re = \frac{inertial\ forces}{viscous\ forces} = \frac{density * velocity * length}{visocity} \tag{1.1}$$

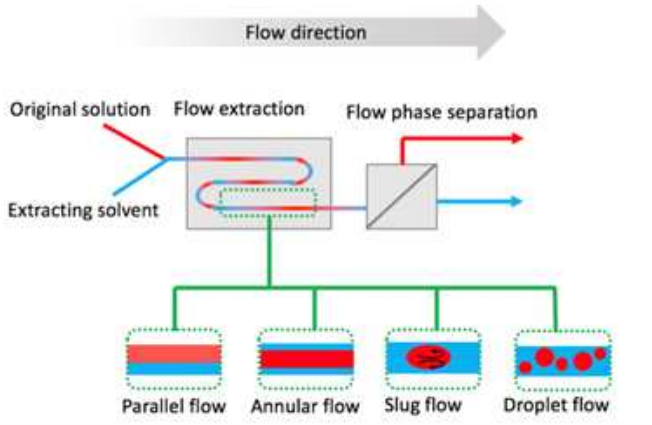

Figure 1.7: Different flow regimes that can be achieved in microfluidics, from [47]

In microfluidics the Reynolds number is so low (below approximately 2000), that laminar flow is expected, and mass transport will be limited mainly by diffusion to the interface [42, 43]. Advantages of microfluidic extraction are the high surface-to-volume ratio and a known effective contact surface, which enables the quantification of extraction kinetics and interfacial mass transfer [44]. A stable flow with a steady flow rate will also lead to more uniform reaction conditions and, thus, reliable and reproducible results. Different flow regimes can be described in microfluidics as shown in Fig 1.7. After the two immiscible fluids are brought in contact with each other they can exhibit either a parallel, annular, slug or droplet flow [45]. Slug flow has the highest surface-to-volume ratio due to internal circulation of slugs leading to an increase in mass transfer [46] and is, therefore, often preferred in industrial applications [47]. Parallel or annular flow give the opportunity to precisely calculate mass transfer rate coefficients due to the known surface-to-volume ratio [44, 48]. Which flow regime will be present is not only determined by the flow rate and channel size, but also by the microfluidic set-up. The most prominent ones are microfluidic chips or membrane separators and are described in detail in the following paragraph.

1.5. Microfluidic solvent extraction

Even though the first uses of micro devices were described in the 1940s, most advancements only began at the end of the 20th century after the introduction of the first Total Analysis System (TAS), in which sample transport, any necessary chemical reactions, chromatographic separations and detection could proceed automatically [49]. This improvement increased the interest of other fields of microfluidics drastically [42]. While a plethora of different microfluidic devices exists to date, due to the relevance for this

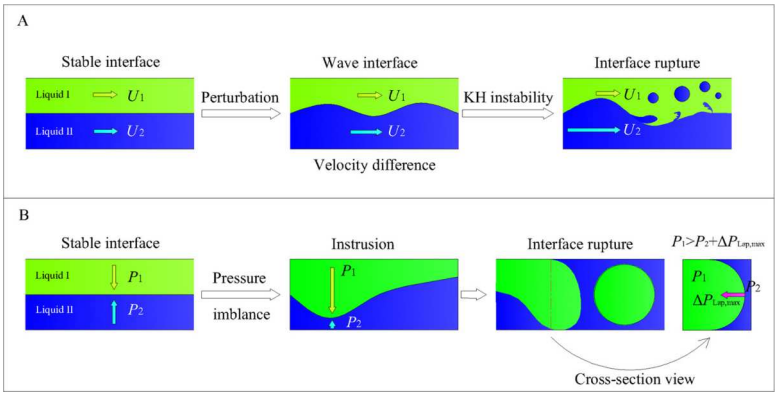

Figure 1.8: Interface instabilities in microfluidic parallel flow. A) Kevin-Helmholtz (KH) instability leading to perturbation and interface rupture due to velocity differences. B) Pressure imbalance at the interface leading to intrusion and surface rupture (from [43]).

dissertation only microfluidic chips and membrane separators are described below.

Microfluidic chips are devices with micro-channels that have been molded or patterned into a specific material. The two most commonly used materials for the production of microfluidic chips are glass and polydimethylsiloxane (PDMS). PDMS is an inexpensive elastomer, that is simple and cost-efficient to produce, resistant to highly acidic or basic solutions and easy to prototype [50]. One disadvantage of PDMS is the possible absorption of small molecules and sensitivity to several organic solvents [50, 51]. While glass chips do not have the same issues, they are more difficult to prototype and far more expensive in production, limiting their applicability to single-use applications such as GMP production of medical radionuclides. Therefore, PDMS is the preferred material for multiple microfluidic devices [50].

Microfluidic chips, as used in this thesis, have an active operation way, which includes the active manipulation of the aqueous and organic solutions by, e.g., syringe pumps, as opposed to passive operation, that makes use of capillary forces, gravity or vacuum [52]. The use of microfluidic chips for solvent extraction began in 2000 when Sato et al. delivered the proof-of-concept with two immiscible fluids in a YY-junction microchannel [53]. Since then, YY-chips are of increasing interest, but to date, they still exhibit several drawbacks that limit their use in solvent extraction.

One major difficulty in operating a microfluidic YY-chip is to maintain a stable interface and, thus, a stable parallel flow. Figure 1.8 shows two main reasons for interface rupture, namely different flow rates causing Kevin-Helmholtz (KH) instability of the flow, and pressure imbalance at the interface leading to interface rupture [43]. Both lead to imperfect phase separation, with either organic or aqueous leakage (see Fig. 1.9). Therefore, YY-microfluidic chips have not been successfully used for the separation of medical radionuclides, yet.

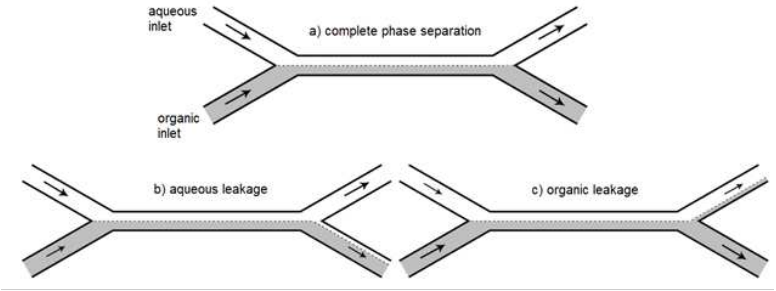

Figure 1.9: Schematic image of different flow patterns. a) complete phase separation. b) aqueous leakage in the organic outlet. c) organic leakage in the aqueous outlet. (Modified after [54])

An alternative to microfluidic chips are membrane separators. When using a membrane separator, it is possible to avoid the issue of imperfect phase separation that usually occurs in commercial microfluidic YY-chips. A commercial microfluidic membrane separator and the one used in this project is the Zaiput Membrane Separator (Fig. 1.10). This separator allows for an easy and sufficient separation of the organic and aqueous phases in solvent extraction experiments. Additionally, the flow regime prominent in the tubing connected to the inlet of the membrane separator is slug flow. Slug flow exhibits the highest surface-to-volume ratio, due to internal circulation, and, thus, has the potential for very high extraction efficiencies. When the two phases enter the membrane separator, one phase will be the wetting phase, depending on the membrane (hydrophilic or hydrophobic). When a hydrophobic membrane is used, the organic phase will be the wetting phase and fill the pores of the membrane, while the aqueous phase will be repelled. An internal pressure controller provides a perfect pressure differential for the wetting phase to pass the membrane without forcing the non-wetting phase to rupture

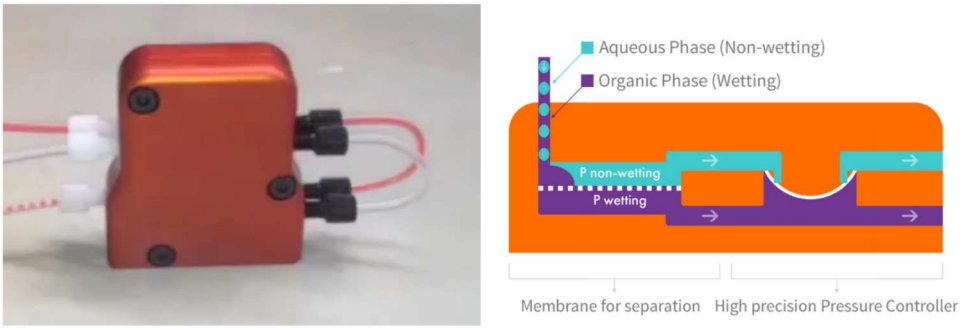

Figure 1.10: Left: Zaiput membrane separator, indicating the separation of two immiscible fluids (red and colorless). Right: Schematic image of the inside of a membrane separator, showing the separation of two immiscible fluid (blue = aqueous; purple = organic), by a hydrophobic membrane [55].

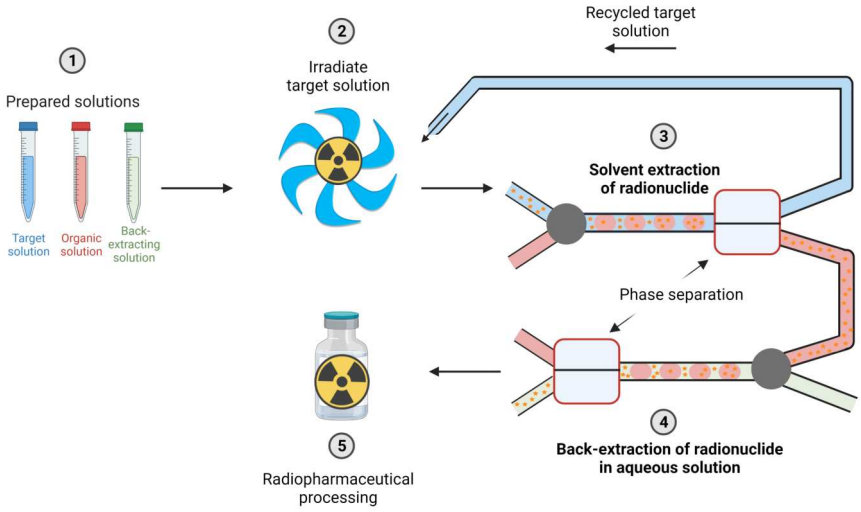

Figure 1.11: Illustration of automated solvent extraction, showing all production steps from 1) the preparation of the necessary solutions, over 2) cyclotron irradiation of the target solution, followed by microfluidic 3) solvent extraction and 4) back-extraction and finally 5) radiopharmaceutical processing.

the membrane. The separator can maintain a constant pressure differential even when different flow rates are applied. Because the membrane separator makes use of wettability differences of the fluids, even two fluids with the same density can be separated [55].

Due to the promising application and the easy handling of membrane separators, initial studies have been done on their application for the separation of medical radionuclides from irradiated targets. Pederson et al. studied the separation of Ti-45 from $ScCl_3$ in 12 M HCl solution as well as the separation of Ga-68 from a $ZnCl_2$ in HCl solutions, and successfully extracted up to 95.7 ± 2.0 % of Ga-68 [56]. However, as $ZnCl_2$ solutions have shown to be unsuitable for irradiation in cyclotrons, due to a rapid pressure increase [57], the study of the separation of Ga-68 from $Zn(NO_3)_2$ in HNO_3 solutions is required for use with liquid targets. Recently, Chakravarty et al [58] published a study about microfluidic solvent extraction of Cu-64 from Zn, using a T-junction microfluidic mixer and subsequent phase separation with a hydrophobic phase separation paper. While the extraction was successful and yielded Cu-64 extraction efficiencies of >85 %, their final collected solution consisted of 25 mL 7 M HCl and H_2O_2 that necessitates drying of the highly radioactive solution before labeling to pharmaceuticals is possible.

While promising proof-of-concept studies exist, detailed consideration of solution compositions (liquid target, as well as final collected solutions), metal and chelator contaminations are still lacking. Additionally, the radiation resistance of those membranes needs to be evaluated, since they are typically made from PTFE, which is known to be-

come brittle upon irradiation [59]. Furthermore, membrane-based microfluidic devices are costly and hence, not applicable for the GMP production of medical radionuclides, that often necessitates single-use equipment [60]. Therefore, the focus in this project lies on the improvement and use of microfluidic chips.

Overall, a microfluidic extraction set-up gives the opportunity for not only the automation of solvent extraction of the produced radionuclide, but also enables direct target recycling of liquid targets, potentially creating a continuous cyclotron irradiation of the target solution [56] as illustrated in Fig. 1.11.

Scope and outline of the thesis

The aim of this thesis is to develop methods for microfluidic solvent extraction of several medical radionuclides of interest. The separation of the nuclides Ga-68, Cu-64, Sc-46, Y-90, La-140 and Ac-225 from their respective targets was studied in batch and later translated to different microfluidic devices, including a membrane separator as well as glass and PDMS microfluidic chips. The effect of extracting chelator contamination on radiopharmaceutical labelling was investigated as well. Furthermore, the use of microfluidic chips for the determination of diffusion coefficients was studied. Finally, an alternative application of chelators was shown in the form of chelators-impregnated PDMS. The outline of this thesis is given below:

Chapter 2 describes the development of a separation method for Ga-68 from $Zn(NO_3)_2$ liquid targets using the batch approach and comparing it to membrane-based microfluidic solvent extraction.

Chapter 3 focuses on the separation of Cu radionuclides from a $Zn(NO_3)_2$ target solution. A method was developed using dithizone as a selective chelator and microfluidic extraction was studied with a commercial glass microfluidic chip.

Chapter 4 shows the microfluidic extraction of Ac-225 with D2EHPA as chelator, using a nano-layer coated PDMS microfluidic chip.

Chapter 5 assesses the applicability of microfluidic chips for the determination of diffusion constants.

Chapter 6 deals with the influence of chelator contamination after solvent extraction on the labelling of radionuclides to pharmaceuticals. A microcolumn was studied for the purification of the Ga-68 solution, obtained after solvent.

Chapter 7 presents an alternative method of chelator-based radionuclide separation from target solutions, namely chelator-impregnated polydimethylsiloxane (PDMS) beads.

Chapter 8 gives a general conclusion and outlook based on the chapters above.

1

References

[1] World-Nuclear-Association. Radioisotopes in medicine. *last update: April 2024, accessed April 2024,* Available at `https://world-nuclear.org/`.

[2] Pande, M. Nuclear medicine market size growth analysis advancements applications and future prospects report 2023-2030 (2023).

[3] Weber, W. A. *et al.* The future of nuclear medicine, molecular imaging, and theranostics. *Journal of Nuclear Medicine* **61**, 263–272 (2020).

[4] Crișan, G. *et al.* Radiopharmaceuticals for PET and SPECT imaging: A literature review over the last decade. *International Journal of Molecular Sciences* **23**, 5023 (2022).

[5] Alqahtani, F. F. SPECT/CT and PET/CT, related radiopharmaceuticals, and areas of application and comparison. *Saudi Pharmaceutical Journal* **31**, 312–328 (2023).

[6] Yang, C.-T. *et al.* PET-MR and SPECT-MR multimodality probes: Development and challenges. *Theranostics* **8**, 6210–6232 (2018).

[7] IAEA. Database of cyclotrons for radionuclide production. *accessed April 2024* Available at `https://nucleus.iaea.org/sites/accelerators/Pages/Cyclotron.aspx`.

[8] Hu, X., Li, D., Wang, R., Wang, P. & Cai, J. Comparison of the application of ^{18}F-FDG and ^{68}Ga-DOTATATE PET/CT in neuroendocrine tumors: A retrospective study. *Medicine* **102**, e33726 (2023).

[9] Anand, S., Singh, H. & Dash, A. Clinical applications of PET and PET-CT. *Medical Journal Armed Forces India* **65**, 353–358 (2009).

[10] Jurcic, J. G. *et al.* Targeted radionuclide therapy. In Gunderson, L. L. & Tepper, J. E. (eds.) *Clinical Radiation Oncology (Fourth Edition)*, 399–418 (Elsevier, Philadelphia, 2016), fourth edition edn.

[11] Khan, A. & T. M. de Rosales, R. Radiolabelling of extracellular vesicles for pet and spect imaging. *Nanotheranostics* **5**, 256–274 (2021).

[12] Malcolm, J., Falzone, N., Lee, B. Q. & Vallis, K. A. Targeted radionuclide therapy: New advances for improvement of patient management and response. *Cancers* **11** (2019).

[13] Kratochwil, C. *et al.* ^{225}Ac-PSMA-617 for PSMA-targeted α-radiation therapy of metastatic castration-resistant prostate cancer. *Journal of Nuclear Medicine* **57**, 1941–1944 (2016).

[14] Vahidfar, N., Aghanejad, A., Ahmadzadehfar, H., Farzanefar, S. & Eppard, E. Theranostic advances in breast cancer in nuclear medicine. *International Journal of Molecular Sciences* **22**, 4597 (2021).

[15] Qaim, S. M. Theranostic radionuclides: recent advances in production methodologies. *Journal of Radioanalytical and Nuclear Chemistry* **322**, 1257–1266 (2019).

[16] Hao, G. *et al.* Copper-67 radioimmunotheranostics for simultaneous immunotherapy and immuno-SPECT. *Scientific Reports* **11**, 3622 (2021).

[17] Rösch, F., Herzog, H. & Qaim, S. M. The beginning and development of the theranostic approach in nuclear medicine, as exemplified by the radionuclide pair 86y and 90y. *Pharmaceuticals* **10** (2017).

[18] Qaim, S. The present and future of medical radionuclide production. *Radiochimica Acta* **100**, 635–651 (2012).

[19] Velikyan, I. ^{68}Ga-based radiopharmaceuticals: Production and application relationship. *Molecules* **20**, 12913–12943 (2015).

[20] Goel, M., Mackeyev, Y. & Krishnan, S. Radiolabeled nanomaterial for cancer diagnostics and therapeutics: principles and concepts. *Cancer Nanotechnology* **14** (2023).

[21] Ballinger, J. R. Mo-99 shortage in nuclear medicine: Crisis or challenge? *Journal of Labelled Compounds and Radiopharmaceuticals* **53**, 167–168 (2010).

[22] Dash, A. & Chakravarty, R. Radionuclide generators: the prospect of availing pet radiotracers to meet current clinical needs and future research demands. *American Journal of Nuclear Medicine and Molecular Imaging* **9**, 30–66 (2019).

[23] Stella, M., Braat, A., van Rooij, R., de Jong, H. & Lam, M. Holmium-166 radioembolization: Current status and future prospective. *CardioVascular and Interventional Radiology* **45**, 1634–1645 (2022).

[24] Das, T. & Banerjee, S. Theranostic applications of lutetium-177 in radionuclide therapy. *Current Radiopharmaceuticals* **9**, 94–101 (2015).

[25] Dash, A., Pillai, M. & Jr., F. K. Production of ^{177}Lu for targeted radionuclide therapy: Available options. *Nuclear Medicine and Molecular Imaging* **49**, 85–107 (2015).

[26] Schmor, P. Review of cyclotrons for the production of radioactive isotopes for medical and industrial applications. *Reviews of Accelerator Science and Technology* **4**, 103–116 (2011).

[27] Synowiecki, M. A., Perk, L. R. & Nijsen, J. F. W. Production of novel diagnostic radionuclides in small medical cyclotrons. *EJNMMI Radiopharmacy and Chemistry* **3** (2018).

[28] Alves, F. *et al.* Production of copper-64 and gallium-68 with a medical cyclotron using liquid targets. *Modern Physics Letters A* **32** (2017).

[29] Alves, V., do Carmo, S., Alves, F. & Abrunhosa, A. Automated purification of radiometals produced by liquid targets. *Instruments* **2**, 1–9 (2018).

[30] Oehlke, E. *et al.* Production of Y-86 and other radiometals for research purposes using a solution target system. *Nuclear Medicine and Biology* **42**, 842–849 (2015).

[31] do Carmo, S. J., Scott, P. J. & Alves, F. Production of radiometals in liquid targets. *EJNMMI Radiopharmacy and Chemistry* **5** (2020).

[32] Naushad, M. & Al-Othman, Z. A. *A Book on Ion Exchange, Adsorption and Solvent Extraction* (Nova, 2013).

[33] Zielinska, B., Apostolidis, C., Bruchertseifer, F. & Morgenstern, A. An improved method for the production of Ac-225/Bi-213 from Th-229 for targeted alpha therapy. *Solvent Extraction and Ion Exchange* **25**, 339–349 (2007).

[34] Hatti-Kaul, R. Aqueous two-phase systems a general overview. *Molecular Biotechnology* **19**, 269–277 (2001).

[35] Sapkale, G. N., Patil, S. M., Surwase, U. S. & Bhatbhage, P. K. Supercritical fluid extraction. *International Journal of Chemical Sciences* **8**, 729–743 (2010).

[36] Hoogerstraete, T. V., Onghena, B. & Binnemans, K. Homogeneous liquid-liquid extraction of metal ions with a functionalized ionic liquid. *Journal of Physical Chemistry Letters* **4**, 1659–1663 (2013).

[37] Payolla, F. B., Massabni, A. C. & Orvig, C. Radiopharmaceuticals for diagnosis in nuclear medicine: A short review. *Ecletica Quimica* **44**, 11–19 (2019).

[38] Pascali, G., Watts, P. & Salvadori, P. A. Microfluidics in radiopharmaceutical chemistry. *Nuclear Medicine and Biology* **40**, 776–787 (2013).

[39] Flett, D. S. Solvent extraction in hydrometallurgy: The role of organophosphorus extractants. *Journal of Organometallic Chemistry* **690**, 2426–2438 (2005).

[40] Herbst, R., Baron, P. & Nilsson, M. *Advanced separation techniques for nuclear fuel reprocessing and radioactive waste treatment*, chap. Chapter 6: Standard and advanced separation: PUREX processes for nuclear fuel reprocessing, 141–175 (Woodhead Publishing Ltd, 2011).

[41] Sears, M. E. Chelation: Harnessing and enhancing heavy metal detoxification - a review. *The Scientific World Journal* **2013** (2013).

[42] Convery, N. & Gadegaard, N. 30 years of microfluidics. *Micro and Nano Engineering* **2**, 76–91 (2019).

[43] Xu, C. & Xie, T. Review of microfluidic liquid-liquid extractors. *Industrial and Engineering Chemistry Research* **56**, 7593–7622 (2017).

[44] Ciceri, D., Perera, J. M. & Stevens, G. W. The use of microfluidic devices in solvent extraction. *Journal of Chemical Technology and Biotechnology* **89**, 771–786 (2014).

[45] Rebrov, E. V. Two-phase flow regimes in microchannels. *Theoretical Foundations of Chemical Engineering* **44**, 355–367 (2010).

[46] Kashid, M. N. *et al.* Internal circulation within the liquid slugs of a liquid-liquid slug-flow capillary microreactor. *Industrial and Engineering Chemistry Research* **44**, 5003–5010 (2005).

[47] Martini, P. *et al.* Perspectives on the use of liquid extraction for radioisotope purification. *Molecules* **24**, 1–17 (2019).

[48] Hellé, G., Mariet, C. & Cote, G. Liquid-liquid extraction of uranium(VI) with Aliquat336 from HCl media in microfluidic devices: Combination of micro-unit operations and online ICP-MS determination. *Talanta* **139**, 123–131 (2015).

[49] Manz, A., Graber, N. & Widmer, H. M. Miniaturized total chemical analysis systems: a novel concept for chemical sensing. *Sensors and Actuators* **B1**, 244–248 (1990).

[50] M, K. R. & Chakraborty, S. PDMS microfluidics: A mini review. *Journal of Applied Polymer Science* **137**, 1–14 (2020).

[51] Toepke, M. W. & Beebe, D. J. PDMS absorption of small molecules and consequences in microfluidic applications. *Lab on a Chip* **6**, 1484–1486 (2006).

[52] Narayanamurthy, V. *et al.* Advances in passively driven microfluidics and lab-on-chip devices: A comprehensive literature review and patent analysis. *RSC Advances* **10**, 11652–11680 (2020).

[53] Sato, K., Tokeshi, M., Sawada, T. & Kitamori, T. Molecular transport between two phases in a microchannel. *Anaytical Sciences* **16**, 455–456 (2000).

[54] Nanninga, T. *An experimental analyses of a two-phased flow patterns inside a microchannel.* Ph.D. thesis, Delft University of Technology (2018).

[55] Zaiput-Flow-Technologies. Development scale liquid-liquid/gas-liquid separators. *last update: 2024, accessed April 2024,* Available at https://www.zaiput.com/product/liquid-liquid-gas-separators/.

[56] Pedersen, K. S., Nielsen, K. M., Fonslet, J., Jensen, M. & Zhuravlev, F. Separation of radiogallium from zinc using membrane-based liquid-liquid extraction in flow: Experimental and COSMO-RS studies. *Solvent Extraction and Ion Exchange* **37**, 376–391 (2019).

[57] Pandey, M. K., Byrne, J. F., Jiang, H., Packard, A. B. & Degrado, T. R. Cyclotron production of 68 ga via the 68 zn(p,n) 68 ga reaction in aqueous solution. *Am J Nucl Med Mol Imaging* **4**, 303–310 (2014). Available at www.ajnmmi.us/ISSN:2160-8407/ajnmmi0000152.

[58] Chakravarty, R. *et al.* Microfluidic solvent extraction of no-carrier-added 64cu from irradiated zn target for radiopharmaceutical preparation. *Chemical Engineering Journal Advances* **13**, 100433 (2023).

[59] Fayolle, B., Audouin, L. & Verdu, J. Radiation induced embrittlement of PTFE. *Polymer* **44**, 2773–2780 (2003).

[60] European Comission. EU GMP Annex 1: Manufacture of sterile medicinal products. (2022). Available at https://health.ec.europa.eu/system/files/2022-08/20220825_gmp-an1_en_0.pdf.

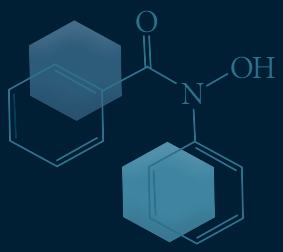

2

Membrane-based microfluidic solvent extraction of Ga-68

2

Membrane-based microfluidic solvent extraction of Ga-68

The radionuclide Ga-68 is commonly used in nuclear medicine, specifically in positron emission tomography (PET). Recently, the interest in producing Ga-68 by cyclotron irradiation of Zn-68 nitrate liquid targets is increasing [1–3]. However, current purification methods of Ga-68 from the target solution consist of long multi-step procedures, thus, leading to a significant loss of activity through natural decay, while often consuming large amounts of chemicals. To eventually allow switching from batch to continuous production, conventional batch extraction and membrane-based microfluidic extraction were compared. In both approaches, Ga-68 was extracted using N-benzoyl-N-phenylhydroxylamine in chloroform as the organic extracting phase. Extraction efficiencies of up to 99.5 % ± 0.6 % were achieved within 10 minutes, using the batch approach. Back-extraction of Ga-68 into 2 M HCl was accomplished within 1 minute with efficiencies of up to 94.5 % ± 0.6 %. Membrane-based microfluidic extraction achieved 99.2 % ± 0.3 % extraction efficiency and 95.8 % ± 0.8 % back-extraction efficiency into 6 M HCl. When executed on a solution irradiated with a 13 MeV cyclotron at TRIUMF, Canada, comparable efficiencies of 97.0 % ± 0.4 % were achieved. Zn contamination in the back-extracted Ga-68 solution was found to be below 3 ppm. Microfluidic solvent extraction is a promising method in the production of Ga-68 achieving high efficiencies in a short amount of time, potentially allowing for direct target recycling.

The content of this chapter has been published in: Trapp, S., Lammers, T., Engudar, G., Hoehr, C., Denkova, A.G., Paulssen, E. and de Kruijff, R.M., 2023. Membrane-based microfluidic solvent extraction of Ga-68 from aqueous Zn solutions: towards an automated cyclotron production loop. EJNMMI radiopharm. chem. 8(9)

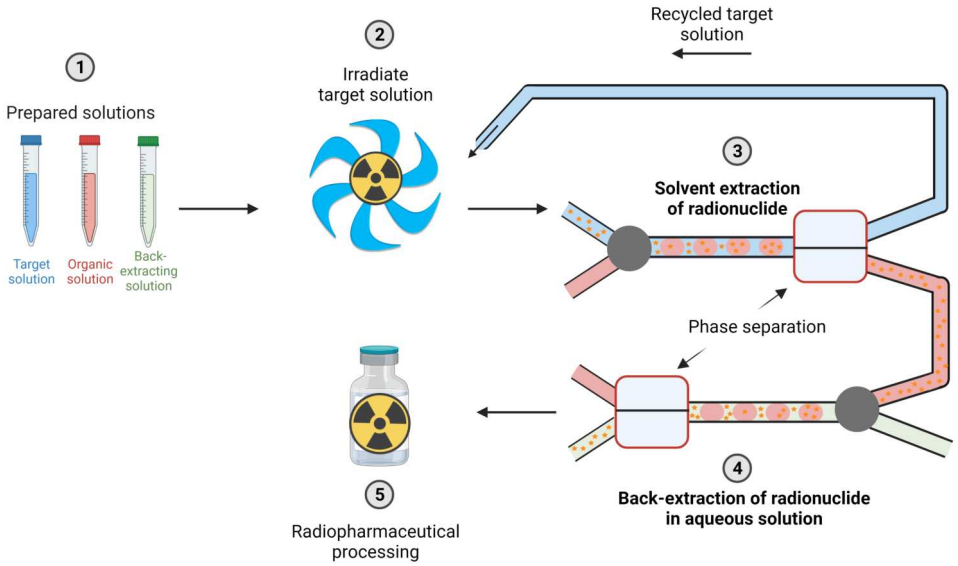

Figure 2.1: Graphical abstract showing the steps of liquid target preparation, irradiation and subsequent solvent extraction and back-extraction with the potential of direct target recycling (created with BioRender.com).

2.1. Introduction

The use of Ga-68-labelled radiopharmaceuticals has become increasingly popular in nuclear medicine over the last two decades. Ga-68 has ideal decay characteristics for high quality PET imaging, such as a positron yield of 89.1 % and an average beta energy of 836 keV [4] while the short half-life of 67.71 minutes minimizes the total dose to the patient and medical personnel. Since its radiolabelling chemistry is well understood, it can easily be applied in a variety of radiopharmaceuticals [5–7]. Recently, a new Ga-68 prostate-specific membrane antigen ligand (^{68}Ga-PSMA-11) for PET imaging of metastasized prostate cancer was approved by US Food & Drug Administration [8], which can detect significantly more prostate lesions than the previously used ^{18}F-fluciclovine [9]. Furthermore, Ga-68 labelled fibroblasts activation protein inhibitors (FAPI) showed remarkable results in PET imaging of up to 30 different tumor types [10]. Currently, over 500 clinical trials are using Ga-68 as a diagnostic agent [11] showing that the applications of Ga-68 in nuclear medicine are steadily expanding. An increase in demand in Ga-68 can therefore be expected.

To date, Ga-68 is mostly produced by Ge-68/Ga-68 generators, due to their easy handling and accessibility for hospitals without an irradiation infrastructure [6, 12]. But several limitations of these generators, such as the high costs, an increasing shortage in the target material to produce Ge-68, the limited amounts of Ga-68 that can be eluted from

a generator in a day [12–14], as well as the high amounts of radioactive Ge-68 waste after the shelf-life of a generator is reached, result in the necessity to investigate other Ga-68 production routes. Proton irradiation of Zn-68 could significantly amplify the production of Ga-68 by the ^{68}Zn(p,n)^{68}Ga reaction [15]. Several studies on the cyclotron production of Ga-68 from solid and liquid Zn targets exist to date [2, 3, 16–19]. Although the irradiation of liquid targets results in lower production yields compared to solid targets, they benefit from reduced target preparation steps pre and post irradiation, while still producing higher activities than generators. Most commercial Ge-68/Ga-68 generators produce a maximum of 1.85 GBq per elution, although this has recently increased with the development of a Ge-68/Ga-68 generator producing up to 3.7 GBq per elution [20]. These generators can only be eluted between one to three times per working day, dependent on the generator, loaded Ge-68 radioactivity, and the generators age [15]. In comparison, Alves et al [17] reported a yield of 6 GBq Ga-68 after a 45 minute irradiation of a Zn-68 liquid target with a 12.9 MeV medical cyclotron and a beam current of 45 μA, which can be up scaled to produce up to 40 GBq per irradiation by increasing the concentration of Zn-68 in the liquid target. Therefore, a single irradiation of a Zn-68 liquid target could produce a more than 10-times higher yield than the best currently available generators, making it a worthy alternative for hospitals that have a medical cyclotron (up to 12 MeV [21]) infrastructure available. But at the same time, current extraction methods of Ga-68 from the target solution after irradiation are multi-step procedures that can lead to a significant loss of activity due to natural decay and do not enable direct recycling of the costly, enriched target material.

Current literature on Ga-68 production using liquid targets focus mostly on the purification of Ga-68 using a combination of anion and cation exchange resins. As a first step cation exchange resins are used (e.g., hydroxamate, DOWEX 50W-X8, AG-50W-X8) to trap Ga-68 and wash most Zn-68. Enriched Zn-68 must be recovered and processed from the washing solutions before it can be reused for irradiation. Next, Ga-68 is eluted from the first column in large volumes of highly concentrated HCl solutions and loaded onto an anion exchange resin (e.g., Biorad 1X8, AG-1X-8, DGA, TK200) from which Ga-68 can be eluted in 0.1 M HCl or water, depending on the resin [2, 3, 16, 17, 22]. These methods usually lead to a purified Ga-68 in 30-60 minutes with yields between 78 % and 90 %. Microfluidic solvent extraction presents a very attractive, fast alternative to column chromatography [23] for the separation of Ga-68 from the target solution, with an efficient two-step procedure that potentially enables extraction automation and direct target recycling. In this approach, the target solution is not changed after irradiation (e.g. change of acid concentration), and can therefore potentially be directly recycled without any further processing steps as shown in Fig 2.1. While several studies exist on microfluidic solvent extraction on other medical radionuclides [24–26], Pedersen et al. [27] were the first to develop a microfluidic solvent extraction method to separate Ga-68 from a

$ZnCl_2$ in HCl target solution. However, the rate of radiolysis of water in HCl-based target solutions is known to lead to rapid pressure increase upon cyclotron irradiation, potentially forcing the abortion of irradiations [16]. It can also lead to strong corrosion of the Havar© foil used in the liquid target body [28]. Hence, irradiation of zinc liquid targets focuses almost exclusively on $Zn(NO_3)_2$ in dilute HNO_3 target solutions [1–3, 17, 22, 28] due to the ability of nitrates to scavenge free radicals produced during the irradiation of water, thereby reducing the target pressure [29]. Zhuravlev et al. [30] took the first steps in the development of a membrane-based microfluidic solvent extraction of Ga-68 from zinc nitrate solutions using an arylamino phosphonate leading to an extraction efficiency of 80 % in flow. However, this compound is not commercially available and was newly synthesized for their approach. In this chapter, a highly efficient microfluidic solvent extraction method for the selective extraction of Ga-68 from zinc nitrate liquid target solutions is presented, using a commercially available chelator, therefore avoiding the need for complex synthesis. Batch experiments are conducted to determine equilibrium extraction efficiencies for different concentrations of potential target solutions, followed by microfluidic experiments including a proof-of-principle run with a irradiated target solution.

2.2. Methods and Materials

2.2.1. Materials and analytical methods

N-benzoyl-N-phenylhydroxylamine (BPHA; CAS: 304-88-1) and zinc nitrate hexahydrate ($Zn(NO_3)_2 \cdot 6\,H_2O$) were purchased from ACROS ORGANICS (VWR, Amsterdam, the Netherlands), nitric acid (HNO_3), hydrochloric acid (HCl) and chloroform and were purchased from Sigma Aldrich (Merck Sigma, Zwijndrecht, the Netherlands). An Eckert & Ziegler IGG100 GMP Ge-68/Ga-68-generator was generously supplied by Erasmus MC, the Netherlands. ^{69m}Zn was produced by neutron irradiation of 6 mg ^{nat}Zn foil at the Hoge Onderwijs Reactor (HOR) of the Reactor Institute Delft (the Netherlands). After subsequent cooling for 10 hours, the foil was dissolved in 0.1 mL 8 M HNO_3 and diluted to 10 mL with distilled water. Microfluidic extractions were executed with a SEP-10 membrane separator with hydrophobic membranes (pore size: 0.45 µm) from Zaiput Flow Technologies (Waltham, Massachusetts, USA). AL-1000 Programmable Syringe pumps (941-371-1003) were purchased from World Precision Instruments Inc. and used to deliver solutions to the membrane separator via PTFE tubing (100 cm length, 0.03 inch inner diameter). A slug flow was achieved by using a Microfluidic Y Connector PEEK from IDEX Health & Science (Oak Harbor, Washington, USA). The Vortex-Genie 2 used for batch extractions was purchased from Scientific Industries, Inc (Bohemia, New York, USA). Metal contaminations were measured with an Inductively Coupled Plasma-Optical

Emission Spectrometer (ICP-OES) Optima 8000 from Perkin Elmer (Groningen, the Netherlands). The Wallac Wizard2 3" 2480 Automatic Gamma Counter from Perkin Elmer (Groningen, The Netherlands) was used for gamma-radiation measurements.

2.2.2. Experimental Methods

Batch Extraction

To optimize the Ga-68 extraction, aqueous solution concentrations ranging from 1-5 M $^{nat}Zn(NO_3)_2$ in 0.01-1M HNO_3 were tested according to reported target concentrations in the literature [1, 2, 17, 22]. 10-15 kBq of Ga-68 from a Ge-68/Ga-68 generator was added to each aqueous solution to trace Ga extraction and 3-5 kBq Zn-69m was added to trace Zn-coextraction. BPHA was chosen as the extractant due to its capability to extract Ga^{3+} from highly acidic media and known kinetics of the Ga-BPHA complex [31–33]. The organic solution used consisted of 0.2 M BPHA in chloroform. Additionally, dithizone was selected as an extractant to selectively extract Cu contaminations from the target solution. Conventional batch extraction experiments were executed in Eppendorf vials with a 1:1 volumetric ratio of aqueous and organic phase with volumes of 0.5 mL each. The Eppendorf vials were shaken with the Vortex for 10 minutes or 1 minute with BPHA or dithizone, respectively, to ensure extraction equilibrium was reached. Afterwards, the organic phase was separated by pipetting. The Ga-68 and Zn-69m radioactivity in the aqueous solution before extraction (A_{start}) and organic phase after extraction ($A_{organic}$) was measured with the Wallac Wizard2 3" 2480 Automatic Gamma Counter and corrected for decay. The extraction efficiencies (EE%) were calculated according to:

$$EE\% = \frac{A_{organic}}{A_{start}} * 100\% \tag{2.1}$$

To evaluate back-extraction of Ga-68 from the organic phase into an aqueous phase, different concentrations of 0.1 M to 6 M HCl were added to the organic phase, again with a 1:1 volumetric ratio. The Ga-68 activity of the HCl solutions was measured separately after back-extraction (A_{HCl}) and back-extraction efficiencies (BEE%) were calculated according to:

$$EE\% = \frac{A_{HCl}}{A_{organic}} * 100\% \tag{2.2}$$

Each extraction experiment was executed in triplicate and errors are given as one standard deviation of the mean. Since Fe, Cu, Ni, Co and Mn are often found as non-isotopic impurities after cyclotron irradiation of $[^{68}Zn]Zn(NO_3)_2$ solutions [3] their co-extraction in the developed extraction system was investigated, following the same procedure. Therefore, 0.1 mM non-radioactive Fe(III), Cu, Ni, Co and Mn were added to the zinc solution. Their co-extraction was measure by ICP-OES.

Microfluidic Solvent Extraction

To achieve complete phase separation after the extraction, a membrane-based separation device (Zaiput Membrane Separator [34]) was used. Solvent extraction was executed in microfluidic PTFE tubing of 100 cm length and an inner diameter of 0.03 inch. The tubing was connected to two syringes, containing the aqueous and organic solutions (Fig 2.2). A constant flow of the aqueous and organic solutions was achieved using syringe pumps and a slug flow was created with a microfluidic Y-connector, to increase the surface-to-volume ratio of the aqueous and organic solution, maximizing extraction. All microfluidic solvent extraction experiments were performed at a 1:1 volumetric ratio with a flow rate of 40 µL/min. The radioactivity of Ga-68 was again measured with the Wallac Wizard2 3" 2480 Automatic Gamma Counter in the aqueous ($A_{aqueous}$) and organic solution ($A_{organic}$) after the extraction. Extraction efficiencies (EE%) were calculated according to:

$$EE\% = \frac{A_{\text{organic}}}{A_{\text{organic}} + A_{\text{aqueous}}} * 100\% \tag{2.3}$$

Additionally, back-extraction was investigated in the microfluidic set-up with 2 and 6 M HCl and varying flow rates from 50 – 150 µL/min. Back-extraction efficiency (BEE%) was calculated according to:

$$BEE\% = \frac{A_{\text{HCl}}}{A_{\text{organic}} + A_{\text{HCl}})} * 100\% \tag{2.4}$$

with A_{HCl} = Ga-68 activity in the aqueous HCl solution after back-extraction and $A_{organic}$ = Ga-68 activity in the organic solution after back-extraction. Solutions used for back-extraction were collected to determine Zn, Cu, Ni, Co, Fe and Mn contamination by ICP-OES. All experiments were executed in triplicate and errors are given as standard deviations of the mean. All measured activities were corrected for decay.

Cyclotron Targetry and Irradiation

Three irradiations on 2 M $^{nat}Zn(NO_3)_2 \cdot 6\,H_2O$ solutions in 0.01 M HNO_3 were executed on TRIUMF's TR13 cyclotron, a 13 MeV self-shielded, negative hydrogen ion cyclotron. This target concentration was selected due to its common use in literature [2, 3, 16–18] as well as extraction performance. The target solutions were irradiated in a siphon-style niobium body target with an internal expansion chamber as described by Hoehr et al. [35] and Lowis et al. [36]. The target chamber has a volume of 1.48 mL and is separated from the cyclotron vacuum by a double foil window with a water-cooling jacket on the back and a helium jet cooling on the front site of the target. Due to the two foils (25 µm thick aluminium foil outside of target and 38 µm HAVAR® foil inside of target) the proton beam gets degraded to 12 MeV. Before the start of the irradiation the internal expansion chamber was pressurized to 200 psi. A 10 µA beam of protons was applied for 30 minutes (n = 3). After irradiation and unloading, 5 mL of radioactive solution were obtained. 2.5

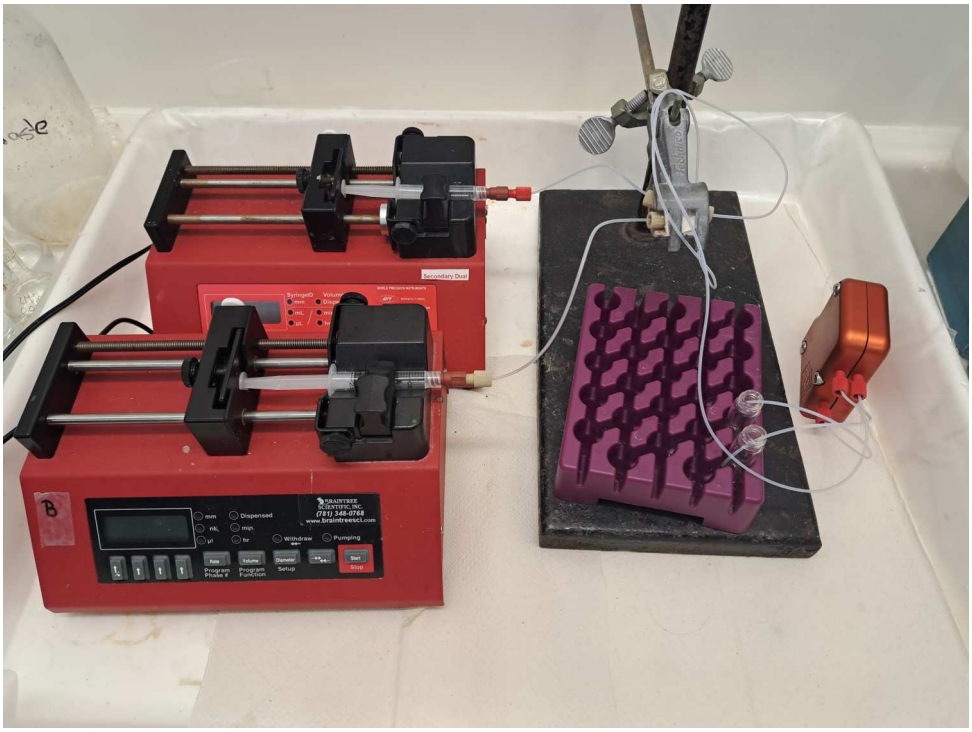

Figure 2.2: Microfluidic solvent extraction set-up using a Zaiput Sep-10 membrane separator. The droplet flow is created by fluidic y-connector.

mL were loaded into a syringe and microfluidic extractions were executed as described above with a flow rate of 40 µL/min. The extraction efficiency of Ga-68 was calculated according to Eq. 2.4 by using the 1077.34 keV identification peak.

2.3. Results

2.3.1. Batch extraction

Batch extraction of different concentrations of target solutions, ranging from 1 - 5 M $Zn(NO_3)_2$ in 0.01 – 1 M HNO_3, were performed to investigate optimal target concentrations to achieve highest extraction efficiencies for Ga-68. 5 M $Zn(NO_3)_2$ solutions all showed maximum extraction efficiencies of over 99.3 %. However, a trend of decreasing extraction efficiencies can be observed with increasing HNO3 concentrations for lower $Zn(NO_3)_2$ concentrations (Fig. 2.3a). Extraction efficiencies in the solutions containing 1 M $Zn(NO_3)_2$ range from 99.5 % ± 1.2 % to 55.5 % ± 0.6 % in 0.01 M and 1 M HNO_3, respectively. Increasing the contact time to up to 60 minutes did not increase extraction efficiencies (Fig. 2.3b), indicating that the results in Fig. 2.3a represent equilibrium.

Table 2.1: Extraction efficiencies for different metals using BPHA (5 min contact time) and dithizone (1 min contact time) from 2 M $Zn(NO_3)_2$ in 0.01 M HNO_3. Fe(III), Cu, Mn, Co and Ni ions were added to the $Zn(NO_3)_2$ solution at concentrations of 0.1 mM. Uncertainty is given as the standard deviation of the mean (n=3).

	BPHA	Dithizone
Zn [%]	0.09 ± 0.06	0.31 ± 0.19
Ga [%]	99.6 ± 0.3	0.03 ± 0.02
Fe [%]	99.45 ± 0.03	9.3 ± 3.0
Cu [%]	99.3 ± 0.4	99.91 ± 0.06
Mn [%]	0.8 ± 0.3	3.3 ± 2.3
Co [%]	4.1 ± 1.6	5.1 ± 1.5
Ni [%]	1.9 ± 1.2	7.3 ± 1.9

Therefore, lower HNO_3 concentrations of 0.01 M HNO_3 are beneficial to achieve highest possible extraction efficiencies of over 99 % for all studied $Zn(NO_3)_2$ concentrations. Zinc co-extraction was measured to be 0.09 % ± 0.06 % from a 2 M $Zn(NO_3)_2$ solution in 0.01 M HNO_3. Back-extraction efficiencies of 94.5 % ± 0.6 % could be achieved within 1 minute by using 2 M HCl as back-extracting agent. Higher HCl concentrations achieve similar results, while lower HCl concentrations lead to decreasing back-extraction efficiencies (Fig. 2.3c). Increasing the contact time for longer than 1 minute does not increase the back-extraction efficiency (Fig. 2.3d) indicating equilibrium could be reached within such a short time.

Co-extraction of other metal impurities

Co-extraction of non-isotopic metal impurities from a 2 M $^{nat}Zn(NO_3)_2$ solution in 0.01 M HNO_3 into BPHA and dithizone was investigated in batch (Tab. 1). Cu and Fe are co-extracted by BPHA with 99.3 ± 0.4 % and 99.45 ± 0.03 % efficiency, respectively, using a contact time of 5 min. Mn, Co and Ni are not extracted in significant amounts by BPHA (< 5%). Using 10 mM dithizone in chloroform, Cu impurities could be extracted from the target solution within 1 min of vortexing with an efficiency of 99.91 % ± 0.06 % without co-extracting Ga-68, giving the opportunity to extract ^{61}Cu which is simultaneously produced by proton irradiation of ^{nat}Zn [37, 38]. All other tested impurities showed very little to no extraction using dithizone (< 10 %).

Metal contamination in final solutions

Metal contamination in the back-extracted 2 M and 6 M HCl solutions after batch extraction from 2 M $^{nat}Zn(NO_3)_2$ in 0.01 M HNO_3 was measured by ICP-OES (Fig 2.4). All measured metal contaminations, including Cu, Ni, Co, Fe, Mn were below 0.5 ppm with Mn being below the detection limit (<10 ppb).

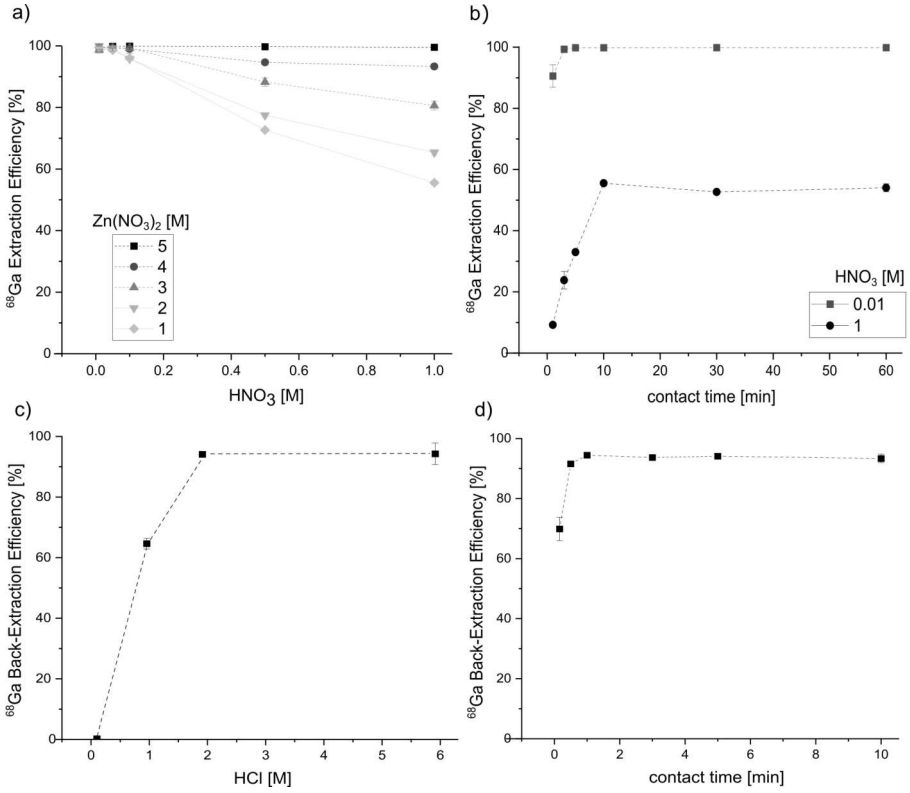

Figure 2.3: a) Extraction efficiencies for batch extraction of Ga-68 from various $Zn(NO_3)_2$ solutions in HNO_3 for a contact time of 10 minutes. b) Extraction efficiencies over time for batch extraction of Ga-68 from 1 M $Zn(NO_3)_2$ in 0.01 and 1 M HNO_3. c) Back-extraction efficiencies for batch extraction of Ga-68 into different HCl concentrations within. 1 minute contact time. d) Back-extraction efficiencies over time for back-extraction of Ga-68 into 2 M HCl. Error bars represent the standard deviation of the mean.

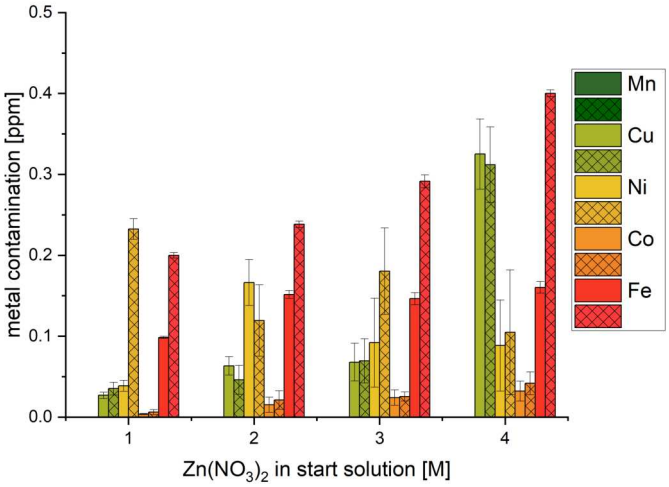

Figure 2.4: Mn, Cu, Ni, Co and Fe contaminations in back-extracted solutions (plain= into 2 M HCl; crossed= into 6 M HCl) after extraction from 2 M $Zn(NO_3)_2$ in 0.01 M HNO_3. Error bars represent the standard deviation of the mean (n=3).

2.3.2. Microfluidic extraction

Microfluidic extraction experiments were performed with varying $Zn(NO_3)_2$ and HNO_3 concentrations (Fig. 2.5). The results show a decreasing extraction efficiency with increasing $Zn(NO_3)_2$ concentrations (Fig. 2.5a). While 1 M $Zn(NO_3)_2$ resulted in an efficiency of 99.2% ± 0.3%, the 4 M $Zn(NO_3)_2$ solution only showed an efficiency of 88.2% ± 6.9% when the same flow rate of 40 µL/min was applied. Increasing the HNO_3 concentration significantly impacted the extraction efficiency (Fig. 2.5b), decreasing it, for instance, for 2 M $Zn(NO_3)_2$ from 97.9 % ± 0.6 % in 0.01 M HNO_3 to 41.2 % ± 4.5 % and 9.5 % ± 1.8 % in 0.1 M and 1 M HNO_3, respectively. Back-extraction exhibits a significant difference when comparing 2 M and 6 M HCl as back-extraction solutions. While 6 M HCl consistently showed efficiencies exceeding 94 % for varying flow rates between 50 and 150 µL/min, 2 M HCl achieved only 60.5 % ± 2.0 % decreasing to 31.5 % ± 1.8 %, for 50 and 150 µL/min, respectively (Fig. 2.5c). Zn contaminations did not exceed 3 ppm for all tested target solutions concentrations (Fig 2.5d), conforming to IAEA TecDoc standards [38]. To estimate the contamination according to the European Pharmacopoeia [37], where a maximum of 10 µg/GBq is allowed, the results were compared to a production of Ga-68 from enriched Zn-68 by Alves et al. [17]. They irradiated a 2.2 M $Zn(NO_3)_2$ solution, which resulted in an Ga-68 activity of 25 GBq at EOB. Taking 2 hour of decay into consideration for processing of the target solution and production of radiopharmaceuticals, while considering a Zn contamination of 3 ppm after the presented separation methods, the resulting contamination would equal to 2.5 µg/GBq. While this is just a

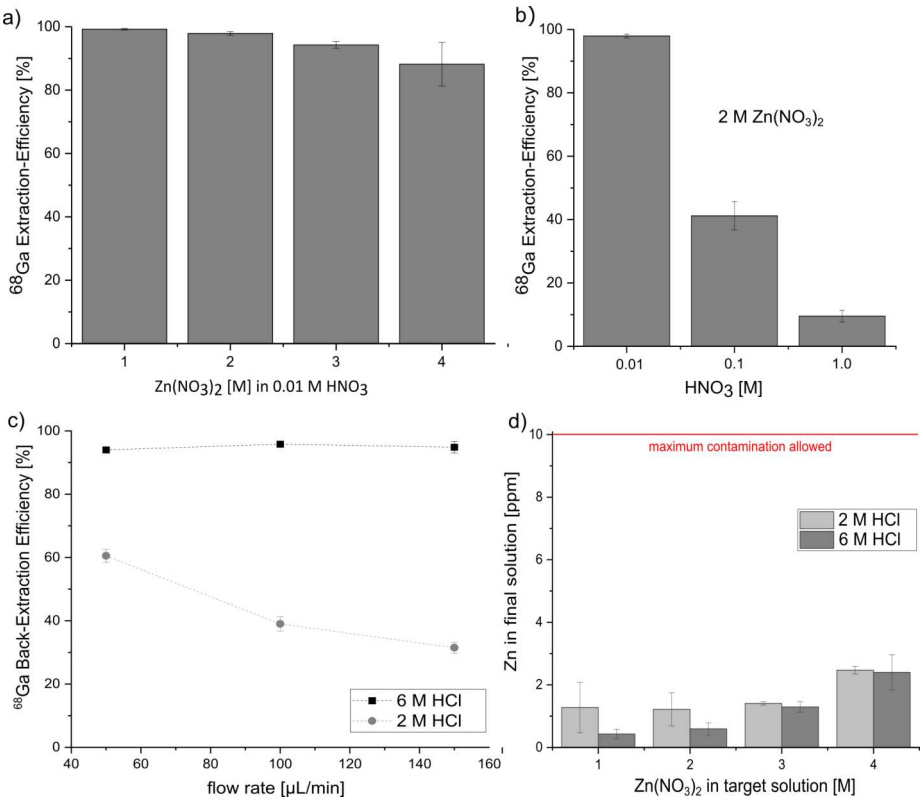

Figure 2.5: a) Extraction efficiencies for microfluidic extraction of Ga-68 from various $Zn(NO_3)_2$ solutions in 0.01 M HNO_3. The flow rate was 40 µL/min for both solutions. b) Extraction efficiencies for microfluidic extraction of Ga-68 from 2 M $Zn(NO_3)_2$ solutions with varying HNO_3 concentrations. The flow rate was 40 µL/min. c) Back-extraction efficiencies for microfluidic back-extraction of Ga-68 into 2 and 6 M HCl with varying flow rates. d) Zn contamination in final HCl solutions after back-extraction. Error bars represent the standard deviation of the mean (n=3).

approximation and results highly depend on irradiation parameters and target concentrations [2], the results look promising to fulfill the European Pharmacopoeia standards [37]. Additionally, a microfluidic extraction was performed on a cyclotron irradiated 2 M $Zn(NO_3)_2$ solution in 0.01 M HNO_3 as described in 2.3.2. Extraction efficiencies of 97.0 % ± 0.4 % (n=3) were obtained and are within uncertainty identical to the results observed with low activity solutions of 97.9 % ± 0.6 %. However, it was observed that the membranes used in these experiments were sensitive to radiolysis and started to break down after being in contact with a target solution containing between 500-600 MBq of Ga-68 for more than 20 minutes.

2.4. Discussion

2.4.1. Extraction behavior

During cyclotron irradiation of liquid targets high amounts of gases can be produced, leading to a drastic pressure increase inside the target body. Adding HNO_3 to Zn target solutions can reduce the pressure build up by scavenging free radicals. Several different HNO_3 target solution concentrations have been used successfully in the literature [2]. Therefore, multiple HNO_3 concentrations (0.01 - 1 M) in the target solutions were studied. These target solutions have a pH between -1.3 and 1.7, which is generally not preferred for solvent extraction purposes. Most conventional extractants only efficiently extract ions at higher pH (> pH 2) [39–44] or from highly acidic chloride solutions that will lead to the formation of chloride species [45–48]. However, in the solutions tested in this study, the dominant species is Ga^{3+} with minor amounts of $Ga(OH)^{2+}$ (calculated with CHEAQS Next software [49]). Therefore, most commercial extractants are not applicable. BPHA on the other hand has the ability to bind to Ga^{3+} and $Ga(OH)^{2+}$ according to reactions in equations 2.5 and 2.6 (adapted from [33] with L representing the ligand BPHA and M the metal Ga), making it a suitable extractant for extracting Ga-68 from $Zn(NO_3)_2$ liquid targets.

$$HL + M^{3+} \rightarrow MHL^{3+} \tag{2.5}$$

$$HL + M(OH)^{3+} \rightarrow ML^{2+} + H_2O \tag{2.6}$$

In the presented experiments, a clear effect of the amount of H^+ ions in the solution can be observed, indicating that lower acid concentration in the target solution (0.01-0.1 M HNO_3) are generally preferable to achieve the highest equilibrium extraction efficiency in the shortest contact time. Intramolecular hydrogen bonding was proposed as a reason for this reduction in extraction efficiencies [33]. However, increasing the $Zn(NO_3)_2$ concentrations in the target solutions leads to an increase in Ga-68 extraction efficiency even when higher acid concentrations are used, probably due to the 'salting-out effect'. This effect describes the positive effect of salt concentration on the partition coefficient and the separation factor of the extractant during the extraction process, consequently improving the extraction efficiency of Ga-68. The high effectiveness of $Zn(NO_3)_2$ as a salting-out agent in solvent extraction has been described before [50]. It could also be observed that higher levels of radioactivity, and the corresponding increase in radiolysis of the target solution after cyclotron irradiation, did not affect the extraction. Most likely the BPHA has sufficient radiation resistance to withstand breakdown during the short contact time, enabling Ga-68 extraction with the same efficiency as at low levels of radioactivity. The membrane on the other hand, seemed to be affected by the radiation dose and the corresponding radiolysis resulting in the formation of radicals in the target solution as well as the chloroform solution (SEM images of irradiated

membranes are included in the Supplements). Therefore, future research about the radiation stability of the membrane is necessary in order to ensure a continuous separation of radioactive nuclides.

Zhuravlev et al. [30] reported a maximum of 89.6 % EE in batch, and 80 % EE in membrane separator experiments from a 1 M $Zn(NO_3)_2$ in 0.01 M HNO_3. They used a comparable set-up for the phase separation utilizing slug flow in a 100 cm long tubing with 0.03 inch inner diameter connected to the Zaiput membrane separator for subsequent phase separation, but the flowrates used in their study where approximately 6 times faster at 250 µL/min. An additional mixing step was also included in their set-up with simultaneous heating of the solution to 50 °C. In comparison, the results from our study show maximum EEs as high as 99.9 % in batch, and 99.2 % ± 0.3 % in membrane separator experiments for the same zinc nitrate solution at room temperature without additional mixing, but with a slower flowrate of 40 µL/min. Finally, the measured zinc concentration in the back-extracted solutions in our study was below 3 ppm, while Zhuravlev et al. [30] reported 11 ppm in their study, which exceeds regulations of maximum 10 ppm, posed by the International Atomic Energy Agency TecDoc Quality Control on the Production of Radiopharmaceuticals [38]. Our results present a robust, highly efficient strategy for the rapid extraction of Ga-68 from cyclotron-irradiated $Zn(NO_3)_2$ liquid target solutions, based on an commercially available chelator allowing for quick implementation in Ga-68-producing cyclotron facilities.

2.4.2. Applicability in clinical setting

The developed method could increase the production of Ga-68 in the future significantly. The total purification time after cyclotron irradiation can be as fast as 10 minutes if applied to a module of multiple microfluidic devices, since one device only has a throughput of 40 µL/min it would take significantly longer otherwise. This method can increase the amount of extracted Ga-68 by almost 25 % compared to other purification methods, for the same irradiation time while potentially allowing for direct target recycling and re-irradiation. With just a single irradiation, produced activities could be 10-fold higher compared to an elution of the best currently available Ge-68/Ga-68 generator. The recyclability of the target solution after the extraction could lead to more irradiations per day, potentially increasing Ga-68 production tremendously. However, before this method can be readily used in clinical settings, some issues have to be overcome. Since the radiolysis in the target solution after irradiation leads to damage in the membrane used for the separation, and to the best of our knowledge no membrane for this specific set-up exists that might have higher radiation stability, further development should focus on a different microfluidic set-up without a radiation-sensitive membrane or on the improvement of the stability of the membranes.

2.5. Conclusion

A new two-step microfluidic extraction method for the efficient extraction of Ga-68 from liquid target solutions was developed. By using BPHA in chloroform as the extracting phase, extraction efficiencies of over 99 % and back-extraction efficiencies of up to 95 % could be achieved, leading to a total Ga-68 recovery of up to 94 % within 5-15 minutes. Best results were achieved when 0.01 M HNO_3 was used as the target solution, while only co-extracting 0.09 % ± 0.06 % Zn. This method presents a very promising new approach to selectively extract Ga-68 from [^{68}Zn]Zn$(NO_3)_2$ liquid targets, which significantly decreases the time required for Ga-68 extraction, and subsequently increasing production yield, while potentially allowing for direct target recycling.

References

[1] do Carmo, S. J., Scott, P. J. & Alves, F. Production of radiometals in liquid targets. *EJNMMI Radiopharmacy and Chemistry* **5** (2020).

[2] Pandey, M. K., Byrne, J. F., Schlasner, K. N., Schmit, N. R. & DeGrado, T. R. Cyclotron production of ^{68}Ga in a liquid target: Effects of solution composition and irradiation parameters. *Nuclear Medicine and Biology* **74-75**, 49–55 (2019).

[3] Riga, S. *et al.* Production of Ga-68 with a General Electric PETtrace cyclotron by liquid target. *Physica Medica* **55**, 116–126 (2018).

[4] Sanchez-Crespo, A. Comparison of gallium-68 and fluorine-18 imaging characteristics in positron emission tomography. *Applied Radiation and Isotopes* **76**, 55–62 (2013).

[5] Banerjee, S. R. & Pomper, M. G. Clinical applications of gallium-68. *Applied Radiation and Isotopes* **76**, 2–13 (2013).

[6] Maecke, H. R. & André, J. P. ^{68}Ga-PET radiopharmacy: A generator-based alternative to ^{18}F-radiopharmacy. *Ernst Schering Research Foundation workshop* 215–242 (2007).

[7] Prata, M. I. M. Gallium-68: A new trend in PET radiopharmacy. *Current Radiopharmaceuticalse* **5**, 142–149 (2012).

[8] U.S. Food and Drug Administration. U.S. Food and Drug Administration: FDA approves first PSMA targeted PET imaging drug (2022). `https://www.fda.gov/news-events/press-announcements` [Accessed: November 1st, 2022].

[9] Calais, J. *et al.* ^{18}F-fluciclovine PET-CT and ^{68}Ga-PSMA-11 PET-CT in patients with early biochemical recurrence after prostatectomy: a prospective, single-centre, single-arm, comparative imaging trial. *The Lancet Oncology* **20**, 1286–1294 (2019).

[10] Kratochwil, C. *et al.* ^{68}Ga-FAPI PET/CT: Tracer uptake in 28 different kinds of cancer. *Journal of Nuclear Medicine* **60**, 801–805 (2019).

[11] National Library of Medicine. Clinical Trials (2022). `https:\clinicaltrials.gov` [Accessed: November 1st, 2022].

[12] Rösch, F. Past, present and future of ^{68}Ge/^{68}Ga generators. *Applied Radiation and Isotopes* **76**, 24–30 (2013).

[13] Lambrecht, R. M. Radionuclide generators. *Radiochimica Acta* **34**, 1–2 (1983).

[14] Dash, A. & Chakravarty, R. Radionuclide generators: the prospect of availing PET radiotracers to meet current clinical needs and future research demands. *American Journal of Nuclear Medicine and Molecular Imaging* **9**, 30–66 (2019).

[15] Velikyan, I. ^{68}Ga-based radiopharmaceuticals: Production and application relationship. *Molecules* **20**, 12913–12943 (2015).

[16] Pandey, M. K., Byrne, J. F., Jiang, H., Packard, A. B. & Degrado, T. R. Cyclotron production of ^{68}Ga via the ^{68}Zn(p,n)^{68}Ga reaction in aqueous solution. *American Journal of Nuclear Medicine and Molecular Imaging* **4**, 303–310 (2014).

[17] Alves, F. *et al.* Cyclotron production of Ga-68 for human use from liquid targets: From theory to practice. *AIP Conference Proceedings* **1845** (2017).

[18] Rodnick, M. E. *et al.* Cyclotron-based production of ^{68}Ga, [^{68}Ga]$GaCl_3$, and [^{68}Ga]Ga-PSMA-11 from a liquid target. *EJNMMI Radiopharmacy and Chemistry* **5**, 1–18 (2020).

[19] Engle, J. W. *et al.* Very high specific activity ^{66}/^{68}Ga from zinc targets for PET. *Applied Radiation and Isotopes* **70**, 1792–1796 (2012).

[20] Radiopharma. Eckert & Ziegler extends gallium-68 generator portfolio in the united states (2022). `https://radiopharma.com/news` [Accessed: November 1st, 2022].

[21] Siikanen, J. *et al.* Cyclotron-produced ^{68}Ga from enriched ^{68}Zn foils. *Applied Radiation and Isotopes* **176** (2021).

[22] Alves, V., do Carmo, S., Alves, F. & Abrunhosa, A. Automated purification of radiometals produced by liquid targets. *Instruments* **2**, 1–9 (2018).

[23] Martini, P. *et al.* Perspectives on the use of liquid extraction for radioisotope purification. *Molecules* **24**, 1–17 (2019).

[24] Trapp, S., Lammers, T., Paulssen, E. & de Kruijff, R. Rapid, automated radionuclide separation with high yield - towards microfluidic solvent extraction for ^{61,64,67}Cu production. *Proceedings at European Research Reactor Conference, Antwerp, The Netherlands* 177–184 (2023).

[25] Martini, P. *et al.* Highly efficient micro-scale liquid-liquid in-flow extraction of ^{99m}Tc from molybdenum. *Molecules* **26**, 5699 (2021).

[26] Dalmázio, I. & Oehlke, E. Cyclohexanone microfluidic extraction of radioactive perrhenate from acid solutions. *International Nuclear Atlantic Conference, Belo Horizonte, Brazil* (2017).

[27] Pedersen, K. S., Nielsen, K. M., Fonslet, J., Jensen, M. & Zhuravlev, F. Separation of radiogallium from zinc using membrane-based liquid-liquid extraction in flow: Experimental and COSMO-RS studies. *Solvent Extraction and Ion Exchange* **37**, 376–391 (2019).

[28] Oehlke, E. *et al.* Production of Y-86 and other radiometals for research purposes using a solution target system. *Nuclear Medicine and Biology* **42**, 842–849 (2015).

[29] Pandey, M. K., Engelbrecht, H. P., Byrne, J. P., Packard, A. B. & DeGrado, T. R. Production of ^{89}Zr via the ^{89}Y(p,n)^{89}Zr reaction in aqueous solution: Effect of solution composition on in-target chemistry. *Nuclear Medicine and Biology* **41**, 309–316 (2014).

[30] Zhuravlev, F., Gulzar, A. & Falborg, L. Recovery of gallium-68 and zinc from HNO_3-based solution by liquid–liquid extraction with arylamino phosphonates. *Molecules* **27** (2022).

[31] Riedel, A. Systematic study of the extraction of metals using n-benzoyl-n-phenylhydroxylamine. *Journal of Radioanalytical Chemistry* **13**, 125–134 (1973).

[32] Lyle, S. J. & Shendrikar, A. D. A separation scheme for gallium, indium, thallium, germanium, tin and lead by solvent extraction with n-benzoyl-n-phenylhydroxylamine. *Analytica Chimica Acta* **32**, 575–582 (1965).

[33] Morroni, L., Secco, F., Venturini, M., Garcia, B. & Leal, J. M. Kinetics and equilibria of the interactions of hydroxamic acids with gallium(iii) and indium(iii). *Inorganic Chemistry* **43**, 3005–3012 (2004).

[34] Flow Technologies, Z. Development scale liquid-liquid/gas-liquid separators (2022). https://www.zaiput.com/product/liquid-liquid-gas-separators [Accessed: November 1st, 2022].

[35] Hoehr, C. *et al.* Producing radiometals in liquid targets: Proof of feasibility with ^{94m}Tc. *14th international workshop on targetry and target chemistry, Playa del Carmen, Mexico,* 56–60 (2012).

[36] Lowis, C., Ferguson, S., Paulßen, E. & Hoehr, C. Improved Sc-44 production in a siphon-style liquid target on a medical cyclotron. *Applied Radiation and Isotopes* **172**, 109675 (2021).

[37] The European Pharmacopoeia Commission. European pharmacopoeia 10.0: Gallium (^{68}Ga) chloride solution for radiolabelling. 1206–1208 (2019).

[38] International Atomic Energy Agency. Quality control in the production of radiopharmaceuticals. (2018).

[39] Vadasdi, G. K. The extraction of gallium with cupferron. *Analytica Chimica Acta* **44**, 469–471 (1969).

[40] Dhond, P. V. & Khopkar, S. M. Solvent extraction of gallium(iii) with 2-thenoyltrifluoroacetone. *Talanta* **23**, 51–53 (1976).

[41] Bhattacharya, B., Mandal, D. & Mukherjee, S. Liquid-liquid extraction of gallium(iii) with LIX 26. *Separation Science and Technology* **38(6)**, 1417–1427 (2007).

[42] Inoue, K., Baba, Y. & Yoshizuka, K. Solvent extraction equilibria of gallium(iii) with acidic organophosphorus compounds from aqueous nitrate media. *Solvent Extraction and Ion Exchange* **6**, 381–392 (1988).

[43] Lee, M., Ahn, J. & Lee, E. Solvent extraction separation of indium and gallium from sulphate solutions using D2EHPA. *Hydrometallurgy* **63**, 269–276 (2002).

[44] De, A. & Asit, K. Solvent extraction and separation of gallium(iii), indium(iii), and thallium (iii) with tributylphosphate. *Talanta* **14**, 629–635 (1967).

[45] Ahmed, I. M., El-Nadi, Y. A. & El-Hefny, N. E. Extraction of gallium(iii) from hydrochloric acid by cyanex 923 and cyanex 925. *Hydrometallurgy* **131-132**, 24–28 (2013).

[46] Song, S. J., Le, M. N. & Lee, M. S. Separation of gallium(iii) and indium(iii) by solvent extraction with ionic liquids from hydrochloric acid solution. *Processes* **8**, 1–14 (2020).

[47] Katsuta, S., Okai, M., Yoshimoto, Y. & Kudo, Y. Extraction of gallium(iii) f rom hydrochloric acid solutions by trioctylammonium-based mixed ionic liquids. *Analytical Sciences* **28**, 1009–1012 (2012).

[48] Maljkovic, D., Maljkovic, D. & Paulin, A. Extraction of gallium(iii) from hydrochloric acid by diiopropyl ether and mixture diisopropyl ether-pentanol. *Solvent Extraction and Ion Exchange* **8**, 659–668 (1990).

[49] Verweij, W. CHEAQS next (0.2.1.8).

[50] Qi, D. Extractants used in solvent extraction-separation of rare earths: Extraction mechanism, properties, and features. *Hydrometallurgy of Rare Earths* 187–389 (2018).

Supplementory Information

A membrane used in the present study (hydrophobic PTFE membranes with a poresize of 0.45 µm) was irradiated in Co-60 chamber with a total dose of 1 MGy, while submerged in water. Afterwards, the membrane was imaged with a SEM JSM-IT100. It was observed that the PTFE-based membrane becomes brittle during irradiation . Subsequently, the fibers of the membrane can break, as can be seen in Fig 2.6. This will ultimately lead to a failure of the membrane, making the membranes unsuitable for highly radioactive substances.

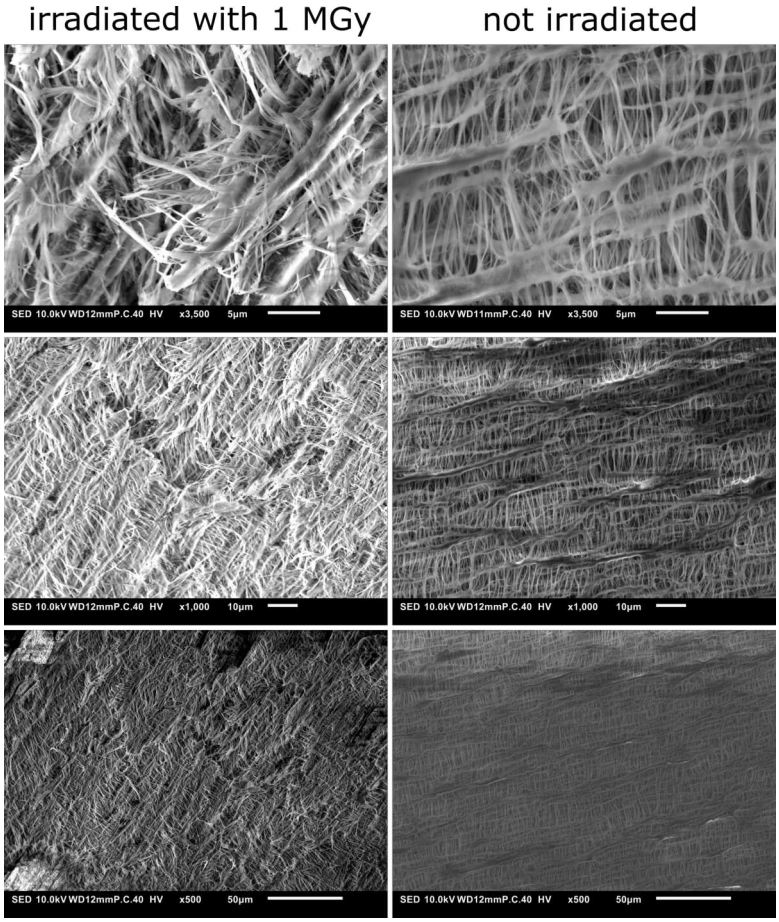

Figure 2.6: SEM images of irradiated (left) and non-irradiated membrane (right). The radiation dose by Co-60 was 1 MGy. This caused the PTFE of the membranes to become brittle, resulting in the breakage of the fibers as can be seen in the left images, ultimately leading to a failure of the membrane.

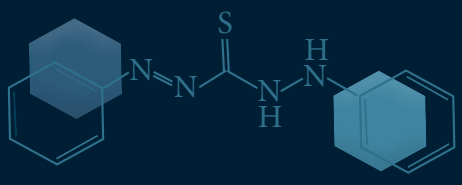

3

Microfluidic solvent extraction of Cu radionuclides from Zn

3

Microfluidic solvent extraction of Cu radionuclides from Zn

Several Cu isotopes can be used in nuclear medicine, such as Cu-61, Cu-64 and Cu-67. Production of these isotopes is mostly done by irradiation of Zn targets in both nuclear reactors and accelerators. Given the generally short half-lives and high activities associated with radionuclide production, fast, automatable separation strategies are warranted. While current separation methods are mainly based ion exchange chromatography, this chapter studies the solvent extraction of Cu-64 from $Zn(NO_3)_2$ in dilute HNO_3 solutions and explores the use of a commercial YY-junction glass microfluidic chip. Several extracting agents were compared for their efficiency and selectivity to extract Cu. In conventional batch extraction, using dithizone as the extracting agent, efficiencies of up to 97% ± 3% for Cu were achieved within 1 minute of contact time. Microfluidic solvent extraction achieved up to 62 % within a contact time of 15 seconds. However, perfect separation could not be achieved with the applied commercial glass microfluidic chip.

Parts of this chapter have been published in: Trapp S, Lammers T, Paulssen E, de Kruijf R. Rapid, automated radionuclide separation with high yield—towards microfluidic solvent extraction for Cu-61,64,67 production. In: European research reactor conference 2023 proceedings. Antwerp; 2023. p. 177–84

3.1. Introduction

Nuclear medicine is seeing a large increase in the development of novel radiopharmaceuticals, following the success of, amongst other, ^{177}Lu-based therapeutic agents for the treatment of a variety of metastasized tumours including neuroendocrine and prostate cancer [1, 2]. Many new beta- and gamma-emitters are currently being investigated as candidates for the development of novel radiotheranostics. So-called 'matched pairs' of radioisotopes, which consist of diagnostic as well as therapeutic radionuclides of the same element, provide an attractive alternative to currently used radioisotopes. Cu radioisotopes represent one of these emerging matched pairs of radionuclides, with two positron-emitting diagnostic isotopes, Cu-61 and Cu-64, and the therapeutic Cu-67. Of these, Cu-64 ($t_{1/2}$=12.7 h) is already well-established in the clinic [3], and the shorter half-life of Cu-61 ($t_{1/2}$=3.33 h) makes it a suitable substitute to Ga-68 [4]. The therapeutic Cu-67 is a beta-emitter with a 2.6 day half-life, and although its low availability has limited research into Cu-67 based therapeutic agents in the past, recent commercial availability is expected to lead to rapid development of new Cu-67-based radiopharmaceuticals [5]. Possible production pathways for high specific activity Cu-64 include neutron irradiation of enriched Zn-64 targets or charged particle irradiation of enriched Zn or Ni targets [6], including both solid and liquid target approaches. Cu-61 can be produced from enriched Zn, Co or Ni targets following cyclotron irradiation [4]. Finally, Cu-67 can be produced in a nuclear reactor using enriched Zn-67 targets, from enriched Zn or Ni targets using charged particle induced reactions or following photonuclear activation of enriched Zn-68 targets [7]. Commonly, the produced Cu radionuclide is then purified from the bulk target material using a series of ion exchange resins, although approaches using solvent extraction or sublimation-based separation [8] have also been reported [6, 7, 9]. However, these approaches suffer from several drawbacks, including relatively long processing times (> 1h to > 1 day [8]) and inherent difficulties concerning automation of the extraction procedures in hot cells. Given the relatively short half-lives of the Cu isotopes of interest, fast separation strategies are required to prevent unnecessary loss of activity. In this study, a fast separation technique was developed based on liquid-liquid extraction, which is capable of selective isolation of Cu from bulk Zn target materials.

3.2. Methods and Materials

Zinc nitrate hexahydrate ($Zn(NO_3)_2{\cdot}6H_2O$) and copper nitrate ($Cu(NO_3)_2{\cdot}6H_2O$) were purchased from ACROS ORGANICS (VWR, Amsterdam, the Netherlands). Nitric acid (HNO_3), hydrochloric acid (HCl), chloroform, acetylacetone (AA), tri-n-butyl phosphate (TBP) and salicylaldoxime (SA) were purchased from Sigma Aldrich (Merck Sigma, Zwijndrecht, the Netherlands). Dithizone, thenoyltrifluoroacetone (TTFA) and di-(2-ethylhexyl)phosphoric acid (D2EHPA) were purchased from VWR International BV (Amster-

Figure 3.1: Microfluidic setup used for the experiments. a) A aqueous syringe pump, B organic syringe pump, C aqueous syringe, D: organic syringe, E microscope, F microfluidic device, G collection vials. b) A aqueous inlet, B organic inlet, C aqueous outlet, D organic outlet, E microfluidic chip, F aluminium hull.

dam, the Netherlands). LIX984N was generously supplied by BASF (Ludwigshafen, Germany).

Batch experiments were executed by adding equal amounts of aqueous and organic phases to Eppendorf vials, vortexing the solution (Vortex Genie 2 from Scientific Industries) and separating the two phases afterwards by pipetting. Unless stated otherwise, these experiments have been carried out with a 1 M HNO_3 solution containing 1 M $Zn(NO_3)_2$ and 0.1 M $Cu(NO_3)_2$, and an organic solution containing 0.2 M chelating agent in chloroform. Microfluidic experiments were performed by connecting two syringes containing the aqueous and organic solution, respectively, to the microfluidic chip via PEEK tubing (0.5 mm o.d. 0.26 mm i.d.) (see Fig. 3.1 for set-up). The microfluidic glass chip was purchased from the Institute of Microchemical Technologies Co. (IMT), and contained a YY junction microchannel, with 46 μm x 160 μm x 12 cm dimensions, a 6 μm guide, and a Y splitter (ICC-DY15G) on a chip holder (ICH-01K). Programmable syringe pumps (AL-1000 from World Precision Instruments Inc.) were used to deliver the solutions from the syringes to the microfluidic chip with a constant flow. An inverted microscope at 250 times magnification was employed for observing the flow behaviour of solutions in the microchannel. 13 mm syringe filters with 0.2 μm PTFE membrane (VWR International BV, Amsterdam, the Netherlands) were used to filter the solutions before introducing them to the microchannel to avoid clogging. In microfluidic experiments, the aqueous flow rate was fixed to 10 μL/min and only the organic flow rate was varied

to assess the effect of the (aqueous) residence time on the extraction behaviour. The aqueous phase consisted of a 1 M HNO_3 solution containing 3.9 M $Zn(NO_3)_2$ and 1 mM $Cu(NO_3)_2$ and the organic phase was 10 mM dithizone in chloroform or pure LIX984N. Metal concentrations in the initial and final solutions for batch and microfluidic experiments were measured with an ICP-OES Optima 8000 from Perkin Elmer (Groningen, The Netherlands). The extraction efficiencies (EE(%)) of Cu shown in study were calculated according to:

$$EE(\%) = \frac{[Cu]_{\text{aq,initial}} - [Cu]_{\text{aq,final}}}{[Cu]_{\text{aq,initial}}} * 100\% \tag{3.1}$$

where $[Cu]_{\text{aq,initial}}$ and $[Cu]_{\text{aq,final}}$ represent the concentration of Cu ions in the initial aqueous HNO_3 solution, and the aqueous solution after solvent extraction, respectively. All experiments were performed in triplicate, and reported errors represent one standard deviation of the mean.

3.3. Results and discussion

3.3.1. Batch extractions

First, seven different extraction agents were screened on their suitability for the selective extraction of Cu from Zn solutions (Fig. 3.2). Unless stated otherwise, these experiments have been carried out with a 1 M $Zn(NO_3)_2$, 0.1 M $Cu(NO_3)_2$ solution in different dilute HNO_3 concentrations and 0.2 M chelating agent in the organic solution. Large differences were observed in the ability of the different extraction agents to extract Cu, with the chelators AA, D2EHPA and TBP failing to extract Cu at all pH levels. On the other hand, dithizone, LIX984N, SA and TTFA did extract Cu, with dithizone extracting up to 97 ± 3 % at pH 0. Three of the chelators, LIX984N, SA and TTFA showed an increasing Cu EE(%) for increasing pH. This can be explained by the abundance of H^+ ions in the solutions, hindering the complex formation of Cu with the extracting agents at decreasing pHs and subsequently lead to lower EE(%). This phenomenon has been typically observed in the literature [10–12].

Dithizone on the other hand displayed a decreasing Cu EE(%) with increasing pH (Fig. 3.2). Increasing Zn co-extraction with increasing pH for dithizone extractions might explain the decrease of EE(%) for Cu, however, due to large uncertainties in the results of the Zn co-extraction, no clear conclusions can be drawn. These occurred due to the fact that highly concentrated solutions were measured by ICP-OES, which necessitate strong dilution, inevitably leading to high uncertainties, and could be mitigated in future work using radiotracers. Generally, relatively low Zn co-extraction was observed for all extraction agents except for SA (Fig. 3.2). After assessing the feasibility of the different extracting agents for the selective extraction of Cu from Zn target solutions, dithizone and LIX984N were selected as the most promising candidates. Next, the concentrations of

Figure 3.2: EE % of non-radioactive Cu (top) and Zn (bottom) for various chelating agents and pH values with 1 min vortexing time. All extractions were carried out with a 1 M HNO_3 solution containing 1 M $Zn(NO_3)_2$ and 0.1 M $Cu(NO_3)_2$, and 0.2 M chelating agent in chloroform as organic phase, except for dithizone and SA. These were carried out with an aqueous solution containing 0.1 M $Zn(NO_3)_2$ and 0.01 M $Cu(NO_3)_2$, and 0.02 M chelating agent in chloroform as the organic phase. Reported uncertainties represent one standard deviation of the mean (n=3).

the selected extracting agents were optimized, as shown in Figs. 3.3 and 3.4 for dithizone and LIX984N, respectively. In the subsequent experiments, the $Zn(NO_3)_2$ concentration in the aqueous solutions was increased to 3.9 M to better represent possible future target solutions [4]. It can be concluded that increasing the concentration of the extracting agent has a significant impact on the effectiveness of the extractions, where higher concentrations lead to higher EE(%) for both extracting agents. An EE(%) of 90.3 ± 1.1 % was achieved for Cu extraction using 10 mM dithizone and 1 min vortexing time. Further increasing the dithizone concentration did not significantly increase the EE(%). Highest EE(%) for LIX984N were observed when left undiluted (160 mM), achieving a maximum of 93.4 ± 0.5 % within 1 min of vortexing time. These concentrations were therefore used in the following microfluidic experiments.

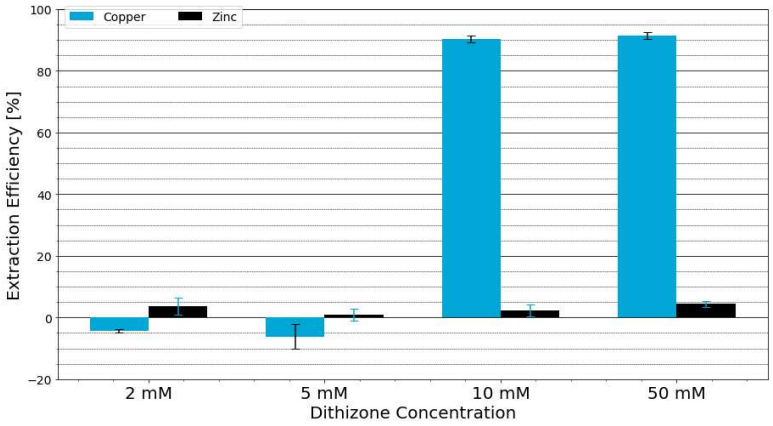

Figure 3.3: EE(%) of Cu and Zn for various dithizone concentrations and 1 min vortexing time. All extractions were carried out with a 1 M HNO_3 solution containing 3.9 M $Zn(NO_3)_2$ and 1 mM $Cu(NO_3)_2$ and. Dithizone was dissolved in chloroform. Reported uncertainties represent one standard deviation of the mean (n=3).

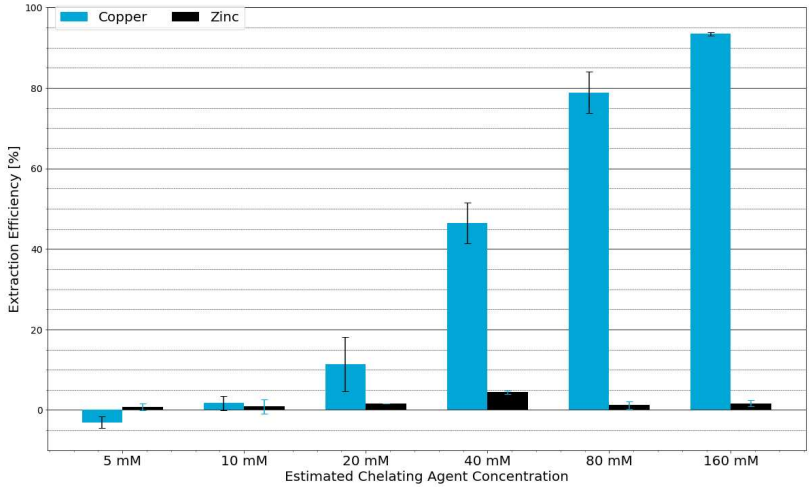

Figure 3.4: EE(%) of Cu and Zn for various LIX984N concentrations and 1 min vortexing time. All extractions were carried out with a 1 M HNO_3 solution containing 3.9 M $Zn(NO_3)_2$ and 1 mM $Cu(NO_3)_2$. LIX984N was diluted with chloroform. 160 mM corresponds to pure LIX984N. Reported uncertainties represent one standard deviation of the mean (n=3).

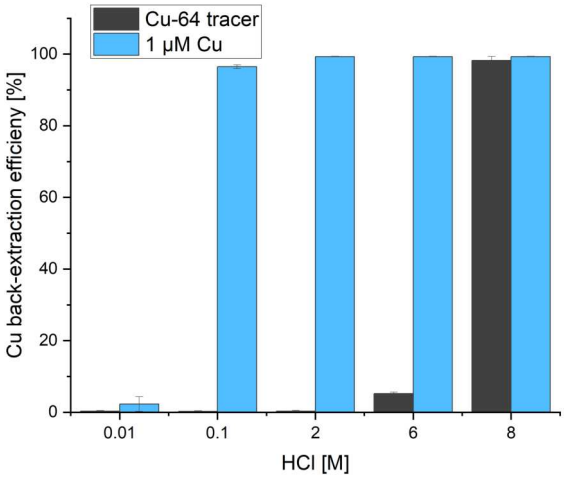

Figure 3.5: BEE(%) of Cu-64 at trace levels and 1 µM Cu into differnt HCl concentrations with 10 min vortex time. Reported uncertainties represent one standard deviation of the mean (n=3).

3.3.2. Microfluidic extractions

After establishing optimal extraction conditions in the batch approach, microfluidic extractions were performed in a YY-junction microfluidic chip. First, a stable, stratified flow had to be established. As reported in the literature [13], this YY-junction chip consistently fails to achieve a perfect phase separation. Depending on the flow rate ratios either aqueous, organic, or even simultaneous leakage was observed, as shown in Fig. 3.6 for both dithizone and LIX984N. The flow rates used were 9.1, 4.6, 2.3 and 1.5 μL/min, which corresponds to residence times of 2.5, 5.0, 10 and 15 s, respectively. To minimize the leakage, the ratio of organic vs aqueous flow rates was 5.2:1 for dithizone, and 1.7:1 for LIX984N due to its higher viscosity (see Fig. 3.7 for aqueous leakage in microfluidic chip).

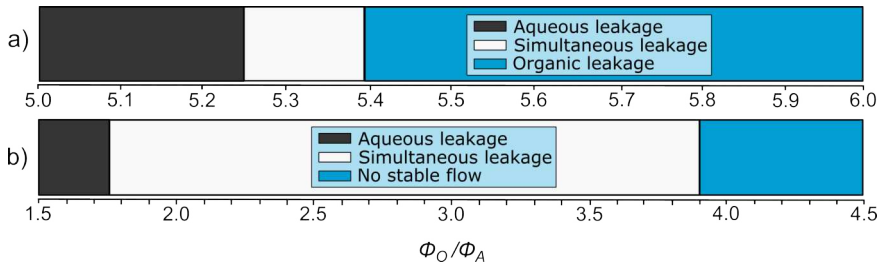

Figure 3.6: Outlet stability at the outlet Y-junction of the microfluidic chip with stratified flow. Aqueous phase is a 1 M HNO_3 solution containing 3.9 M $Zn(NO_3)_2$ and 1 mM $Cu(NO_3)_2$ and the organic phase is a) 10 mM dithizone in chloroform and b) pure LIX984N. Flow rate of the aqueous phase was set at 10 μL/min. The axis shows the flow rate ratio, which is the organic flow rate Φ_O divided by the aqueous flow rate Φ_A.

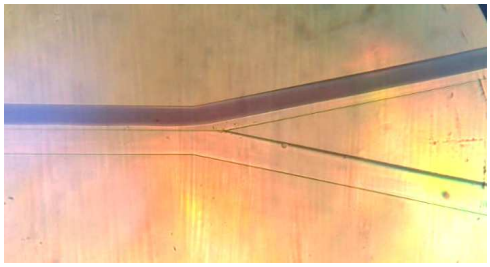

Figure 3.7: Aqueous leakage at the outlet of the microfluidic chip. Top phase is the organic phase bottom phase is the aqueous solution.

Both LIX984N and dithizone only achieved between 40 - 50 % EE(%) within the longest possible contact time of 15 seconds. Additionally, because these parallel flow microfluidic chips are currently not able to achieve perfect phase separation [13], the results presented in Fig. 3.8 should be regarded as a proof-of-principle, for final application further chip optimization will be required. Furthermore, while it might be implicitly assumed that the Cu concentration in the aqueous phase is uniform, this is not expected to be the case in these microfluidic chips. Solvent extraction in laminar flow leads to a concentration gradient within the aqueous phase due to the extraction at the interface. Therefore, it is expected that the Cu concentration in the aqueous phase is lowest at the interface. This means that under the presented operating conditions, with minimal aqueous leakage, the aqueous part with the lowest Cu concentration is leaking. Since only the aque-

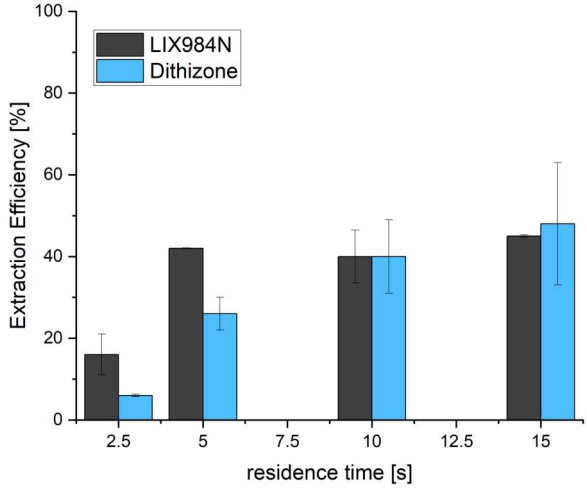

Figure 3.8: EE(%) of Cu in the microfluidic device for dithizone and LIX984N. The aqueous phase is a 1 M HNO_3 solution containing 3.9 M $Zn(NO_3)_2$ and 1 mM $Cu(NO_3)_2$, and the organic phase is pure LIX984N (grey) or 10 mM dithizone in chloroform (blue). Reported uncertainties represent one standard deviation of the mean (n=3).

ous phase is analyzed, the results might slightly underestimate the real EE(%). This underestimation of the EE(%) is expected to be more pronounced for extractions with the LIX984N solution in flow, as there was a slight aqueous flow observed surrounding the organic solution, thus increasing the amount of aqueous leakage in the organic outlet channel. This can be explained by the fact that LIX984N works as a surfactant, changing the contact angle between the aqueous and organic solution, leaving the aqueous solution preferred in contact to the glass. Furthermore, a much lower EE(%) of Cu was found using the microfluidic chips, plateauing out at approximately 40 % (Fig. 3.8), compared to the batch experiments (with EE(%) up to 90 ± 5 %). Longer contact times would be needed to further increase the EE(%) in flow, which the microfluidic setup in this study did not allow for. A different type of microfluidic chip that allows for longer contact times and perfect phase separation, preventing both aqueous and organic leakage, would need to be developed to fully characterize this system and allowing for its implementation for radionuclide separation.

3.4. Conclusion

The presented study focused on the development of a solvent extraction system to separate Cu from Zn targets, suitable for automation the separation using microfluidic solvent extraction. Extraction efficiencies up to 97 ± 3 % and 90 ± 5 % for dithizone and LIX984N, respectively, were found within 1 min contact time in batch experiments. While dithizone and LIX984N were both still able to extract Cu from Zn solutions in flow, observed EE(%) were significantly lower than the batch extractions, only reaching around 45%. Longer contact times are needed to increase the EE(%) in flow. Unfortunately, the experimental setup did not allow for further optimization of the EE(%), as the chip geometry could not achieve longer contact times. However, the batch experiments leave us confident that EE(%) exceeding 90% can be obtained with longer microfluidic chips. Future work, therefore, includes optimizing the chip geometry such that longer contact times and a perfect phase separation can be realized. Overall, this study presents very promising first steps, that when optimized will pose an interesting alternative to traditional column separation, allowing for a continuous radionuclide production.

References

[1] Sartor, O. *et al.* Lutetium-177–PSMA-617 for metastatic castration-resistant prostate cancer. *New England Journal of Medicine* **385**, 1091–1103 (2021).

[2] Mittra, E. S. Neuroendocrine tumor therapy: ^{177}Lu-DOTATATE. *American Journal of Roentgenology* **211**, 278–285 (2018).

[3] Anderson, C. J. & Ferdani, R. Copper-64 radiopharmaceuticals for PET imaging

of cancer: Advances in preclinical and clinical research. *Cancer Biotherapy and Radiopharmaceuticals* **24**, 379–393 (2009).

[4] Fonseca, A. I. *et al.* Production of GMP-compliant clinical amounts of copper-61 radiopharmaceuticals from liquid targets. *Pharmaceuticals* **15** (2022).

[5] Isotopes. Routine production of high specific activity Cu-67! *https://www.isotopes.gov/node/443,* updated November 25, 2019; accessed February 23, 2023.

[6] *Copper-64 Radiopharmaceuticals: Production, Quality Control and Clinical Applications, in: Radioisotopes and Radiopharmaceuticals Series.* 7 (International Atomic Energy Agency, Vienna, 2022).

[7] Mou, L. *et al.* ^{67}Cu production capabilities: A mini review. *Molecules* **27** (2022).

[8] Merrick, M. J. *et al.* Imaging and dosimetric characteristics of Cu-67. *Physics in Medicine and Biology* **66**, 035002 (2021).

[9] Sen, N., Chakravarty, R., Singh, K., Chakraborty, S. & Shenoy, K. Selective separation of Cu from large excess of zn using a microfluidic platform. *Chemical Engineering and Processing - Process Intensification* **159**, 108215 (2021).

[10] Harris, D. *Quantitative Chemical Analysis, 9th ed.* (W.H. Freeman and Company: New York, 2016).

[11] Minczewski, J., Chwastowska, J. & Dybczynski, R. *Separation and Preconcentration Methods in: Inorganic Trace Analysis, 1st ed.* (Ellis Horwood Limited: Chichester, UK, 1982).

[12] Sinha, M., Sahu, S., Meshram, P., Pandey, B. & Kumar, V. Solvent extraction and separation of copper and zinc from a pickling solution. *International Journal of Metallurgical Engineering* **1**, 28–34 (2012).

[13] Dalamzio, I. & Oehlke, P. Cylohexanona microfluidic extraction of radioactive perrhenate from acid solutions. *International Nuclear Atlantic Conference - INAC 2017, Belo Horizonte, MG, Brazil* (October 22-27, 2017).

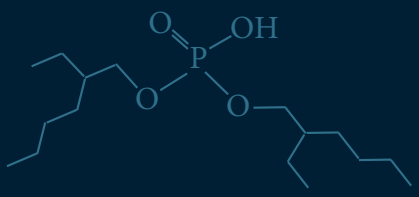

4

Solvent extraction of Ac-225 in nano-layer coated PDMS microfluidics

4

Solvent extraction of Ac-225 in nano-layer coated PDMS microfluidics

.

With the rise of polydimethylsiloxane (PDMS) microfluidic chips, solvent extraction processes can take place in a simple and reproducible chip platform continuously and automatically. Furthermore, the microfluidic chips can be coated with metal-oxide nanolayers, increasing their resistance against the employed organic solvents. Such chips were fabricated and demonstrated a parallel flow at a considerably large range of flow rates using the aqueous and organic solutions commonly used in medical radionuclide extraction. In the following case study for the separation of Ac-225 from radium with the chelator di(2-ethylhexyl)phosphoric acid (D2EHPA), a remarkable extraction efficiency of 97.1 % ± 1.5 % was reached within 1.8 seconds of contact time, while maintaining a near perfect phase separation of the aqueous and organic solutions. This method will enable the automation of solvent extraction and faster target recycling, and serves, therefore, as a proof-of-concept for the applicability of microfluidic chip solvent extraction of (medical) radionuclides.

Parts of this chapter have been published in: Trapp, S., Santoso, A., Hounat, Y., Paulssen, E., van Ommen, J.R., van Steijn, V., de Kruijff, R., (2024) Solvent extraction of Ac-225 in nano-layer coated, solvent resistant PDMS microfluidics. *Scientific Reports* **14**, 29988. https://doi.org/10.1038/s41598-024-81177-5

4.1. Introduction

In nuclear medicine, radionuclides are utilized for imaging and treatment of various diseases [1]. Despite numerous existing potential radionuclides, only a handful reach clinical use, partly due to their limited availability [2, 3]. Increasing the global supply requires a production system that is not only fast and efficient, but also continuous and automatable, incorporating the necessary steps to separate the produced radionuclide from its initial target material [2, 4]. Solvent extraction, among other methods, offers a simple, selective, and efficient means of separation [5]. By bringing an aqueous solution that contains the product radionuclide as well as its target material in contact with an immiscible organic solution that contains a chelator, the chelator selectively binds to the product radionuclide [5, 6]. As a result, the product radionuclide gets extracted into the organic solution, while the valuable target material stays in the aqueous solution, potentially ready to be recycled. To prepare the product radionuclide for further use, it needs to be transferred to a fresh aqueous solution, which is possible through a simple second (back-) extraction step. Microfluidic devices offer precise control over two-phase flows and their interfaces, enabling the design of a continuous and potentially automatable extraction system [7–12]. With short diffusion paths, these devices consistently achieve high extraction efficiencies for many radionuclides [9].

Polydimethylsiloxane (PDMS), among the most used materials for microfluidic devices stands out as it (1) allows rapid prototyping through a simple molding technique [13], (2) has a high radiation resistance as opposed to commercial membranes used for radionuclide separation [14], and (3) resists solution with extreme pH used in the (back-) extraction step for the separation of medical radionuclides [15–17]. Furthermore, PDMS has also been used in medical industries, easily complying with regulatory demands [15]. The only downside is that it swells and deforms when it comes in contact with organic solutions commonly used for extraction [18]. To overcome this issue, direct contact between the organic solution and the PDMS microfluidic chip must be prevented. Recently, a simple approach was developed to coat the channels of PDMS chips with metal oxide nano-layers using atomic layer deposition (ALD) [17]. These nano-layers are grown by alternatingly flowing the two gaseous ALD reactants through the chips, a metal precursor and an oxidizing agent, with a purge of inert gas in between. The number of repeats allows high control over the layer thickness and its properties due to the self-limiting nature of the ALD reactions [19]. This invention now opens the door to develop a PDMS-based microfluidic system for radionuclide solvent extraction.

In this chapter, a PDMS-based microfluidic radionuclide extraction system is presented, in which the PDMS is rendered inert against the use of organic solutions through a silicon oxide nano-layer deposited by means of ALD. Besides the nano-layer, a second important feature of the microfluidic chip is the difference in height between the channels for the organic phase containing the chelator and the aqueous phase containing the

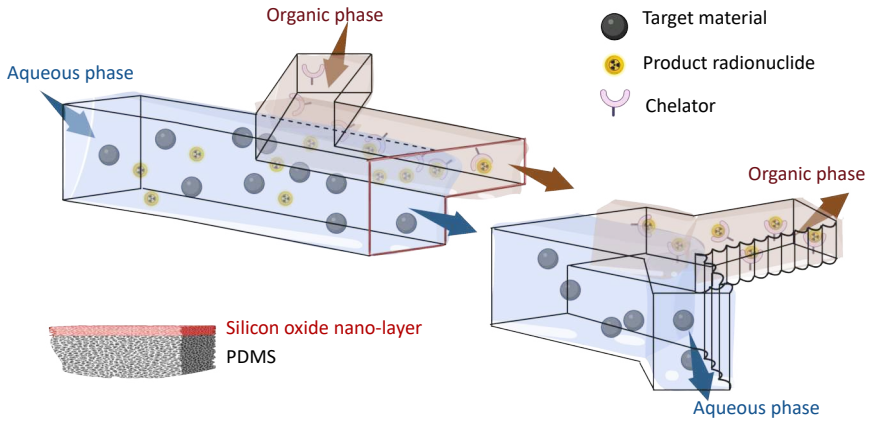

Figure 4.1: Illustration of continuous two-phase liquid-liquid extraction of radionuclides in a PDMS-based microfluidic chip, with the product radionuclide and its target supplied in the aqueous phase and the chelator in the organic phase. The silicon oxide nano-layer coated on the walls using atomic layer deposition renders the wall inert against the organic phase. The difference in height between the side where aqueous phase and the organic phase flow ensures pinning of the interface, ensuring stable parallel flow. The wavy wall near the exit pins the interface as well, ensuring perfect phase separation.

product radionuclide and its target material (see Fig. 4.1). The height difference ensures pinning of the interface [20], securing stable parallel flow, even at the lowest flow rates. A third important feature is the wavy-wall near the exit, securing that the interface remains pinned, achieving perfect phase separation. As a proof of concept, a case study was done for the separation of Ac-225 from radium, using di-2-ethylhexylphosphoric acid (D2EHPA) as the chelator, after initial experiments on the separation of La-140 from barium as substitutes. Ac-225 is a medical radionuclide, currently researched for targeted alpha therapy, showing very promising clinical results [21–23]. However, so far, the global supply of Ac-225 is severely limited and does not meet the predicted clinical demand [3]. Therefore, many efforts are made to produce Ac-225 via a plethora of different production routes [24], including the irradiation of Ra-226 [3, 25–27]. The presented case study showcases a fast, continuous, and efficient process using microfluidic solvent extraction, with the potential for establishing an automated purification system for medical radionuclides.

4.2. Methods and Materials

4.2.1. Microfluidic device

Working principle of the microfluidic device design

Two key requirements for continuous two-phase flow extraction are that the two phases (1) flow stably side by side through the main channel, without breaking up into slugs,

and (2) leave the device separately via the two dedicated outlet channels. To accommodate these requirements, the geometry often used in solvent extraction was adapted [5], namely a simple straight channel (500 μm wide and 11.6 mm long in our work) with a Y-junction for the introduction of the two phases and another Y-junction for their exit. Two important geometries were added to pin the interface throughout the device: a vertical guiding structure in the form of a step height [20, 28] and a lateral guiding structure in the form of a wavy wall at the outlet junction (see Fig. 4.1). The position of the step height in the main channel is determined by the estimated interface position of the two fluids. Assuming two-dimensional flow and considering continuity of velocity and shear stress, the interface position is a function of the viscosity ratio and the flow rate ratio [29–31]. In this study, the viscosities of the fluids used for the radionuclide separations are of a comparable order of magnitude. Additionally, extraction is done at comparable flow rates. Therefore, the step height is placed in the middle of the main channel to account for most of the used operating conditions. The channel for the aqueous phase was 100 μm deep, while the channel for the organic phase was 50 μm deep. This difference was based on preliminary experiments, in which it was found that this step height was enough to guide the two phases without compromising the contact area too much.

Ideally, pinning of the interface near the outlet occurs at the outlet junction point. In case of unpinning, the wavy wall at the end provides a new pinning point, similar to the pinning in pillar-based or array-based microfluidic devices [32, 33]. This wavy wall comprises of half-circles (diameter of 5 μm) pattern starting from the outlet junction point and extends for 1 cm into each outlet channel. The joining points between two half-circles facilitate the new pinning of the interface, lowering the risk of phase contamination from one side of the channel to the other.

Microfluidic device fabrication

The microfluidic devices were fabricated using soft lithography [34]. In short, a 4-inch silicon wafer was spin-coated at 2000 rpm for 30 seconds with a negative photoresist (SU8-2050, Kayaku Advanced Materials, Inc.) and soft-baked at 100°C for 15 minutes. The thickness of this first layer of photoresist was 50 μm as determined by a profilometer (DektakXT 2, Bruker, Billerica, US). Instead of transferring the two-dimensional channel design to the coated wafer by exposing it through a patterned mask as commonly done in soft lithography, the design made in AutoCAD 2023 (Autodesk) was directly written on the coated wafer with a tabletop LaserWriter (μmLA, Heidelberg Instruments, Germany; raster scan with 1 μm laser beam at 365 nm), using an exposure dose of 300 mJ/cm^2. The patterned wafer was then post-exposure-baked at 100°C for 5 minutes. To obtain the step height, a second 50 μm thick layer of SU8-2050 photoresist was spin-coated on top of the post-exposure-baked wafer. After aligning the design of the second layer to the design of the first layer using the embedded inspection camera of the LaserWriter, the second layer was written. The wafer was then post-exposure-baked at 100°C for

5 minutes. After this second post-exposure-bake, the fully patterned wafer was developed using propylene glycol monomethyl ether acetate (Sigma-Aldrich, 99.5 %), washed with isopropyl alcohol (Sigma-Aldrich, 70 %), and hard-baked at 200°C for 20 minutes. Before its first use, the patterned wafer was silanized by exposing it to 1H,1H,2H,2H-perfluorooctyltrichlorosilane (Sigma-Aldrich, 95 %) vapour in a vacuum desiccator for one hour to prevent polydimethylsiloxane (PDMS) from sticking to the wafer.

The microfluidic devices were made from PDMS. They were prepared by mixing polymer elastomer and curing agent (Sylgard 184 Elastomer Kit, Dow Corning Comp.) in a mass ratio of 5:1. After degassing the mixture in a vacuum desiccator, it was poured over the patterned wafer in a glass 5-inch Petri dish and cured at 150°C for at least 2 hours [17]. The cured PDMS was then gently removed from the patterned wafer and cut to size. The inlets and outlets were subsequently punched using a 1.5 mm biopsy puncher. The chips were cleaned with ethanol (Sigma-Aldrich, 70 %) and dried using compressed air, before being bonded on a glass slide spin-coated with a 20 µm thick layer of PDMS (2000 rpm for 2 minutes, Laurell WS-650Mz-23NPPB) after oxygen plasma treatment for 140 seconds at 0.2-0.4 mbar (Harrick, PDC-002). The microfluidic devices were stored at 70°C for at least 12 hours before further modification to allow the PDMS to recover to its hydrophobic state.

Atmospheric pressure atomic layer deposition in microfluidic devices

To coat a thin layer of silicon oxide on the inner walls of the microfluidic channels in order to render the walls inert against the solvents used in the extraction experiments, a home-built atomic layer deposition setup was used [17, 35, 36]. In-channel growth of a layer of silicon oxide was achieved by sequentially flowing gas phase ALD precursors through the microchannels as described in our recent work [37]. In short, silicon tetrachloride (Alfa Aesar) was used as the metal precursor, while ozonated air (Sander Certizon) combined with deionized water was used as the oxygen precursor. A gas flow rate of 0.2 L/min was used, with the metal precursor flowing for 10 seconds and the oxygen precursor for 30 seconds, with nitrogen purges for 100 seconds in between. Each microfluidic channel was coated with 25 of such ALD cycles (i.e., the described sequence was repeated 25 times), carried out at 60°C.

Stability of parallel two-phase flow in bare and ALD-treated PDMS microfluidic devices

The stability of the two-phase flow was studied over a wide range of flow rates (0.1-150 µL/min) of the aqueous and organic solutions. As model liquids, a 1 M nitric acid (HNO_3, 65 %, Merck Sigma) solution was used as the aqueous phase and chloroform ($CHCl_3$, Merck Sigma) as the organic phase. The viscosity of 1 M HNO_3 at 20°C is estimated to be 0.99 mPa.s (measured using a VWR falling ball viscometer, comparable with reported values in the literature[38]). The viscosity of chloroform at 20°C as provided by

the supplier is 0.57 mPa.s. To estimate the interfacial tension between 1 M HNO_3 and chloroform, pendant drop tensiometry (Kruss easydrop) was conducted by forming a 10 µL chloroform droplet (Worthington number was ~1[39]) in a cuvette filled with 1 M HNO_3. Using the Young-Laplace equation, the interfacial tension was calculated to be 31.6 mN/m, comparable to reported values in the literature [40].

The liquids were loaded in separate 5 mL syringes (Beckton-Dickinson, Discardit II) with a plastic plunger. The syringes were connected to the inlets of the microfluidic device with polytetrafluorethylene (PTFE) tubing (outer diameter 1.6 mm, inner diameter 0.5 mm, length 300 mm, Diba, 008T16-050-200) and the liquids were driven into the device using individual syringe pumps (Harvard Apparatus Pump 11 Pico Elite Plus). The aqueous phase was injected at the inlet leading to the deeper part of the main channel, while the organic phase was injected at the inlet leading to the shallower part. Snapshots of the flow were taken using a camera (ImagingSource DFK33UX273) through an LWD plan phase 10X lens on a microscope (Euromex Oxion Inverso PLPH).

To rationalize the flow stability experiments, the outcome was compared against an available simple theoretical model [41]. In short, the transition between stable and unstable parallel flow is expected when the difference in organic and aqueous phase pressure drop over the length of the main channel due to viscous flow exceeds the difference in organic and aqueous phase pressure due to interfacial forces, known as the Laplace pressure jump. At the onset of this transition, small perturbations in the flow, for example due to the step motor of a syringe pump [42–44] lead to unpinning of the interface at the step height. The Laplace pressure jump ($\Delta P_{Laplace}$) can be estimated using the following expression [28]

$$\Delta P_{Laplace} = \frac{2\gamma \sin(\theta - 90^\circ)}{d}, \tag{4.1}$$

where γ represents the interfacial tension between two liquids, θ represents the solid-liquid-liquid contact angle, and d represents the height between the ceiling of the main channel and the step (i.e., 50 µm in our work). A simple estimate of the pressure drop over the channel (ΔP_F) in both the aqueous and the organic phase is obtained through the pressure drop of a single phase flow in a rectangular channel [28, 30, 45], i.e.,

$$\Delta P_F = \frac{12 Q \eta L}{\left(1 - 0.630 \frac{d}{w}\right) d^3 w}, \tag{4.2}$$

where Q represents the flow rate of the considered phase, η represents the dynamic viscosity of the considered phase, L represents the length of the main channel, and d and w represent the height and width of considered phase (approximated as 100 µm × 250 µm for the aqueous phase and 50 µm × 250 µm for the organic phase. The transitions between stable and unstable parallel flow is estimated as

$$\left|\Delta P_{F,aqueous} - \Delta P_{F,organic}\right| = \Delta P_{Laplace}. \tag{4.3}$$

4.2.2. Radionuclide separation experiments

Radiotracer production and radioactivity measurements

Initial experiments were focused on the separation of La-140 from $Ba(NO_3)_2$ in Milli-Q. The radiotracers Ba-139 and La-140 were produced by neutron irradiation of BaO and La_2O_3 (Merck Sigma), respectively, at the Hoge Onderwijs Reactor (HOR) of the TU Delft Reactor Institute (the Netherlands) with a thermal neutron flux of $4.69 \cdot 10^{16}$ $s^{-1}m^{-2}$ for 3 hours. They were subsequently dissolved in 1 M HNO_3, dried down, and redissolved in ultrapure water (Milli-Q; Merck Milli-Q Advantage A10). Ac-225 was supplied in 0.05 M HCl by Eckert & Ziegler, and Ra-223 was supplied as $^{223}RaCl_2$ (Xofigo) by GE Healthcare (Leiderdorp, the Netherlands). Ba-139, La-140, and Ra-223 were measured directly with the Wallac Wizard2 3" 2480 Automatic Gamma Counter (Perkin Elmer). Ac-225 was measured indirectly at equilibrium (> 30 minutes after experiments) through its daughter Fr-221, emitting 218 keV γ-rays. Additional experiments for the separation of Sc-46 from $Ca(NO_3)_2$ and Y-90 from $Sr(NO_3)_2$ are presented as Supplementary Information.

Solution preparation

The aqueous solutions used in the solvent extraction experiments were prepared by dissolution of different amounts of $Ba(NO_3)_2$ (Merck Sigma) in Milli-Q water and subsequent addition of radiotracers. Note that for the separation of Ac-225 from Ra-223, rather than using 0.1 M $Ra(NO_3)_2$ as the (target) solution, a 0.1 M $Ba(NO_3)_2$ was used. This is justified by the chemical similarities of Ra and Ba, making it an often used substitute [46, 47]. The organic solution used in the solvent extraction experiments contains the chelator di-2-ethylhexylphosphoric acid (D2EHPA, reagent grade < 98 %; Merck Sigma) and was prepared as a 10 %v/v D2EHPA in chloroform (Merck Sigma) solution.

Batch solvent extraction experiments

Batch extraction experiments were performed to determine the equilibrium extraction efficiency, which is the highest possible extraction efficiency that can be obtained in the continuous-flow microfluidic experiments for a given combination of solutions and chelator. Next to these (forward) extraction experiments, also back-extraction experiments were performed to determine the optimal conditions, i.e., the lowest HCl concentration required for maximum back-extraction.

The batch forward extraction experiments were done in Eppendorf vials at a 1:1 volumetric ratio, with 0.5 mL of the aqueous and 0.5 mL of the organic solution. The vials containing both solutions were shaken on a Vortex-Genie 2 mixer (Scientific Industries, Inc.) for 1 minute at the highest speed setting, to reach equilibrium. Afterwards, the solutions were separated by pipetting and the radioactivity of both solutions was measured

in order to determine the extraction efficiency. The extraction efficiency of the batch experiments ($EE\%_{batch}$) was defined as the radioactivity of the organic solution after extraction ($A_{org,out}$) relative to the radioactivity of the aqueous solution before extraction ($A_{aq,in}$), i.e.,

$$EE\%_{batch} = \frac{A_{org,out}}{A_{aq,in}} \times 100\%. \tag{4.4}$$

The extraction efficiency was determined for the 'produced' radionuclide as well as for the target material.

The batch back-extraction experiments were performed in a similar manner, to release the 'produced' radionuclide from the organic solutions into an aqueous solution for further use in radiopharmaceutical production. The organic solution obtained after forward extraction containing the complexed radionuclide was brought into contact with an aqueous HCl (Merck Sigma) solution. The organic and aqueous solution were pipetted into a vial at equal volumes, shaken on the Vortex mixer for 5 minutes, and subsequently separated by pipetting. Different HCl concentrations were tested to determine the lowest HCl concentration necessary. The back-extraction efficiency ($BEE\%_{batch}$) was defined as the radioactivity in the resulting aqueous HCl solution ($A_{HCl,out}$) relative to the total radioactivity of the HCl and the organic solution ($A_{HCl,out} + A_{org,out}$), i.e.,

$$BEE\%_{batch} = \frac{A_{HCl,out}}{A_{HCl,out} + A_{org,out}} \times 100\%. \tag{4.5}$$

All batch experiments were done in triplicate and errors in the obtained values of the extraction and back-extraction efficiency were given as one standard deviation of the mean.

Microfluidic continuous-flow solvent extraction experiments

Microfluidic extraction experiments were performed in ALD-treated PDMS microfluidic chips. The aqueous, radionuclide-containing $Ba(NO_3)_2$ solution and the D2EHPA/$CHCl_3$ organic solution were loaded into 2.5 mL syringes, which were loaded on two separate syringe pumps (AL-1000 Programmable Syringe pumps 941-371-1003, World Precision Instruments, Inc.) and connected to the chips using PTFE tubing (outer diameter 1.6 mm, inner diameter 0.5 mm, length 200 mm). The extraction efficiency was studied for different contact times between the two phases in the microfluidic chips. The contact times were adjusted by varying the total volumetric flow rate of the two solutions, while keeping the ratio of flow rates at 1:1. The contact time t was calculated as $t = L/v$, with the length L of the main channel being equal to 11.63 mm and the average velocity v estimated from the sum of the volumetric flow rates ($Q_{aq} + Q_{org}$) over the cross-sectional channel area (S), i.e., $v = (Q_{aq} + Q_{org})/S$, with S equal to the sum area of both rectangular channel parts (deeper and shallower). At the outlet of the chip the organic solution,

enriched in the 'produced' radionuclide with radioactivity $A_{org,out}$, and the aqueous solution, depleted in the 'produced' radionuclide with radioactivity $A_{aq,out}$, were collected separately and measured for their radioactivity to determine the extraction efficiency ($EE\%_{continuous}$) determined as

$$EE\%_{continuous} = \frac{A_{org,out}}{A_{aq,out} + A_{org,out}} \times 100\%. \tag{4.6}$$

Microfluidic back-extraction experiments were performed by injecting the organic solutions containing the 'produced' radionuclide and different aqueous HCl solutions through microfluidic chips for varying contact times. The aqueous solution with radioactivity $A_{HCl,out}$ and the organic solution with radioactivity $A_{org,out}$ were collected at the outlets and the continuous back-extraction efficiency ($BEE\%_{continuous}$) was determined as

$$BEE\%_{continous} = \frac{A_{HCl,out}}{A_{org,out} + A_{HCl,out}} \times 100\%. \tag{4.7}$$

All microfluidic experiments were done in triplicate and errors in the obtained extraction and back-extraction efficiency were given as one standard deviation of the mean.

4.3. Results and discussion

4.3.1. Stability of parallel two-phase flow in bare and ALD-treated PDMS microfluidic devices

Figure 4.2 a) shows the three possible flow profiles taking place in the ALD-treated PDMS microfluidic chip when using 1 M HNO_3 as the aqueous phase and $CHCl_3$ as the organic phase: stable parallel flow with the interface pinned at the step height, unstable parallel with the interface not pinned at the step height, and break-up of the parallel flow into slugs. A map of these flow profiles shows that stable parallel flow with a pinned interface (filled squares) is obtained for a relatively wide range of flow rate combinations (see Fig. 4.2 b)). This window of stable operation is much larger than in microfluidic chips without the guiding structure [29–31], especially at a low flow rate, indicating the importance of the guiding structure. For the larger flow rates studied in this work, parallel flow is still observed, but with the interface not pinned to the step height over the full length of the microchannel (open squares). For this flow profile, occasional break-up of the unpinned interface into slugs was observed. For the highest flow rate ratios, the unpinned interface breaks-up downstream the Y-junction and slug flow (red circles) was observed. The transition between parallel flow with (partly) pinned interface (squares) and slug flow, represented by the solid lines, is reasonably well captured by the simple model (Eq. 4.1 - 4.3).

For reference, an attemp was made to perform the same measurements in a bare (un-

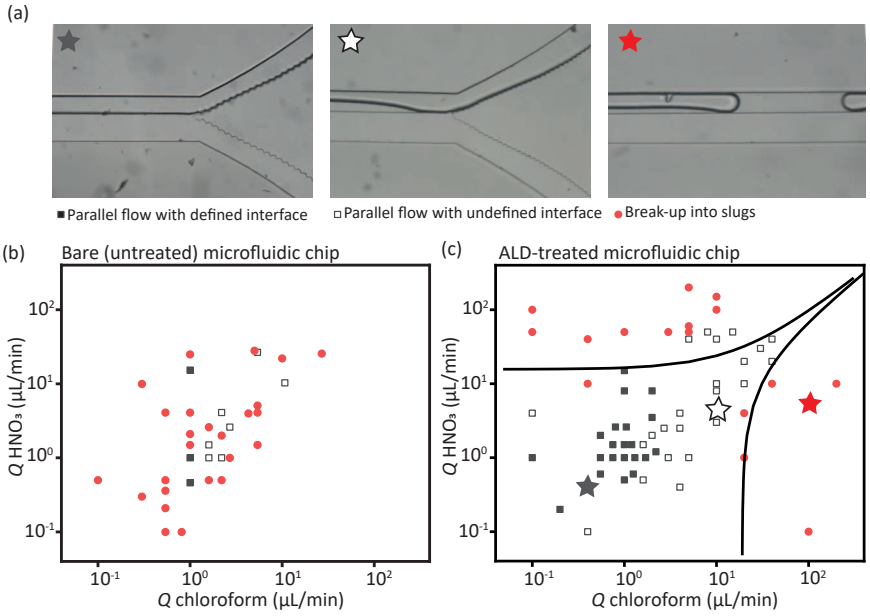

Figure 4.2: a) Optical microscopy photos taken in an ALD-treated PDMS microfluidic chip, illustrating the three types of two-phase flow observed at different combinations of the flow rate of the aqueous and organic solution. The solution in the upper and lower half of the channel is 1 M HNO_3 and $CHCl_3$, respectively. b) Flow map of 1 M HNO_3 and $CHCl_3$ inside ALD-treated PDMS microfluidic chips (n=3). The stars correspond to the photos shown in a). The lines represent the calculated transition between stable and unstable parallel flow using Eq. 4.1 - 4.3. c) Flow map of 1 M HNO_3 and $CHCl_3$ inside a bare (untreated) microfluidic chip (n=1).

treated) microfluidic chip. As expected, during these experiments, many chips leaked due to the swelling and deformation of PDMS under exposure to organic solvents [48]. The employed $CHCl_3$ induces matrix swelling inside the microfluidic channel, estimated at around 1.39 (length swelling ratio [18]). Swelling also reduces the channel space, leading to an undefined flow profile. While the experiments in ALD-treated chips were reproducible, strong variations from experiment to experiment were observed in untreated chips. An example experiment in a single untreated chip is shown in Fig. 4.2 c), illustrating the importance of the silicon oxide nano-layer of the ALD-treated chip to increases the organic solvent resistance of PDMS by preventing direct contact between the organic solvent and PDMS, as further detailed in earlier works [17, 37].

4.3.2. Batch solvent extraction

Batch extraction of La-140 (simulated 'produced' radionuclide) from Ba (simulated target material) and of Ac-225 from Ra-223 (in 0.1 M $Ba(NO_3)_2$) showed high extraction efficiencies (> 98 %) for all tested solutions (see Fig. 4.3 a)). With a mixing time of (less than) 1 minute, the complexation of D2EHPA is considered very fast. Simultaneously,

co-extraction of the target material into the organic phase remained low in all solutions: below 2 % for Ba-139 and below 0.3 % for Ra-223. However, it should be noted that the aqueous solution did not consist purely of Ra, but a Ra-223 tracer dissolved in a 0.1 M $Ba(NO_3)_2$ solution (commonly written as $[^{223}Ra]Ba(NO_3)_2$). Because of the chemical similarities of group 2 and 3 elements, additional extraction experiments were conducted for the separation of Y from Sr and Sc from Ca, which can be found in the Supplementary Information. All the extractions also show considerably high efficiency (> 80 %), as expected.

Back-extraction experiments show back-extraction efficiencies over 98 % for both La-140 and Ac-225 (as well as for Ba-139 and Ra-223) when using 0.1 M HCl (see Fig. 4.3 b)). These efficiencies decrease with decreasing HCl concentration. When using 0.01 M HCl as back-extraction solution, the back-extraction efficiency is significantly higher for Ac-225 compared to La-140. These results indicate a higher complex stability of ^{140}La-D2EHPA over ^{225}Ac-D2EHPA. The complex stability is dependent on the electronegativity and the ionic size and therefore, on the charge density, resulting in a lower complex stability for the larger Ac. This trend of decreasing complex stability with decreasing charge density is often found in chelate complexation [49] and was shown for La and Ac before [50]. The back-extraction results, including the results shown in the Supplementary Information for the separation of Y from Sr and Sc from Ca, are in line with this trend.

4.3.3. Microfluidic continuous-flow solvent extraction

The batch experiments were instrumental in determining the maximum achievable extraction efficiency with the continuous-flow microfluidic experiments. The insights gathered from the batch experiments were used to design and perform the microfluidic (forward) extraction experiments with (target) solution concentrations of 0.1 M $Ba(NO_3)_2$ and 1 µM $Ba(NO_3)_2$ in Milli-Q for La-140 and 0.1 M $Ba(NO_3)_2$ for Ac-225. Additionally, the back-extraction experiments were designed and performed with HCl solutions with concentrations higher than 0.1 M. For La-140 extraction from the 0.1 M and 1 μM $Ba(NO_3)_2$ solutions, the extraction efficiency for the longest contact time (1.7 seconds) was 97.44 % ± 0.71 % and 99.01 % ± 0.22 %, respectively (see Fig. 4.3c)). For Ac-225 extraction from the 0.1 M $Ba(NO_3)_2$ solution, a comparable extraction efficiency of 97.2 % ± 1.5 % was obtained for the same contact time (see Fig. 4.3 e)).

The speed of extraction is slightly influenced by the target concentration, as seen from the two curves in Fig. 4.3 c), which are different in target concentration by 5 orders of magnitude. The salting-out-effect, usually increasing extraction efficiency and separation because of a higher ionic strength of the solution, only has a minor influence on the results. A comparison of the curves in Fig. 4.3 c) and e) suggests that the speed of extraction is insensitive to the radionuclide concentration, which is six orders

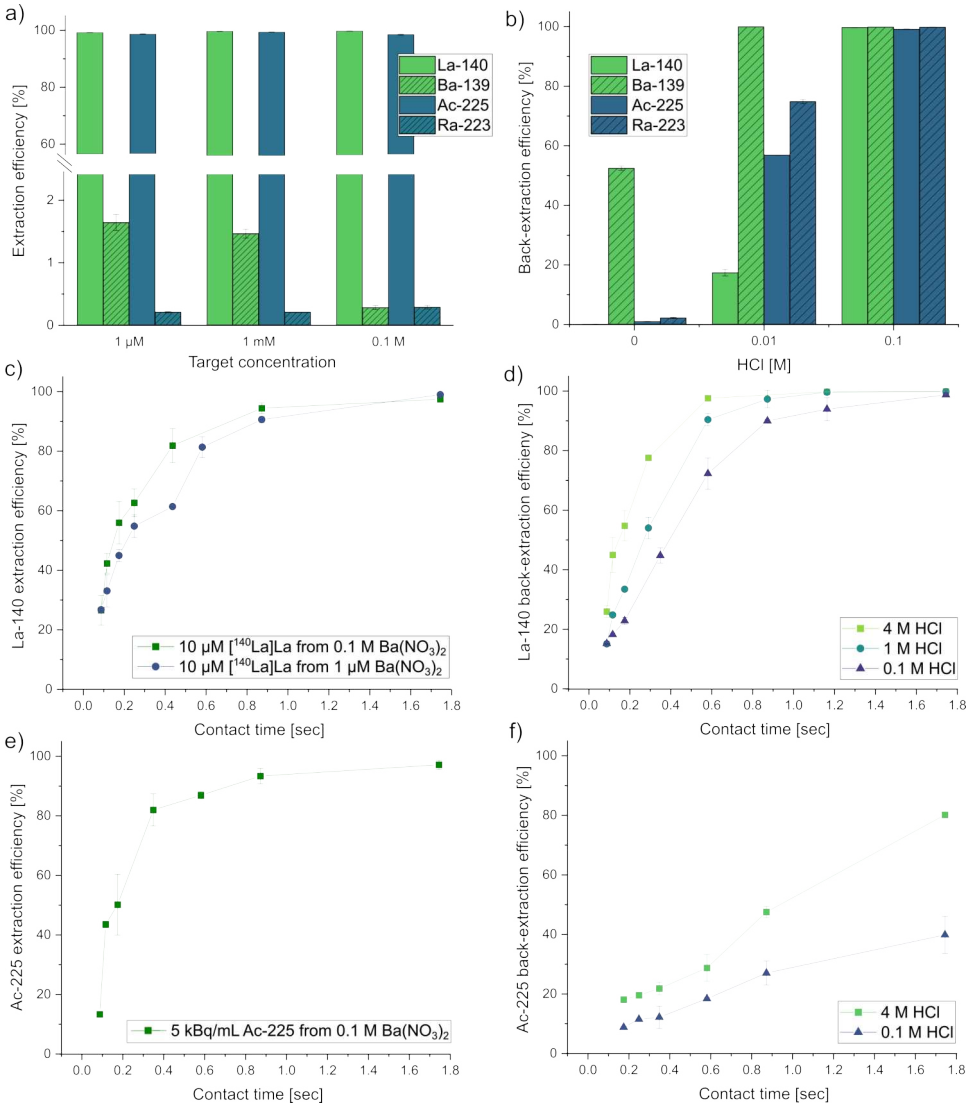

Figure 4.3: a) Batch extraction of Ba-139, La-140, Ac-225, and Ra-223 for varying target concentrations. b) Batch back-extraction of Ba-139, La-140, Ac-225, and Ra-223 for varying HCl concentrations. c) Microfluidic extraction of La-140 from two different $Ba(NO_3)_2$ solutions for varying contact times. d) Microfluidic back-extraction of La-140 into different HCl solutions for varying contact times. e) Microfluidic extraction of Ac-225 from 0.1 M $Ba(NO_3)_2$ solutions for varying contact times. f) Microfluidic back-extraction of Ac-225 into different HCl solutions for varying contact times. All experiments were done in triplicate and error bars represent the standard deviation of the mean.

of magnitude higher for La-140 than for Ac-225. Usually, the metal concentration (both radionuclide and target) plays a major role during the extraction in a microfluidic device because the concentration drives the diffusive flux [51]. The results indicate that the concentration of the radiometal that is to be extracted does not have a large influence on the extraction when using D2EHPA. Others have shown before that the D2EHPA concentration and its reaction kinetics have the highest influence on the extraction speed [52, 53]. Based on the molecular structure of D2EHPA illustrated in Fig. 4.4 a), Sun et al. (2021) [54] proposed that D2EHPA first transfers into the aqueous phase where it forms a complex with the product radionuclide, which subsequently transfers into the organic phase (see Fig. 4.4 b), shortening the diffusion distance of the radiometal. These steps, including the electrostatic pull of D2EHPA towards the metal ions[55], influence the extraction speed. While the full set of Ac-225 extraction experiments was performed with fixed radionuclide and target concentrations, it can be expected based on the aforementioned reasons that the Ba (or Ra) target concentration and the Ac-225 concentration have no major influence on Ac-225 extraction.

The back-extraction efficiency of La-140 into 0.1 M, 1 M, and 4 M HCl solutions exceeded 99 % within 1.7 seconds of contact time (see Fig. 4.3 d)). The back-extraction efficiency of Ac-225 with the same contact time is considerably lower, i.e., 80.16 % ± 0.77 % and 39.9 % ± 6.2 % for extraction into 4 M and 0.1 M HCl solutions, respectively (see Fig. 4.3f)). While the speed of back-extraction depends on the used HCl concentration, the extraction efficiency plateaus within 1.7 seconds for all three used HCl concentrations for La-140. For Ac-225, the plateau is not visible within 1.7 seconds. A comparison of the La-140 and Ac-225 back-extraction experiments for the same HCl concentrations suggests that the concentration of the radionuclide/D2EHPA complex has a higher influence on the back-extraction speed compared to the speed of the (forward) extraction. This implies that diffusion plays a more prominent role in back-extraction. Additionally, the now-neutral charge of the complex does not offer the ability of electrostatic pull of the complex near the interface. Therefore, the movement to the interface is slower. An increase in the back-extraction efficiency of Ac-225 could likely be accomplished by increasing the HCl concentration or increasing the contact time.

Overall, excellent extraction and back-extraction efficiencies can be achieved with the developed microfluidic solvent extraction method for both La-140 (97.44 % ± 0.71 % and 99.86 % ± 0.12 %, respectively) and Ac-225 (97.2 % ± 1.5 % and 80.16 % ± 0.77 %, respectively). Ac-225 currently receives enormous attention for its potential in targeted alpha therapy. Other commonly used methods for the separation of Ac-225 include the use of ion-exchange column chromatography [3, 56, 57], microfluidic ion-exchange [58], or solvent impregnated resins [59]. While achieving comparable results for the total recovery (the combination of extraction and back-extraction efficiency) of Ac-225, the developed microfluidic solvent extraction method exceeds the above-mentioned methods

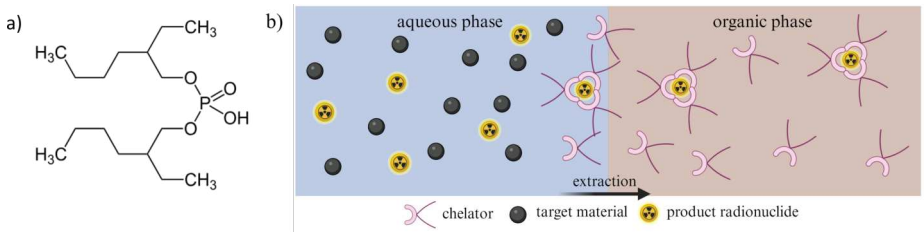

Figure 4.4: a) Structure of D2EHPA. b) Illustration of the extraction mechanism proposed by Sun et al.[54] showing that D2EHPA transfers into the aqueous phase where it forms a complex with the product radionuclide, which subsequently transfers into the organic phase.

in terms of minimizing chemical volumes [56, 57, 59], reducing the acidity of the final solution [56, 58, 59], or lowering processing time [58, 59].

Thus, the developed microfluidic solvent extraction of Ac-225 presents a promising alternative to conventional separation methods. The newly developed nano-layer coated PDMS microfluidic chip with a step-height and wavy outlet geometry solves the issue of insufficient phase separation and unstable parallel flow in microfluidic chips, and enables the future use and automation of solvent extraction for the separation of medical radionuclides.

4.4. Conclusion

A microfluidic PDMS-based chip was developed for fast, continuous, and efficient solvent extraction of radionuclides. To overcome the general issue that PDMS is incompatible with common organic solvents used in solvent extraction experiments, the recently developed atomic layer deposition method was used to deposit a layer of silicon oxide on the inside of the microchannels, rendering them inert. Two key features incorporated in the microfluidic chip, a difference in height in the channel for the organic and aqueous phase and a wavy wall near the exit, proved essential to obtain a stable parallel flow and a near-perfect separation of the phases at the exit. With the newly designed microfluidic chip and using the chelator D2EHPA in chloroform as the organic solution, a high extraction efficiency of 97.2 % ± 1.5 % of Ac-225 was accomplished in less than 1.8 seconds of contact time, while only co-extracting a maximum of 0.293 % ± 0.034 % of Ra, according to batch experiments. Back-extraction can be achieved in 0.1 M HCl, where increasing the contact time or the HCl concentration was found to speed up the back-extraction process. The presented proof-of-concept showcases the potential of microfluidic chips, for fast, continuous, and potentially automatable liquid-liquid extraction for the separation of medical radionuclides.

References

[1] https://world nuclear.org. Radioisotopes in medicine. *(last updated April 2024, accessed April 2024)* Available at `https://world-nuclear.org/`.

[2] Qaim, S. M. & Spahn, I. Development of novel radionuclides for medical applications. *Journal of Labelled Compounds and Radiopharmaceuticals* **61**, 126–140 (2018).

[3] Robertson, A. K. H., Ramogida, C. F., Schaffer, P. & Radchenko, V. Development of ^{225}Ac radiopharmaceuticals: Triumf perspectives and experiences. *Current Radiopharmaceuticals* **11**, 156–172 (2018).

[4] Boersma, H. H. *GMP in radiopharmacy: The current situation in its context. In: Nuclear Medicine and Molecular Imaging: Basic concepts, radiopharmacy and instrumentation*, 243–249 (Elsevier, 2022).

[5] Martini, P. *et al.* Perspectives on the use of liquid extraction for radioisotope purification. *Molecules* **24**, 334 (2019).

[6] Ramogida, C. F. *et al.* Evaluation of polydentate picolinic acid chelating ligands and an alpha-melanocyte-stimulating hormone derivative for targeted alpha therapy using ISOL-produced ^{225}Ac. *EJNMMI Radiopharmacy and Chemistry* **4** (2019).

[7] Pedersen, K. S., Nielsen, K. M., Fonslet, J., Jensen, M. & Zhuravlev, F. Separation of radiogallium from zinc using membrane-based liquid-liquid extraction in flow: Experimental and cosmo-rs studies. *Solvent Extraction and Ion Exchange* **37**, 376–391 (2019).

[8] Trapp, S. *et al.* Membrane-based microfluidic solvent extraction of Ga-68 from aqueous zn solutions: towards an automated cyclotron production loop. *EJNMMI Radiopharmacy and Chemistry* **8**, 9 (2023).

[9] Chakravarty, R. *et al.* Microfluidic solvent extraction of no-carrier-added ^{64}Cu from irradiated Zn target for radiopharmaceutical preparation. *Chemical Engineering Journal Advances* **13**, 100433 (2023).

[10] Helle, G., Mariet, C. & Cote, G. Microfluidic tools for the liquid-liquid extraction of radionuclides in analytical procedures. *Procedia Chemistry* **7**, 679–684 (2012).

[11] Mariet, C. *et al.* Microfluidics devices applied to radionuclides separation in acidic media for the nuclear fuel cycle. *Micro and Nano Engineering* **3**, 7–14 (2019).

[12] Abdollahi, P., Karimi-Sabet, J., Moosavian, M. A. & Amini, Y. Microfluidic solvent extraction of calcium: Modeling and optimization of the process variables. *Separation and Purification Technology* **231**, 115875 (2020).

[13] Whitesides, G. M. The origins and the future of microfluidics. *Nature* **442**, 368–373 (2006).

[14] Liu, Q., Huang, W., Liu, B., Wang, P.-C. & Chen, H.-B. Gamma radiation chemistry of polydimethylsiloxane foam in radiation-thermal environments: experiments and simulations. *ACS Applied Materials & Interfaces* **13**, 41287–41302 (2021).

[15] Victor, A., Ribeiro, J. & Araújo, F. F. Study of PDMS characterization and its applications in biomedicine: A review. *Journal of Mechanical Engineering and Biomechanics* **4**, 1–9 (2019).

[16] Ren, K., Zhou, J. & Wu, H. Materials for microfluidic chip fabrication. *Accounts of Chemical Research* **46**, 2396–2406 (2013).

[17] Santoso, A., Damen, A., van Ommen, J. R. & van Steijn, V. Atmospheric pressure atomic layer deposition to increase organic solvent resistance of PDMS. *Chemical Communications* **58**, 10805–10808 (2022).

[18] Lee, J. N., Park, C. & Whitesides, G. M. Solvent compatibility of poly (dimethylsiloxane)-based microfluidic devices. *Analytical Chemistry* **75**, 6544–6554 (2003).

[19] Van Bui, H., Grillo, F. & Van Ommen, J. Atomic and molecular layer deposition: off the beaten track. *Chemical Communications* **53**, 45–71 (2017).

[20] Vulto, P. *et al.* Phaseguides: a paradigm shift in microfluidic priming and emptying. *Lab on a Chip* **11**, 1596–1602 (2011).

[21] Kratochwil, C. *et al.* ^{225}Ac-PSMA-617 for psma-targeted a-radiation therapy of metastatic castration-resistant prostate cancer. *Journal of Nuclear Medicine* **57**, 1941–1944 (2016).

[22] Anderson, P. M., Subbiah, V. & Trucco, M. M. Current and future targeted alpha particle therapies for osteosarcoma: Radium-223, actinium-225, and thorium-227. *Frontiers in Medicine* **9**, 1030094 (2022).

[23] Mastren, T. *et al.* Simultaneous separation of actinium and radium isotopes from a proton irradiated thorium matrix. *Scientific Reports* **7**, 8216 (2017).

[24] Engle, J. W. The production of Ac-225. *Current Radiopharmaceuticals* **11**, 173–179 (2018).

[25] Apostolidis, C. *et al.* Cyclotron production of Ac-225 for targeted alpha therapy. *Applied Radiation and Isotopes* **62**, 383–387 (2005).

[26] Nagatsu, K. *et al.* Cyclotron production of ^{225}Ac from an electroplated ^{226}Ra target. *European Journal of Nuclear Medicine and Molecular Imaging* **49**, 279–289 (2021).

[27] Melville, G. & Allen, B. J. Cyclotron and linac production of Ac-225. *Applied Radiation and Isotopes* **67**, 549–555 (2009).

[28] Hibara, A. *et al.* Surface modification method of microchannels for gas- liquid two-phase flow in microchips. *Analytical Chemistry* **77**, 943–947 (2005).

[29] Pohar, A., Lakner, M. & Plazl, I. Parallel flow of immiscible liquids in a microreactor: modeling and experimental study. *Microfluidics and Nanofluidics* **12**, 307–316 (2012).

[30] Bruus, H. *Theoretical microfluidics*, vol. 18 (Oxford university press, 2007).

[31] Hibara, A., Fukuyama, M., Chung, M., Priest, C. & Proskurnin, M. A. Interfacial phenomena and fluid control in micro/nanofluidics. *Analytical Sciences* **32**, 11–21 (2016).

[32] Saha, A. A. & Mitra, S. K. Effect of dynamic contact angle in a volume of fluid (VOF) model for a microfluidic capillary flow. *Journal of Colloid and Interface Science* **339**, 461–480 (2009).

[33] Gumuscu, B., Bomer, J. G., van den Berg, A. & Eijkel, J. C. Large scale patterning of hydrogel microarrays using capillary pinning. *Lab on a Chip* **15**, 664–667 (2015).

[34] Duffy, D. C., McDonald, J. C., Schueller, O. J. & Whitesides, G. M. Rapid prototyping of microfluidic systems in poly (dimethylsiloxane). *Analytical Chemistry* **70**, 4974–4984 (1998).

[35] Santoso, A. *et al.* Robust surface functionalization of PDMS through atmospheric pressure atomic layer deposition. *Atomic Layer Deposition* **1**, 1–13 (2023).

[36] Goulas, A. & Van Ommen, J. R. Atomic layer deposition of platinum clusters on titania nanoparticles at atmospheric pressure. *Journal of Materials Chemistry A* **1**, 4647–4650 (2013).

[37] Santoso, A., David, M. K., Boukany, P. E., van Steijn, V. & van Ommen, J. R. Atmospheric pressure atomic layer deposition for in-channel surface modification of pdms microfluidic chips. *Chemical Engineering Journal* 155269 (2024).

[38] Sohnel, O. & Novotny, P. *Densities of aqueous solutions of inorganic substances* (Elsevier, 1985).

[39] Berry, J. D., Neeson, M. J., Dagastine, R. R., Chan, D. Y. & Tabor, R. F. Measurement of surface and interfacial tension using pendant drop tensiometry. *Journal of Colloid and Interface Science* **454**, 226–237 (2015).

[40] Demond, A. H. & Lindner, A. S. Estimation of interfacial tension between organic liquids and water. *Environmental Science & Technology* **27**, 2318–2331 (1993).

[41] Kralj, J. G., Sahoo, H. R. & Jensen, K. F. Integrated continuous microfluidic liquid–liquid extraction. *Lab on a Chip* **7**, 256–263 (2007).

[42] Baeckert, M. *et al.* Performance of modern syringe infusion pump assemblies at low infusion rates in the perioperative setting. *British Journal of Anaesthesia* **124**, 173–182 (2020).

[43] Li, Z., Mak, S. Y., Sauret, A. & Shum, H. C. Syringe-pump-induced fluctuation in all-aqueous microfluidic system implications for flow rate accuracy. *Lab on a Chip* **14**, 744–749 (2014).

[44] Korczyk, P. M., Cybulski, O., Makulska, S. & Garstecki, P. Effects of unsteadiness of the rates of flow on the dynamics of formation of droplets in microfluidic systems. *Lab on a Chip* **11**, 173–175 (2011).

[45] Amini, Y. *et al.* Computational fluid dynamics simulation of two-phase flow patterns in a serpentine microfluidic device. *Scientific Reports* **13**, 9483 (2023).

[46] Brown, M. A. Metal oxide sorbents for the separation of radium and actinium. *Industrial & Engineering Chemistry Research* **59**, 20472–20477 (2020).

[47] Toro-González, M., Dame, A. N., Mirzadeh, S. & Rojas, J. V. Encapsulation and retention of 225ac, 223ra, 227th, and decay daughters in zircon-type gadolinium vanadate nanoparticles. *Radiochimica Acta* **108**, 967–977 (2020).

[48] Dangla, R., Gallaire, F. & Baroud, C. N. Microchannel deformations due to solvent-induced PDMS swelling. *Lab on a Chip* **10**, 2972–2978 (2010).

[49] Chapman, D. Electronegativity and the stability of metal complexes. *Nature* **174**, 887–888 (1954).

[50] Mishustin, A. Estimate of the stability constants of trivalent actinide and lanthanide complexes with o-donor ligands in aqueous solutions. *Russ. J. Inorg. Chem.* **55**, 746–752 (2010).

[51] Holden, M. A., Kumar, S., Castellana, E. T., Beskok, A. & Cremer, P. S. Generating fixed concentration arrays in a microfluidic device. *Sensors and Actuators B: Chemical* **92**, 199–207 (2003).

[52] Suyanti & Amiliana, R. A. Extraction of Yttrium from Nd Hydroxide concentrate by using D2EHPA. *Journal of Physics: Conference Series* **1436**, 012002 (2020). Available at https://dx.doi.org/10.1088/1742-6596/1436/1/012002.

[53] STARÝ, J. *The Solvent Extraction of Metal Chelates* (Pergamon, 1964). Available at https://www.sciencedirect.com/science/article/pii/B9780080108216500028.

[54] Sun, P. *et al.* Antagonistic role of aqueous complexation in the solvent extraction and separation of rare earth ions. *ACS Central Science* **7**, 1908–1918 (2021).

[55] Jing, Y. *et al.* Deep insights into the solution and interface behaviors in heavy rare earth extraction: A molecular dynamics study. *Journal of Molecular Liquids* **296**, 111790 (2019). Available at https://www.sciencedirect.com/science/article/pii/S0167732217351218.

[56] Fitzsimmons, J. *et al.* Optimization of cation exchange for the separation of actinium-225 from radioactive thorium, radium-223 and other metals. *Molecules* **24**, 1921 (2019).

[57] Zielinska, B., Apostolidis, C., Bruchertseifer, F. & Morgenstern, A. An improved method for the production of Ac-225/Bi-213 from Th-229 for targeted alpha therapy. *Solvent Extraction and Ion Exchange* **25**, 339–349 (2007).

[58] Davern, S. *et al.* Microfluidics-based separation of actinium-225 from radium-225 for medical applications. *Separation Science and Technology* **54**, 1994–2002 (2019).

[59] Friend, M. T. *et al.* Extraction chromatography of ^{225}Ac and lanthanides on n, n-dioctyldiglycolamic acid/1-butyl-3-methylimidazolium bis (trifluoromethylsulfonyl) imide solvent impregnated resin. *Journal of Chromatography A* **1624**, 461219 (2020).

Supplementary Information

Because of the chemical similarities of group 2 and group 3 elements, additional extraction experiments were conducted for the separation of Sc-46 from $Ca(NO_3)_2$ and Y-90 from $Sr(NO_3)_2$ solutions. The radionuclides Ca-45, Sc-46, Sr-85, and Y-90 were produced by neutron irradiation of [^{44}Ca]CaO (Neonest AB, Sweden), Sc_2O_3 (ACROS ORGANICS; VWR, Amsterdam, the Netherlands), SrO, and Y_2O_3, respectively, at the Hoger Onderwijs Reactor (HOR) of the TU Delft | Reactor Institute (the Netherlands). [^{44}Ca]CaO and SrO were irradiated with a thermal neutron flux of 4.24 $\cdot 10^{17}$ $s^{-1}m^{-2}$ for 10 days and 1 day, respectively. Sc_2O_3 was irradiated with a thermal neutron flux of 4.69 $\cdot 10^{16}$ $s^{-1}m^{-2}$ for 5 hours, and Y_2O_3 was irradiated with a thermal neutron flux of 4.69 $\cdot 10^{16}$ $s^{-1}m^{-2}$ for 3 hours. The irradiated [^{44}Ca]CaO and Sr were subsequently dissolved in dilute HNO_3, dried down, and redissolved in ultrapure water. Ca-45 and Y-90 were measured with a Liquid Scintillation Counter (tri-carb 2750TR/LL, Packard). Sc-46 and Sr-85 were measured directly with the Wallac Wizard2 3" 2480 Automatic Gamma Counter (Perkin Elmer).

The aqueous solutions used in the solvent extraction experiments were prepared by dissolution of different amounts of $Ca(NO_3)_2$ and $Sr(NO_3)_2$ (Merck Sigma, Zwijndrecht, the Netherlands) in Milli-Q and subsequent addition of above mentioned radiotracers. Both batch and microfluidic extraction were performed as described in the main manuscript. The results of all batch and microfluidic extration experiments are shown in Fig. S5. The batch extraction of Sc-46 from 1 M $Ca(NO_3)_2$ resulted in a very good separation, with over 99 % extraction of Sc-46 and below 1 % of Ca-45 co-extraction. However, results differed tremendously for the 1 mM and 1 µM $Ca(NO_3)_2$ solution. Here, the Ca co-extraction increased up to 80 %, while the Sc-46 extraction decreased to 70 %. Back-extraction of Sc-46 was unsuccessful for every tested HCl solution, and therefore no microfluidic back-extraction of Sc-46 was done. The extraction of Y-90 from $Sr(NO_3)_2$ yielded successful efficiencies of over 95 % for all three $Sr(NO_3)_2$ solutions while the Sr-89 co-extraction remained below 2 %. Back-extraction of Y-90 could be achieved with efficiencies over 99 % into HCl concentrations above 0.1 M HCl. Microfluidic extraction of 10 µM [^{46}Sc]Sc was achieved with maximum efficiencies as shown during batch extraction in 1.8 seconds of contact time. Microfluidic extraction of 100 µM [^{90}Y]Y resulted in efficiencies of 99 % in approximately 1 second of contact time from 1 µM $Sr(NO_3)_2$ and in around 0.3 seconds from 1 M $Sr(NO_3)_2$. Microfluidic back-extraction of Y-90 however was slower and resulted in around 90 % back-extraction efficiency into 4 M HCl within 1.2 seconds and only 60 % into 1 M HCl within 1.8 seconds of contact time.

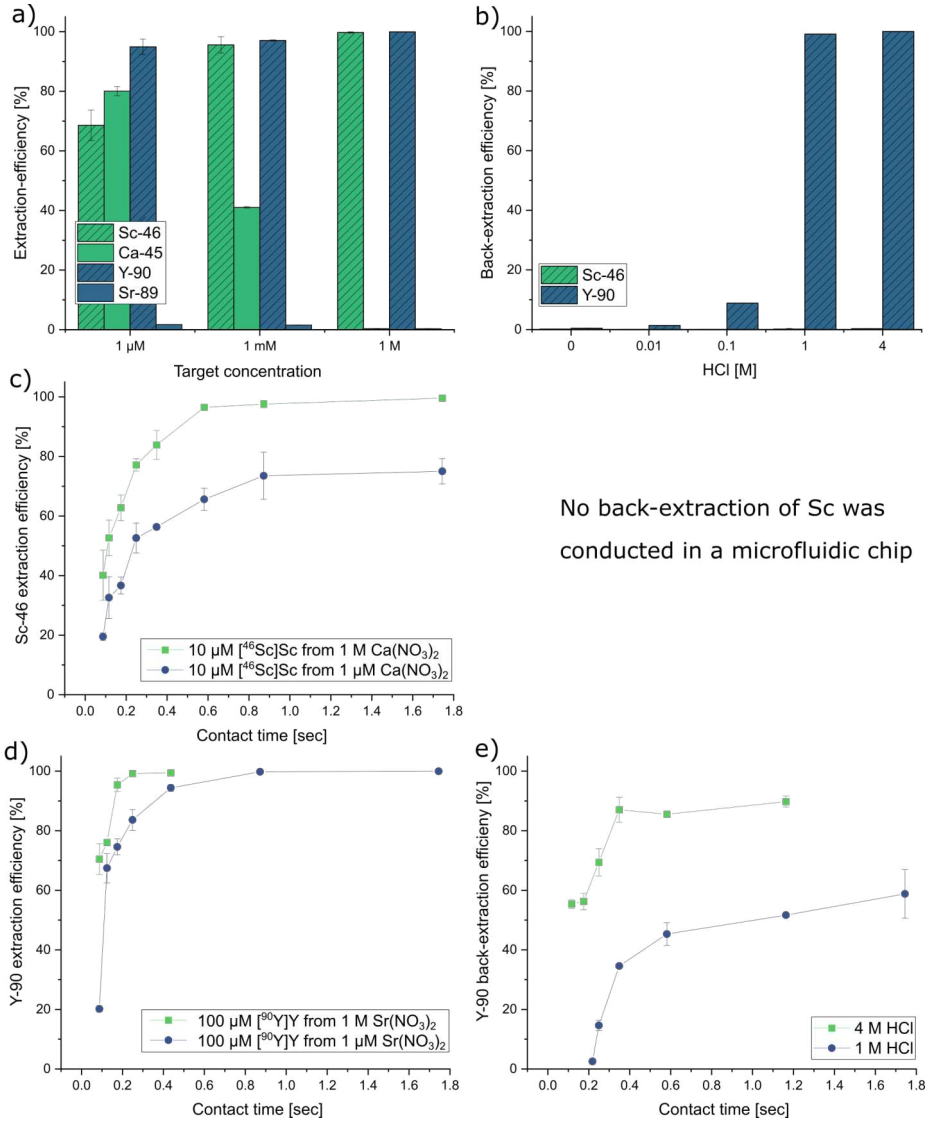

Figure S5: a) Batch extraction of Ca-45, Sc-46, Sr-89, and Y-90 for varying target concentrations. b) Batch back-extraction of Sc-46 and Y-90 for varying HCl concentrations. c) Microfluidic extraction of Sc-46 from two different $Ca(NO_3)_2$ in MQ solutions for varying contact times. d) Microfluidic extraction of Y-90 from two different $Sr(NO_3)_2$ in MQ solutions for varying contact times. e) Microfluidic back-extraction of Y-90 into different HCl solutions for varying contact times. All experiments were done in triplicate and error bars represent the standard deviation of the mean.

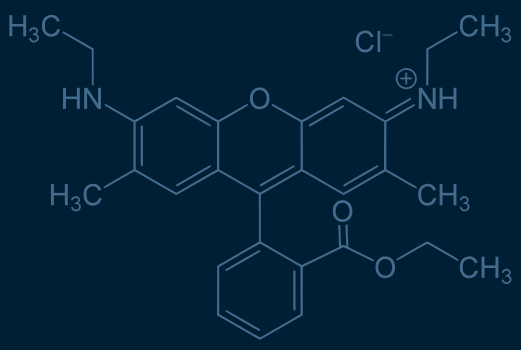

5

Using microfluidic chips for the determination of diffusion coefficients

5

Using microfluidic chips for the determination of diffusion coefficients

The diffusion coefficient is a characteristic physical constant of a compound under given hydrodynamic conditions. They are needed, amongst others, for numerical modeling of mass transfer, which can be used to understand chemical processes or optimize experimental set-ups, such as microfluidic solvent extraction of medical radionuclides. Multiple microfluidic chips were utilized to develop a method for the determination of diffusion coefficients at various flow rates/contact times. After validating the method with methylene blue and rhodamine-6G, the diffusion coefficient of Ga^{3+} in a 2 M $Zn(NO_3)_2$ solution was determined. The diffusion coefficients were determined by measuring the outlet concentrations after parallel flow in microfluidic chips. The results showed a trend of increasing diffusion coefficients with increasing flowrates and an exponential trend with increasing contact times. An exponential decay function was fitted to determine the diffusion coefficients of rhodamine-6G and Ga^{3+} from the measured apparent diffusion coefficients, resulting in values of $4.47 \pm 0.21 \cdot 10^{-10}$ m^2/s and $2.78 \pm 0.09 \cdot 10^{-10}$ m^2/s, respectively. This method showed the feasibility of using microfluidic chips for the determination of diffusion coefficients of (medical) radionuclides, that can be used amongst others for numerical models optimizing the separation of radionuclides from their targets.

5.1. Introduction

The diffusion coefficient (D) is an important physical constant describing the relation between the molar flux (J) and the concentration gradient of a compound or species ($\frac{d\varphi}{dx}$), which can appear in gases, liquids as well as solids in the absence of bulk movement. It is given by:

$$J = -D\frac{d\varphi}{dx} \tag{5.1}$$

The concept of diffusion was first described by Adolf Fick in 1855 in liquid solutions [1] and is therefore known as Fick's Law of diffusion. Nowadays, it is a fundamentally applied concept essential for the numeric modeling of a vast variety of applications, such as semiconductors, nuclear materials, plasma physics and transport phenomena, to name a few. There are multiple methods to determine the diffusion coefficient of a compound mainly consisting of estimations done by empirical correlation equations combined with experimental methods. One of the most used empirical correlation equations is the Stokes-Einstein equation, which specifically applies to a solute consisting of spherical particles, and is valid typically when these spherical molecules are dissolved in a solvent consisting of smaller size molecules compared to the solute [2]. Many empirical correlation relations for estimating liquid phase diffusion coefficients have been derived from it. The Stokes-Einstein equation is given by:

$$D = \frac{k_b T}{6\pi\mu r_h} \tag{5.2}$$

where D is the diffusion coefficient in $m^2 s^{-1}$, k_b the Boltzmann constant in J/K, T the temperature in K, μ the dynamic viscosity in $Pa \cdot s$ and r_h the hydrodynamic radius of the solute. In the context of microfluidic solvent extraction of medical radionuclides, the diffusion coefficient is a necessary parameter to model the mass transfer of the radionuclide in microfluidic chips [3, 4]. Modeling of this mass transfer in a microfluidic chip can aid in optimizing the chip geometry and improve the extraction efficiency. Unfortunately, diffusion data is often lacking, partially due to the complexity and time demand of available techniques for diffusion coefficient measurements, as well as the difficulty when concentrations are very low, limiting inter-molecular interactions that drive diffusion. A plethora of methods have been described over time [5] to determine diffusion coefficients of compounds in aqueous solution, including Taylor dispersion [6], dynamic light scattering [7], fluorescent correlation spectroscopy [8] or electrochemical techniques [9]. They all have pros and cons depending on the specific compound, concentration of the compound, volume of the solution, measurability of the compound, cost and time constraints. The development of microfluidic devices and lab-on-a-chip technology promised an improvement in available methods to measure diffusion coefficients of hard-to-measure compounds [10].

The two main experimental approaches to determine diffusion in a microfluidic device are static or dynamic. In a static set-up, a long channel is used where all solvents are stationary (no flow), because of which only diffusion can occur. Dynamic diffusion experiments rely on contacting two co-flowing streams of different composition in a microchannel and on the observation of mass transfer between them. Due to the low Reynolds number in microfluidic chips (which describes the ratio between inertial and viscous forces), the flow is exclusively laminar and the only mass transfer mechanisms are convection along the laminar flow direction and perpendicular diffusion. Therefore, stream wise diffusion can be neglected [11]. The numerical approach to this type of pressure-driven, dynamic diffusion studies include the use of the convection-diffusion equation (Eq. 5.3), where the transient term described the evolution of the concentration C in time, the convective term describes the rate of change in C due to bulk motion, the diffusive term accounts for molecular transport of the species C and the source term describes any creation/destruction of the species.

$$\underbrace{\frac{\partial \rho C}{\partial t}}_{\text{Transient term}} + \underbrace{\nabla \cdot (\rho \mathbf{u} C)}_{\text{Convection term}} = \underbrace{\nabla \cdot (D \nabla C)}_{\text{Diffusion term}} + \underbrace{S_C}_{\text{Source term}} \tag{5.3}$$

Previous work has demonstrated the potential of this microfluidic diffusion measurement principle focusing on the detection of fluorescent dyes [12]. Several studies have used microfluidic devices for the determination of diffusion coefficients in a dynamic setting (as opposed to static diffusion measurements), including T-, H-, an Y-geometries [12–16]. In most studies, (fluorescent) dyes or pH indicators were used, to measure the diffusion by optical detection inside the microchannel, which is not feasible for the measurement of the diffusion of radiotracers. While several of those studies work under comparable conditions, including the application of syringe pumps and collection of the co-flowing solutions at the outlets, the effect of different flowrates is often neglected [12, 14]. It was also found that dynamic diffusion measurements often result in overestimation of the diffusion coefficient [10], which is discussed to be due to the friction between the solute and the channel wall. In this chapter the aim is to investigate diffusion coefficient of Ga-68 for the later application in numerical models of microfluidic solvent extraction. First, this approach was validated by determining the diffusion coefficients of methylene blue and rhodamine-6G, which are known from literature.

5.2. Methods and Materials

5.2.1. Materials and analytical methods

Gallium nitrate hydrate ($Ga(NO_3)_3 \cdot xH_2O$) and zinc nitrate hexahydrate ($Zn(NO_3)_2 \cdot 6\ H_2O$) were purchased from Acros Organics (VWR, Amsterdam, the Netherlands), ni-

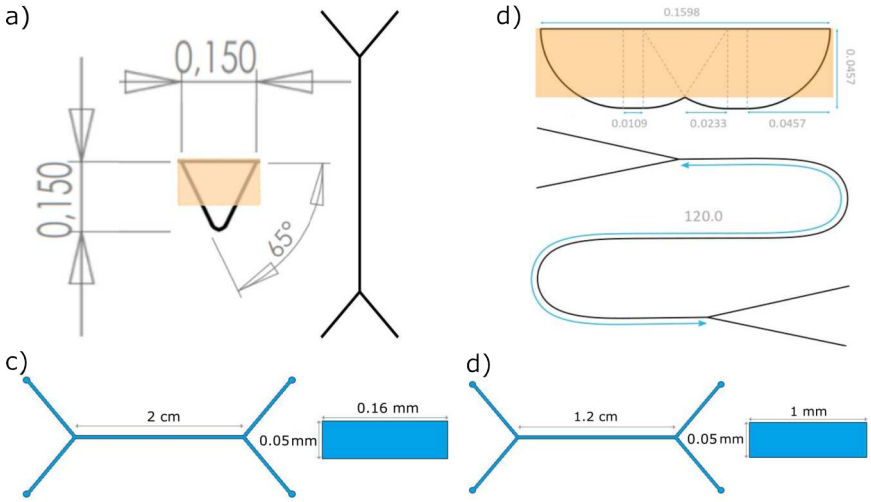

Figure 5.1: Dimension of microfluidic chips. a) Chip 1 Micronit glass chip with v-shaped channel. b) Chip 2 glass chip with w-shaped channel. c) Chip 3 IMT glass chip with rectangular channel. d) Chip 4 PDMS chip with rectangular channel, made in-house.

tric acid (HNO_3) and rhodamine-6G (CAS: 989-38-8) were purchased from Merck Sigma (Zwijndrecht, the Netherlands), and methylene blue was obtained from J.T. Baker Chemicals B.V. (CAS: 7220-79-3; VWR, Amsterdam, the Netherlands). The radiotracer Ga-68 that was used in the experiments was eluted from an Eckert & Ziegler IGG100 GMP Ge-68/Ga-68-generator (generously supplied by Erasmus MC, the Netherlands). AL-1000 Programmable Syringe pumps (941-371-1003) were purchased from World Precision Instruments Inc. The Wallac Wizard2 3" 2480 Automatic Gamma Counter from Perkin Elmer (Groningen, The Netherlands) was used for radioactivity measurements of Ga-68. Rhodamine-6G and methylene blue concentrations were measured with a UV-6300PC Spectrophotometer. Ga speciation was calculated using CHEAQS (Verweij Wi. CHEAQS Next (0.2.1.8)). Viscosity measurements were done using a capillary viscometer (SI Analytics Type 509 04) at room temperature. Microfluidic diffusion studies were executed with four different microfluidic YY-chips. The dimensions of the chips are shown in Fig. 5.1. Chip 1 was a commercial glass YY-chip from Micronit, with a triangular channel. Chip 2 was a commercial glass YY-chip with a w-shaped channel. Chip 3 was a commercial glass chip from IMT with a rectangular channel, and Chip 4 was a PDMS-based chip made in-house with a rectangular channel. The PDMS chips were fabricated by mixing PDMS elastomer and its curing agent with a mass ratio of 10:1 and pouring the mixture onto a 4-inch silicon wafer with a microcolumn pattern. The pattern was printed on the silicon wafer using soft lithography technique. Microscope images showing the channel roughness, were done on a Motic AE2000 optical microscope (Fig. 5.2).

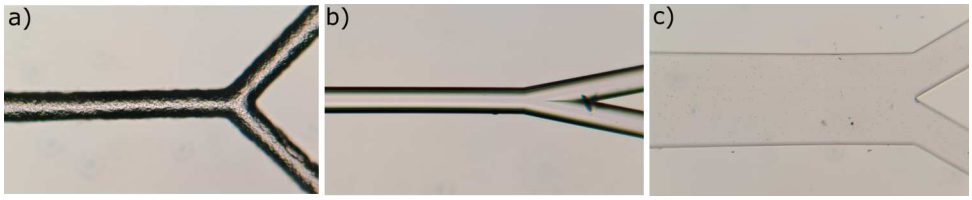

Figure 5.2: Microscope images of microchannels a) Chip 1, b) Chip 2 and c) Chip 4, showing the roughness of the channel walls.

5.2.2. Microfluidic diffusion experiments

The experimental setup consisted of two syringe pumps, a microfluidic device (as described above) and collection vials. A digital microscope allowed for direct observation of diffusion in the microchannel. A schematic overview of the set-up can be seen in Fig. 5.3. Two syringes were connected to the chip via flexible tubing. One syringe held the solution containing the compound of which the diffusion coefficient was to be determined, e.g. Ga-68, methylene blue or rhodamine-6G, while the second syringe contained the solution without the compound, which was ultrapure water in case of methylene blue and rhodamine-6G, and 2 M $Zn(NO_3)_2$ in 10 mM HNO_3 in the case of Ga-68. The syringes were placed in their respective flow rate configurable syringe pumps, and the tubes were connected to the inlets of the microfluidic channel. Because of the concentration gradient of the two co-flowing solutions, the compound diffused into the parallel flowing solution (see Fig. 5.4). Subsequently, the solutions were collected at the outlets in sample vials and the concentrations of rhodamine-6G, methylene blue and Ga-68 were measured in both solutions. All experiments were executed at room temperature (approximately 21°C) in triplicate. Uncertainties are given as one standard deviation of the mean.

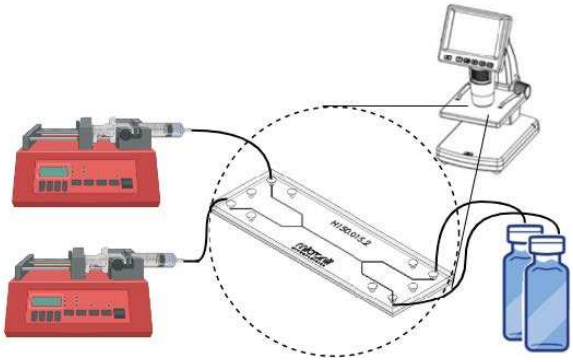

Figure 5.3: Schematic images of diffusion experiment set-up, including syringe pumps, the microfluidic chip, the optical microscope and the collection vials.

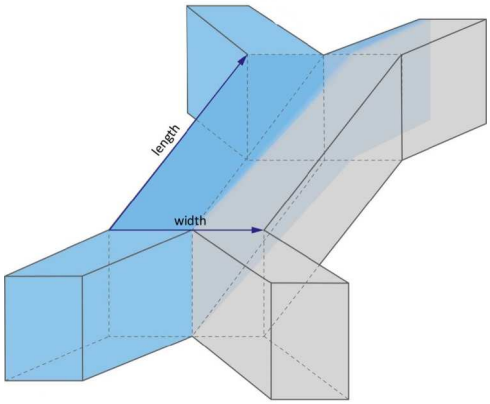

Figure 5.4: Schematic images of diffusion in a parallel flow YY-microfluidic chip. The blue side represents the compound that diffuses along the width of the channel.

5.2.3. Determination of diffusion coefficients

The apparent diffusion coefficients (D_{app}) were estimated numerically from the outlet concentrations obtained in the experiments using a finite difference model for mass transfer [13, 17] based on the convection-diffusion equation (Eq. 5.3).

Additionally, contact times (t) were estimated according to Eq. 5.4.

$$t[s] = \frac{\text{volume of the microchannel } [mm^3]}{\text{flow rate } [\mu L/min]} * 60 \tag{5.4}$$

Finally, the measured apparent diffusion coefficients were plotted against the contact time and an exponential decay function was fitted to the data to determine the final diffusion coefficient (D) for rhodamine-6G and Ga-68, from the asymptote.

Validation of the numerical model

A finite difference model for mass transfer (based on the convection-diffusion equation) was developed to determine diffusion coefficients from the measured outlet concentrations [13, 17]. An analytical Poiseuille flow profile was used to feed the finite difference model corresponding to the flow rates used in the experiments. A no-slip boundary condition was applied at the channel walls. A no-penetration boundary condition was applied (see Fig. 5.5), which ensures that there is no diffusion through the channel wall.

Concentrations of the solute at the outlets of the microchannel were subsequently obtained by integrating over the concentration profile at this particular location. The diffusion coefficient was then altered step by step until the numerically obtained concentrations at the outlets matched the experimentally observed concentrations to within 0.1 %.

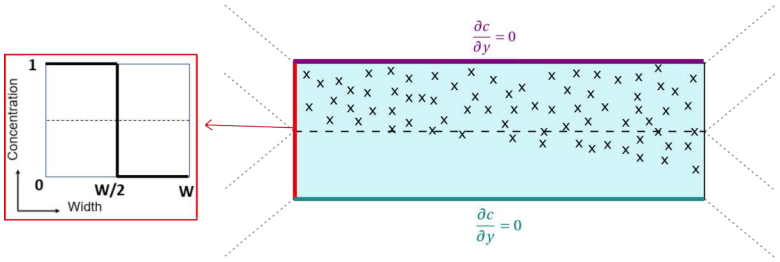

Figure 5.5: Visualization of implemented boundary conditions for mass transfer in microfluidic channels. At the inlets a sharp step function is defined, to simulate an assumed uniform distribution of solute flowing in from the top inlet into the microchannel. This step function is expected to diffuse into similar profiles as represented by the graph with the dashed line on the right.

The numerical approach was then tested for grid independence. Simulations for the grid refinement were done for chip 2 and 3. The ratio for the amount of grid points in the X- and Y-direction was chosen as X:Y=5:1 with the X-direction being along the length of the microfluidic channel and the Y-direction being its width.

5

5.3. Results

5.3.1. Model validation

Before the model could be used to determine the diffusion coefficients the grid independence was evaluated. Simulations on two different channels (chip 2 and 3) show similar results with a converging trend as the amount of grid points increases. In both cases, at 500 nodes in the X-direction (N_x), the value of the concentration at the lower concentration outlet is within 0.5% of the value it would have with 1000-nodes in the X-direction ($C_{Nx}/C1000$). The grid spacing with 500 nodes in the X-direction is therefore deemed sufficiently accurate (see Fig. 5.6). Additionally, visualization of the computed mass transfer and corresponding outlet concentration profile are shown in Fig. 5.7.

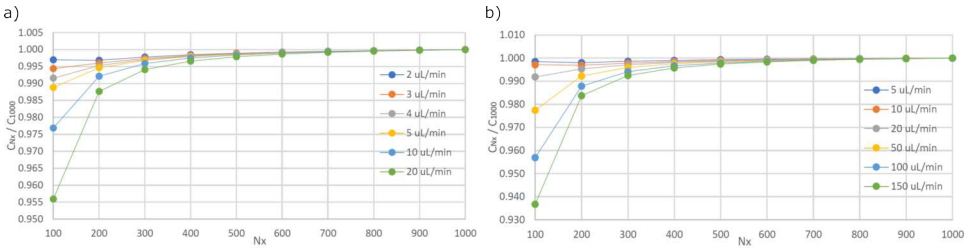

Figure 5.6: a) Grid refinement with 5:1 ratio for straight channel (chip 3). b) Grid refinement with 5:1 ratio for serpentine channel (chip 2).

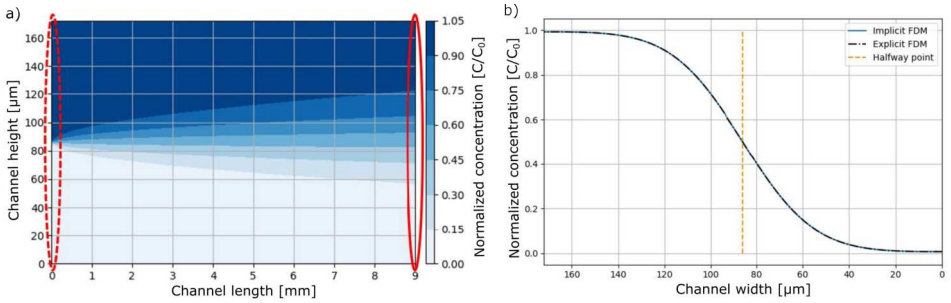

Figure 5.7: a) Visualization of the computed mass transfer in the microfluidic channel. The dotted circle on the left indicates the inlets, and the full circle on the right illustrates concentration distribution at the outlets, shown in b). b) Developed concentration profile at the outlets, as numerically computed by the methods presented in this study.

5.3.2. Diffusion coefficients

First, the apparent diffusion coefficient (D_{app}) of methylene blue was determined using chips 1 and 2. A significant difference in the measured D_{app} can be observed between the two chips with different length, as well as between the two tested flow rates within one chip. It varied between $8.3 \pm 0.3 \cdot 10^{-10} m^2/s$ and $13.6 \pm 0.1 \cdot 10^{-10} m^2/s$ in chip 1 and between $12.1 \pm 0.4 \cdot 10^{-10} m^2/s$ and $12.7 \pm 0.1 \cdot 10^{-10} m^2/s$ in chip 2.

To determine the D_{app} of rhodamine-6G, chips 3 and 4 were compared and varying flow rates were applied. The results are shown in Fig. 5.8 b). It can be seen again, that for both chips that were used, the D_{app} increases with increasing flow rates and as a result, varies significantly, between $2.8 \pm 0.1 \cdot 10^{-10} m^2/s$ and $11.4 \pm 1.6 \cdot 10^{-10} m^2/s$.

It becomes clear that different flow rates have a large impact on the D_{app}, independent of the chip that is used. Results for the measurement of the D_{app} of Ga-68 are shown in Fig 5.9. Here, two different Ga concentrations were compared, using only chip 3. In

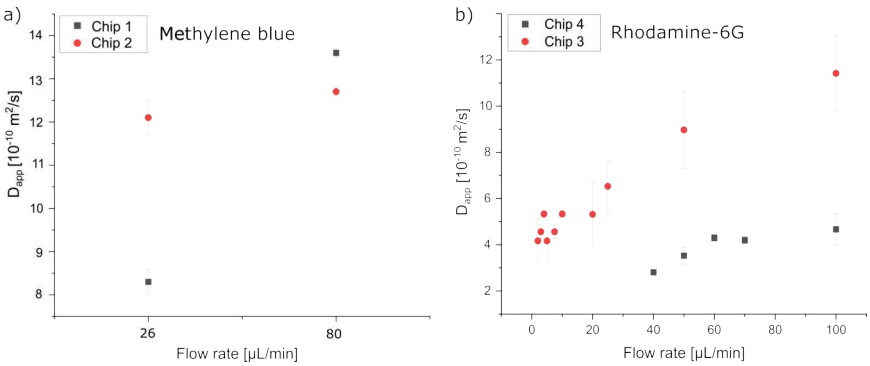

Figure 5.8: a) Methylene blue diffusion coefficient results for various flow rates (n=3) with Chip 1 and 2. b) Rhodamine-6G diffusion coefficient results for various flow rates (n=3) with Chip 3 and 4.

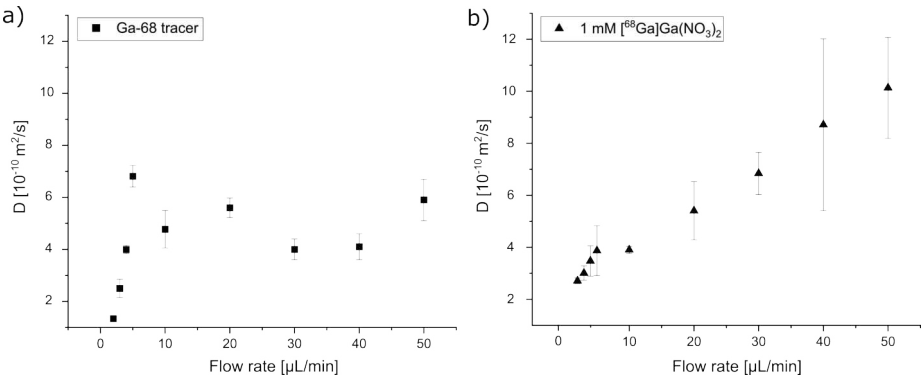

Figure 5.9: a) D_{app} results of Ga using only Ga-68 tracer in a 2 M $Zn(NO_3)_2$ in 0.01 M HNO_3 solution (chip 3) b) D_{app} results of of Ga using 1 mM $[^{68}Ga]Ga(NO_3)_2$ in a 2 M $Zn(NO_3)_2$ in 0.01 M HNO_3 solution (chip 3).

Fig 5.9 a) only a Ga-68 radiotracer was added to the solution, resulting in a total Ga concentration in the femtomolar range. Usually, measuring the diffusion of compounds with concentrations in the pico- to femtomolar range becomes increasingly challenging, due to the very low inter-molecular forces that drive diffusion [16]. It was found that in the presented microfluidic set-up, diffusion coefficient results for Ga-68 tracer where comparable to the results of 1 mM Ga. However, the uncertainties were higher due to the above mentioned effect of low inter-molecular forces. Between both cases, no significant difference in the Ga speciation in the solution was observed (see Tab. 5.1). Therefore, the effect of different species on the diffusion can be neglected. The results prove the possibility of measuring diffusion coefficients for radiotracers.

To determine the actual diffusion coefficient D of rhodamine-6G and Ga from the measured D_{app}, the data was plotted against the contact time instead of the flow rate, resulting in an exponential trend. After fitting an exponential decay equation to the data, the asymptote of the exponential fit gives the actual diffusion coefficient (D) of $4.48 \pm 0.21 \cdot 10^{-10} m^2/s$ for rhodamine-6G in water (with an R-square of 0.84) and $2.78 \pm 0.09 \cdot 10^{-10} m^2/s$ for Ga in a 2 M Zn solution (with an R-square of 0.93).

Table 5.1: Ga speciation in $Zn(NO_3)_2$ in 0.01 M HNO_3 for 1 mM and 1 pM Ga, as given by CHEAQS.

Speciation	% for 1 mM Ga	% for 1 pM Ga
free Ga^{3+}	98.06	98.51
$Ga(OH)^{2+}$	1.49	1.49
$Ga_2(OH)_2{}^{4+}$	0.45	-

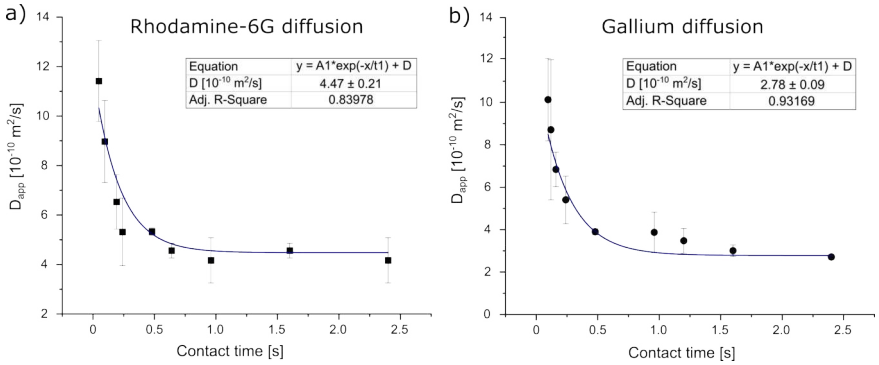

Figure 5.10: a) Rhodamine-6G diffusion coefficients against contact time including exponential fit. b) Ga^{3+} diffusion coefficients against contact time including exponential fit.

5

5.4. Discussion

Compared to literature values for the diffusion coefficient of methylene blue, the presented results of $8.3 \pm 0.3 \cdot 10^{-10} m^2/s$ and $13.6 \pm 0.1 \cdot 10^{-10} m^2/s$ both resulted in higher diffusion coefficients then previously reported. Miložič et al. applied similar methods, using a microfluidic chip and measuring the outlet concentration, and reported a diffusion coefficient of $4.6 \cdot 10^{-10} m^2/s$ [13]. Others have found the diffusion coefficient of methylene blue to range between 2.6 and $7.6 \cdot 10^{-10} m^2/s$ by employing voltammetric methods [18, 19]. Compared to the above-mentioned literature values for the diffusion of methylene blue, the results in the presented study significantly overestimate the diffusion coefficient. When looking at the results for the diffusion of rhodamine-6G, if purely considering the flow rate specific D_{app}, there is a trend of increasing diffusion coefficients with increasing flow rate. After plotting the results against the contact time and fitting an exponential function to it, a diffusion coefficient of $4.48 \pm 0.21 \cdot 10^{-10} m^2/s$ could be determined, falling within reported literature values, that vary between 4.0 and 4.6 $\cdot 10^{-10}$ m^2/s [10, 16, 20, 21]. The same was done for the diffusion of gallium, specifically in a 2 M $Zn(NO_3)_2$ in 0.01 M HNO_3 solution, resulting in a D of $2.78 \pm 0.09 \cdot 10^{-10} m^2/s$. Ga diffusion coefficient values in literature are up to one order of magnitude higher, between 8.4 and $30.6 \cdot 10^{-10} m^2/s$ [22], indicating that the increased viscosity of the highly concentrated zinc solution (see Fig 5.12 in Supplementary Information) reduces the diffusion rate. Irrespective of the chip design and diffusing compound, increasing diffusion coefficients with increasing flow rates were found. This trend has also been observed in other studies, e.g. for the determination of the diffusion coefficient of [^{177}Lu]Lu-DOTA-TATE [23] or bromocresol green sodium salt [17] using microfluidic chips. Schaap (2017) also found a trend of increasing diffusion coefficients with increasing flow rate by measuring outlet concentrations [23], while Binda et al (2022) applied a very long chip and measured the diffusion at different places throughout the chip to show the results for dif-

ferent contact times [17]. Their results similarly show the trend of increasing diffusion coefficients with decreasing contact time, indicating that not the flow rate directly, but the contact time is the major influencing factor.

Another potential reason for the increasing diffusion coefficients with increasing flow rates might be friction between the solution and the channel walls. Increasing flow rates cause increased friction to the channel wall and as a result increases disturbance in the flow [24, 25]. Culbertson et al. (2002) compared multiple static and dynamic microfluidic methods to determine diffusion coefficients and found that dynamic studies result in significantly larger (11%) measured diffusion coefficients compared to static experiments, which is argued to be caused mainly by friction in the dynamic studies [10]. This effect corresponds to our observation in Fig 5.8 a). While the D_{app} as determined using chip 2 only differed slightly between the two flowrates, the results from chip 1 showed a much more significant difference. Chip 1 has the highest roughness compared to all other chips (as can be seen in Fig. 5.2), so the difference in measured diffusion coefficients between different flow-rates should be the greatest according to the reasoning above. Chips 3 and 4, however are produced similarly and have a comparable roughness, so there the increase/slope should be similar.

The main argument found in literature explaining this effect of overestimated D_{app} during pressure-driven diffusion measurements, is the so-called butterfly effect (as established by [26]). Ismagilov et al. (2000) found, that in the initial stages in a microfluidic channel, the diffusion is faster closer to the channel wall compared to the center (see Fig. 5.11), which is caused by the parabolic velocity profile of the solution (Poiseuille flow). This leads to a secondary concentration gradient in the vertical direction, that equilibrates along the length of the channel. Therefore, if the contact time is too low, this butterfly effect will result in an overestimation of the measured diffusion coefficients. This explains why this effect of overestimated diffusion coefficients not only appears when the outlet concentrations are measured, but also when point measurements where executed along the channel length as done by Binda et al [17]. It is therefore of high importance to determine the diffusion coefficient at varying contact times, to avoid overestimation due to the butterfly effect.

Our detailed investigations have given us valuable insights on the feasibility of measuring diffusion coefficients with microfluidic chips. To get best possible results, several experimental set-up designs should be considered. First, microfluidic chips with only minor roughness should be used. Herefore, either polymer based chips as used in this study (PDMS), or HF-eched glass chips would be optimal. Using a pressure pump instead of a syringe pump can lead a more steady flow with less pressure fluctuations as shown by Zeng et al. 2015 [28], potentially reducing the uncertainties on the estimated diffusion coefficient. It is additionally advised to filter the solutions before use, to avoid particle accumulations causing undesirable disturbance in the chip. Finally,

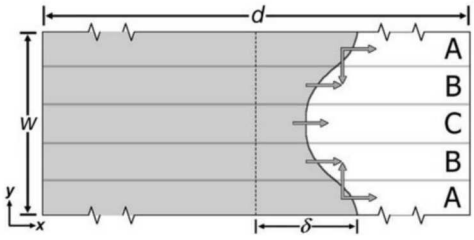

Figure 5.11: From Kamholz et al. (2001) [27]. The shape of the interface in a microfluidic channel during diffusion study is shown. The diffusive compound is shown in grey and the original interface is demonstrated by the dotted line.

the methods of increasing the contact time and fitting the data with an exponential fit to determine the diffusion coefficient was successful. Varying contact times also aid in observing when the D plateaus out, i.e. when the minimum contact time necessary for determining the actual diffusion coefficient is reached, without overestimation due to the butterfly effect.

In Chapter 2 a droplet-based microfluidic solvent extraction method was described to separate Ga-68 from a $Zn(NO_3)_2$ in 0.01 M HNO_3. A 1 m long microfluidic tube (with an inner diameter of 0.03 inch) was necessary to extract 99.2 % ± 0.3 % of Ga-68 at a flow rate of 40 μL/min, corresponding to a residence time of over 5 minutes. Considering the results presented in this study, it can be concluded that the diffusion of Ga-68 is not the limiting factor of the extraction speed, but the speed of complex-formation at the solvent interface.

Overall, these results show that it is not only possible to measure the diffusion coefficient with a microfluidic chip under optimal conditions, but that they can also aid in understanding underlying chemical processes during solvent extraction and hence, aid in optimizing separation processes.

5.5. Conclusion

Microfluidic chips have been used successfully to determine the diffusion of rhodamine-6G in water and Ga^{3+} in a 2 M $Zn(NO_3)_2$ solution, resulting in diffusion coefficients of $4.47 \pm 0.21 \cdot 10^{-10}$ m^2/s and $2.78 \pm 0.09 \cdot 10^{-10}$ m^2/s, respectively. It was demonstrated that it is necessary to measure the apparent diffusion coefficients over varying contact times to determine the actual diffusion coefficient of the compound. A decreasing exponential trend with increasing contact times was found, from which the diffusion coefficient was determined by fitting an exponential decay function to it. These results show that it is possible to measure the diffusion coefficient with a microfluidic chip under optimal conditions. They can therefore be used to optimize future experiments to determine diffusion coefficient of medical radionuclides and hence aid in optimizing their separation

from the target material, as well as aid in understanding underlying chemical processes during solvent extraction.

References

[1] Fick, A. Ueber diffusion. *Annalen der Physik* **170**, 59–86 (1855).

[2] Edward, J. T. Molecular volumes and the stokes-einstein equation. *Journal of Chemical Education* **47**, 261 (1970).

[3] Chevalier, S. Semianalytical modeling of the mass transfer in microfluidic electrochemical chips. *Physical Review E* **104**, 035110 (2021).

[4] Chaurasiya, R. K. & Singh, K. Cfd modelling of mass transfer in liquid–liquid core-annular flow in a microchannel. *Chemical Engineering Science* **249**, 117295 (2022).

[5] Kariuki, S. & Dewald, H. D. Evaluation of diffusion coefficients of metallic ions in aqueous solutions. *Electroanalysis* **8**, 307–313 (1996).

[6] Alizadeh, A., de Castro, C. A. N. & Wakeham, W. A. The theory of the taylor dispersion technique for liquid diffusivity measurements. *International Journal of Thermophysics* **1**, 234–284 (1980).

[7] Fröba, A. P. & Leipertz, A. Diffusion measurements in fluids by dynamic light scattering. *The Open-Access Journal for the Basic Principles of Diffusion Theory, Experiment and Application* (2005).

[8] Enderlein, J., Gregor, I., Patra, D., Dertinger, T. & Kaupp, U. B. Performance of fluorescence correlation spectroscopy for measuring diffusion and concentration. *ChemPhysChem* **6**, 2324–2336 (2005).

[9] Baur, J. E. 19 - diffusion coefficients. In Zoski, C. G. (ed.) *Handbook of Electrochemistry*, 829–848 (Elsevier, Amsterdam, 2007).

[10] Culbertson, C. T., Jacobson, S. C. & Ramsey, J. M. Diffusion coefficient measurements in microfluidic devices. *Talanta* **56**, 365–373 (2002).

[11] Salmon, J.-B. & Ajdari, A. Transverse transport of solutes between co-flowing pressure-driven streams for microfluidic studies of diffusion/reaction processes. *Journal of Applied Physics* **101**, 074902 – 074902 (2007).

[12] Kamholz, A. E., Weigl, B. H., Finlayson, B. A. & Yager, P. Quantitative analysis of molecular interaction in a microfluidic channel: The t-sensor. *Analytical Chemistry* **71**, 5340–5347 (1999).

[13] Miložič, N., Lubej, M., Novak, U., Žnidaršič Plazl, P. & Plazl, I. Evaluation of diffusion coefficient determination using a microfluidic device. *Chemical and Biochemical Engineering Quarterly* **28**, 215–223 (2014).

[14] Yu, M. *et al.* The investigation of protein diffusion via h-cell microfluidics. *Biophysical Journal* **116**, 595–609 (2019).

[15] Häusler, E., Domagalski, P., Ottens, M. & Bardow, A. Microfluidic diffusion measurements: The optimal h-cell. *Chemical Engineering Science* **72**, 45–50 (2012).

[16] Müller, C. B. *et al.* Precise measurement of diffusion by multi-color dual-focus fluorescence correlation spectroscopy. *Europhysics Letters* **83**, 46001 (2008).

[17] Binda, L., Bolado, M., D'Onofrio, A. & Freytes, V. M. Analysis of a microfluidic device for diffusion coefficient determination of high molecular weight solutes detectable in the visible spectrum. *European Physical Journal E* **45** (2022).

[18] Chakraborty, A., Ahmed, S. & Saha, S. K. Electrochemical studies of progressively alkylated thiazine dyes on a glassy carbon electrode (gce) in water, ethanol, and triton x-100 media. *Journal of Chemical & Engineering Data* **55**, 1908–1913 (2010).

[19] Vetter, K. & Bardeleben, J. Überspannung und Gleichgewichtspotentiale der Methylenblau/Leukomethylenblau–Redoxelektrode. *Zeitschrift für Elektrochemie, Berichte der Bunsengesellschaft für physikalische Chemie* **61**, 135–141 (1957).

[20] Gendron, P. O., Avaltroni, F. & Wilkinson, K. J. Diffusion coefficients of several rhodamine derivatives as determined by pulsed field gradient-nuclear magnetic resonance and fluorescence correlation spectroscopy. *Journal of Fluorescence* **18**, 1093–1101 (2008).

[21] Effenhauser, C. S., Bruin, G. J. M. & Paulus, A. Integrated chip-based capillary electrophoresis. *Electrophoresis* **18**, 2203–2213 (1997).

[22] Chung, Y. & Lee, C.-W. Electrochemistry of gallium. *Journal of Electrochemical Science and Technology* **4**, 1–18 (2013).

[23] Schaap, K. *Computational study of the use of microfluidics for the synthesis of the radiopharmaceutical [^{177}Lu]Lu-DOTA-TATE.* Master's thesis, Delft University of Technology (2017).

[24] Jia, J., Song, Q. & Liu, Z. Effect of wall roughness on performance of microchannel applied in microfluidic device. *Microsystem Technologies* **25**, 2385–2397 (2019).

[25] Cheng, W. L., Erbay, C., Sadr, R. & Han, A. Dynamic flow characteristics and design principles of laminar flow microbial fuel cells. *Micromachines* **9** (2018).

[26] Ismagilov, R. F., Stroock, A. D., Kenis, P. J. A., Whitesides, G. & Stone, H. A. Experimental and theoretical scaling laws for transverse diffusive broadening in two-phase laminar flows in microchannels. *Applied Physics Letters* **76**, 2376–2378 (2000).

[27] Kamholz, A. E. & Yager, P. Theoretical analysis of molecular diffusion in pressure-driven laminar flow in microfluidic channels. *Biophysical Journal* **80**, 155–160 (2001).

[28] Zeng, W., Li, S. & Wang, Z. Characterization of syringe-pump-driven versus pressure-driven microfluidic flows. In *2015 International Conference on Fluid Power and Mechatronics (FPM)*, 711–715 (2015).

Supplementary Information

Viscosity measurements

Viscosities of varying $Zn(NO_3)_2$ solutions in 0.01 M HNO_3 are plotted against Ga diffusion coefficients (determined at a set flow-rate and therefore unoptimized) in varying $Zn(NO_3)_2$ solutions in 0.01 M HNO_3, showing the strong influence of viscosity on diffusion.

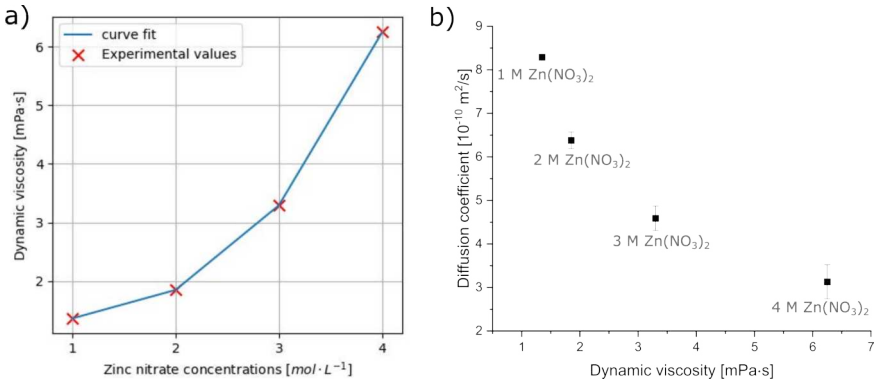

Figure 5.12: a) Dynamic viscosities of varying $Zn(NO_3)_2$ solutions in 0.01 M HNO_3. b) Dynamic viscosities of varying $Zn(NO_3)_2$ solutions in 0.01 M HNO_3 against diffusion coefficient of Ga^{3+}

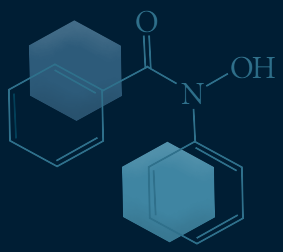

6

Assessing organic contaminations after solvent extraction and their removal using microcolumns

6

Assessing organic contaminations after solvent extraction and their removal using microcolumns

Production of medical radionuclides such as Ga-68, Cu-64 or Ac-225 are usually done by irradiation of enriched target materials in cyclotrons or nuclear reactors. After irradiation, the radionuclide needs to be separated from its target. While this is mostly done by ion-exchange chromatography, an emerging method includes the use of (microfluidic) solvent extraction. However, it has not been studied to which extent the chelators and organic solvents used during solvent extraction contaminate the final radionuclide-containing solution, and how this might impact subsequent radiolabelling applications. In this study, the contamination of the chelators N-benzoyl-N-phenylhydroxilamine (BPHA), dithizone (DIZ) and di(2-ethylhexyl)phosphoric acid (D2EHPA) after solvent extraction of Ga-68, Cu-64 and Ac-225 was investigated, and a microcolumn purification method is proposed. It was found that BPHA and DIZ contaminations can significantly interfere with DOTA-labelling. The applied microcolumn purification method eliminated the BPHA contamination from the Ga-68 solution completely, while simultaneously drastically reducing the total volume and acidity of the solution. It is therefore a promising purification method that can be included in an automated microfluidic solvent extraction procedure.

6.1. Introduction

Because of an ever increasing demand in medical radionuclides, radiochemists are extensively researching different ways to produce a large range of medical radionuclides [1, 2]. Different separation and purification methods are studied to optimize yield, automation and recyclability, including ion-exchange, solvent extraction, co-precipitation, electrochemical separation, as well as combinations of them [3].

One promising way to purify radionuclides is by microfluidic solvent extraction [4–7]. This method is not only interesting due to the very high selectivity of chelators, it also potentially allows for easier or direct target recycling and enables automation of solvent extraction [4]. While several studies have been published investigating the efficiency and selectivity of this separation process, to the best of our knowledge no studies have considered the possible organic contamination of the extracting chelator in the final solution after back-extraction, or their potential interference during labelling of the radionuclide to pharmaceuticals. The presence of organic contaminations after solvent extraction might therefore necessitates further purification steps.

Since high purity is needed for the manufacturing of radiopharmaceuticals, production and separation of the radionuclide needs to comply to good manufacturing processes (GMP). The official requirements include a high radiochemical and radionuclidic purity, meaning that no other isotopes of the medical radionuclide and chemically different radionuclides are present, as well as the chemical purity (including metal-, buffer- and other chemical impurities) [8, 9].

In many cases, even after initial chemical separation methods based on ion-exchange or extraction chromatography, additional purification and/or concentration steps are necessary before radiolabelling. Examples for this include the production of radiolanthanides such as Lu-177 or Tb-161 after irradiation of Yb and Gd targets, respectively. The separation of Lu-177 from its Yb target and Tb-161 from its Gd target using a TK221 extraction chromatographic resin column (Triskem) results in elution volumes of several tens to hundreds of milliliters [10]. The concentration of the solution volume is usually achieved by either additional anion-exchange resin columns or open tabletop drying of the solution [11]. Especially the open drying of highly radioactive solutions is undesirable and further complicates automation of the separation and labelling process. Another example where additional purification/concentration is necessary is the production of Ga-68 via ^{68}Ge/^{68}Ga generators. Here, elution of Ga-68 is typically achieved in 4-7 mL, followed by additional purification/concentration using cation-exchange resin columns [12–14].

While metal impurities in the final solutions have been studied before in this thesis (chapters 2 and 4), as well as in the literature [7, 15], organic contaminations caused by the solvent extraction process are typically neglected.

In earlier studies (Chapters 2, 3 and 4) microfluidic solvent extraction was investi-

gated for the extraction of Ga-68, Cu-64 and Ac-225 using the chelators BPHA, DIZ and D2EHPA, respectively. This study aims to investigate organic contamination in obtained solutions after these solvent extractions, to which extend they influence radiolabelling, and suggests a microcolumn-based method to further purify these solutions. The presented microcolumn purification method can also be extended to purification and concentration of solutions collected during different separation methods then solvent extraction.

6.2. Methods and Materials

6.2.1. Organic contamination detection

To determine the presence of chelator contaminations, solutions obtained after back-extraction were analyzed by ultraviolet–visible spectroscopy (UV-Vis) using a UV-6300PC Double Beam Spectrophotometer. Back-extractions were done according to methods described in earlier chapters (2, 3 and 4). However, the initial extraction step was skipped to avoid interferences with co-extracted metal ions during UV measurements. Therefore, no metals were present to back-extract, but the same experimental procedure was followed. The 'back-extractions' were done from three different chelator solutions due to their use in chapters 2, 3 and 4, namely (I) 0.2 M N-benzoyl-N-phenylhydroxylamine (BPHA; VWR International; CAS 304-88-1) in chloroform and back-extraction into 6 M HCl, (II) 0.01 M dithizone (DIZ; VWR International; CAS 60-10-6) in chloroform and back-extraction into 8 M HCl and (III) 10 v/v% di-2-ethylhexylphosphoric acid (D2EHPA, reagent grade < 98 %; Merck Sigma) in chloroform and back-extraction into 0.1 M HCl. The contact time during the back-extraction was 10 minutes. The obtained aqueous solutions were first measured by UV-Vis and afterwards slowly dried, redissolved in ultrapure water (MQ; Merck Milli-Q Advantage A10) and measured again, to compare the spectra and determine potential chloroform contamination. Analyses were done in quartz cuvettes over a wavelength range of 200 - 700 nm.

6.2.2. DOTA radiolabelling

The chelator dodecane tetraacetic acid (DOTA; CAS 60239-18-1) was chosen for radiolabelling studies with Ga-68, Cu-64 and Ac-225, due its frequent application in radiopharmaceuticals [16]. Ga-68 was eluted from an Eckert & Ziegler IGG100 Ge-68/Ga-68-generator (generously supplied by Erasmus MC) and Ac-225 was supplied by Eckert & Ziegler. Cu-64 was produced at the Hoger Onderwijs Reactor (HOR) in Delft (the Netherlands) by neutron activation of a Zn metal foil with a thermal neutron flux of 3.5 x 10^{13} $s^{-1}m^{-2}$ for 5 hours. After irradiation the Zn foil was dissolved in 8 M HCl and Cu-64 was separated from the solutions using a DOWEX 2x8 200/400 mesh resin (Merck). After pre-conditioning of the column, Cu-64 was adsorbed to the column and subsequently

eluted in 1 M HCl. To obtain chelator-contaminated solutions, extractions and back-extractions of Ga-68, Cu-64 and Ac-225 were executed as described in chapters 2, 3 and 4, respectively. The labelling of the radionuclides to DOTA was performed in a solution consisting of 120 µL acetic acid buffer (pH 4.2), 25 µL 0.42 mM DOTA in MQ and 10-30 kBq of Ga-68, Cu-64 or Ac-225, either obtained from the extraction process or used directly from the source (therefore without potential organic contaminants). The solutions were equilibrated in a thermoshaker for 15 minutes, at 90 °C and 300 rpm. Labeling efficiencies were determined by instant-thin layer chromatography (iTLC). Herefore, instant thin layer chromatography strips (iTLC-SG Agilent) were applied, using acetonitrile 5% v/v (CAS 75-05-08; Central warehouse L&M) as the mobile phase. After the (labelled) radionuclide solutions were pipetted onto the strip, they were left to dry for 30 minutes, before being submerged 1cm into acetonitrile 5% v/v. The mobile phase was left to run for 5 minutes and the strips were dried afterwards for another 30 minutes before measurements. During this chromatography step, the DOTA-labelled radionuclide were separated from the unlabelled radionuclides on the strip. To determine the radiolabelling efficiency, the strips were cut in half and both the top (A_{top}) and bottom (A_{bottom}) of the strip were measured separately for their radioactivity with the Wallac Wizard 2480 automatic gamma counter (Perkin Elmer). The DOTA labelling efficiency (LE%) was calculated as follows:

$$LE\% = \frac{A_{top}}{A_{bottom} + A_{top}} * 100\% \tag{6.1}$$

While Ga-68 and Cu-64 were measured directly, Ac-225 was measured indirectly with its daughter Fr-221 after >30 minutes of equilibration.

6.2.3. Phosphor imaging

For visual representation of the labelled and unlabelled Ga-68 activity, the iTLC strips were imaged with a Typhoon Trio+ phosphor imager (Amersham GE) and images were analyzed with ImageQuant TL. The screen of the phosphor imager was exposed to the iTLC strips for 10 minutes, and subsequently placed into the phosphor imager. The phosphor images of the iTLC strips were taken with a pixel size of 50 microns.

6.2.4. Microcolumn purification

For the specific case of Ga-68 with BPHA contamination, a purification method was developed consisting of an ion-exchange resin-based microcolumn. The microcolumn was fabricated by mixing PDMS elastomer and its curing agent with a mass ratio of 10:1 and pouring the mixture onto a 4-inch silicon wafer with a microcolumn pattern. The pattern was printed on the silicon wafer using a soft lithography technique. Two microcolumns were made with differing width of 2 mm and 5 mm, both 3 cm long and 0.1 mm high. The ion-exchange resin AG 1-X8 (Bio-Rad) was preconditioned in 6 M HCl and loaded

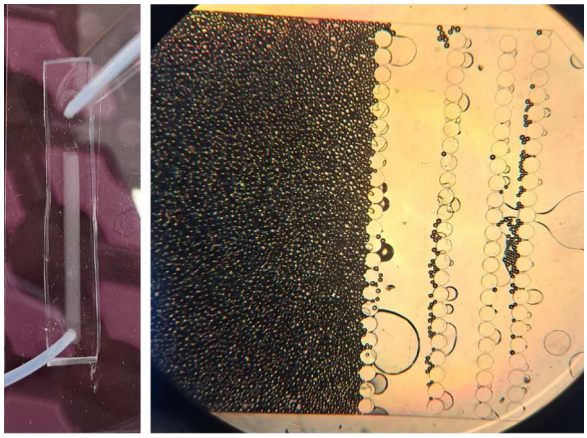

Figure 6.1: Left: Image of 2 mm wide column containing ~8 mg of AG 1-X8 resin. Right: Microscopic images of 5 mm wide microcolumn containing AG 1-X8 resin.

into the microcolumn with a syringe via flexible tubing until filled, resulting in a content of approximately 8 mg in the 2 mm wide column and 21 mg in the 5 mm wide column. A picture of the 2 mm wide column as well as a microscope image of the 5 mm wide column are shown in Fig 6.1. The Ga-68 solution was obtained in 6 M HCl from batch back-extractions as described earlier, and the total Ga concentration was adjusted by addition of $Ga(NO_3)_2$ to be at 1 pM to simulate a realistic concentration of several GBq Ga-68. The 5 mL solution was loaded into a syringe, and connected to the microcolumn via flexible tubing. An AL-1000 Programmable Syringe Pump (941-371-1003; World Precision Instruments Inc.) was used to push the solution through the microcolumn at a set flow rate. The radioactivity of the solution was measured before ($A_{initial}$) and after adsorption (A_{after}) of Ga-68 to the microcolumn and adsorption efficiencies ($AE\%$) were calculated as:

$$AE\% = (1 - \frac{A_{after}}{A_{initial}}) * 100\% \tag{6.2}$$

These experiments were done in triplicate and uncertainties are given as one standard deviation of the mean.

After adsorption of Ga-68 to the microcolumn, elution was done into MQ. The solution was collected in small fractions (of 50 µL in the 5mm wide column and approximately 20 µL in the 2mm wide column) to evaluate the elution profile, and thus determine the minimum amount of solution necessary for complete elution. Additionally, the above-mentioned steps were repeated with a 6 M HCl solution obtained from the back-extraction process with BPHA and chloroform but without Ga-68, to investigate the MQ solutions eluted from the microcolumn for any residual BPHA contamination. Measurements of the BPHA contamination in the 6 M HCl solution and the obtained MQ

solutions were done by UV-Vis spectroscopy as described above. To further investigate the potential reduction of common metal contaminants Zn, Fe and Cu during the microcolumn purification experiments, a 2.5 mL solution containing 5 mg/L Zn, Fe and Cu in 6 M HCl was pushed through the column and eluted into 250 µL MQ. The metal concentrations before adsorption ($C_{initial}$) and after elution ($C_{elution}$) were measured by inductively coupled plasma optical emission spectroscopy (ICP-OES; Optima 8000 from Perkin Elmer) and the total recovery (R%) was calculated as shown below:

$$R\% = (1 - \frac{C_{elution}}{C_{initial}}) * 100\% \tag{6.3}$$

6.3. Results and Discussion

6.3.1. Organic contamination detection

To determine the presence of chloroform, BPHA, DIZ or D2EHPA in the aqueous solutions, UV-Vis measurement were first done on solutions obtained after the back-extraction process. Fig. 6.2 displays the measured spectra of the solutions collected after back-extraction, showing contaminations with a) BPHA, b) DIZ and c) D2EHPA, before and after being dried to evaporate the chloroform contamination. The most prominent peaks can be seen in the spectra of BPHA. It has been reported that BPHA is soluble in water at levels detectable by UV-Vis [17], and its presence was therefore expected in the solutions. After evaporation the peak representative for BPHA [17] can be seen at around 270 nm. The significant difference in the spectra before evaporation is due to the presence of chloroform contaminations and the resulting interaction between chloroform and BPHA.

The spectrum obtained for DIZ shows a peak at 250 nm which is not in line with literature reports of DIZ spectra (having peaks at around 445 nm and 590 nm [18]). This peak likely represents an oxidation product of dithizone as shown by [19]. Since DIZ is known to have a low temperature and photostability [20], the concentration decreases during open tabletop heating, resulting in a lower concentration in the measurement after drying. D2EHPA is not present as a contamination in a concentration within the detection range of the UV-Vis spectrophotometer (<1 ppm), although this of course does not fully exclude its presence. The spectra of the DIZ and D2EHPA solutions before drying also indicate minor chloroform contaminations, due to the steep absorbance at wavelength between 200 and 230 nm [21]. From these measurements it can be concluded that some chelators contaminate the aqueous solution after back-extraction, a fact that has not been discussed in the literature yet [7].

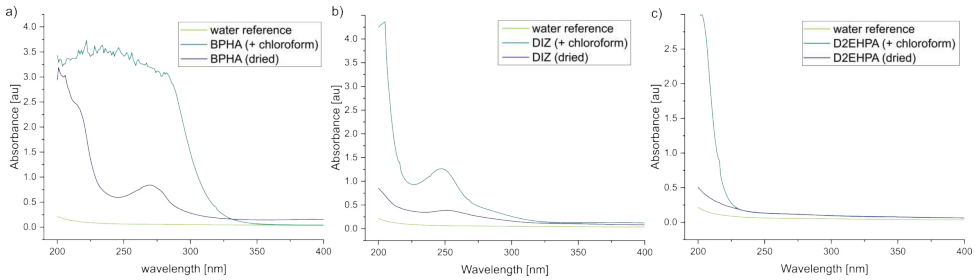

Figure 6.2: UV-VIS spectra showing the presence or absence of contaminations after back-extraction by a) BPHA, b) DIZ and c) D2EHPA, before (light blue) and after (dark blue) evaporation (and re-dissolution) to show the difference with and without chloroform contamination.

6.3.2. DOTA radiolabelling

From the previous experiments it was clear that BPHA and DIZ chelators, as well as chloroform, contaminate the aqueous solution during back-extraction to varying degrees. The potential interference of chelator contamination was therefore investigated during the labelling of the radionuclides Ga-68, Cu-64 and Ac-225 to DOTA. The results (Fig 6.3) indicate that BPHA interferes with the labelling of Ga-68 to DOTA. Interference of DIZ during Cu-64 radiolabelling to DOTA can be assumed from the results. For Ac-225, no significant difference can be seen during the radiolabelling to DOTA, indicating that no interfering D2EHPA contamination was present, which was expected based on the UV-Vis results shown in Fig. 6.2 c). While the radiolabelling of Ga-68 to DOTA yielded a LE% of 99.58 ± 0.70 % in absence of BPHA contamination, in its presence the LE% drops significantly dependent on the amount of BPHA contamination. Phosphor imaging of

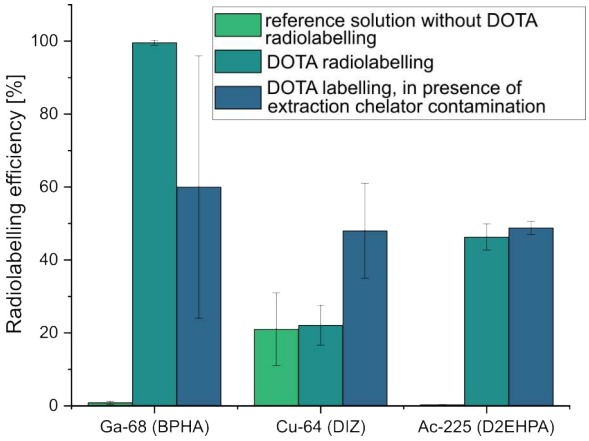

Figure 6.3: Labelling efficiencies of Ga-68, Cu-64 and Ac-225 to DOTA in the presence and absence of contamination by extraction chelators BPHA, DIZ and D2EHPA, respectively.

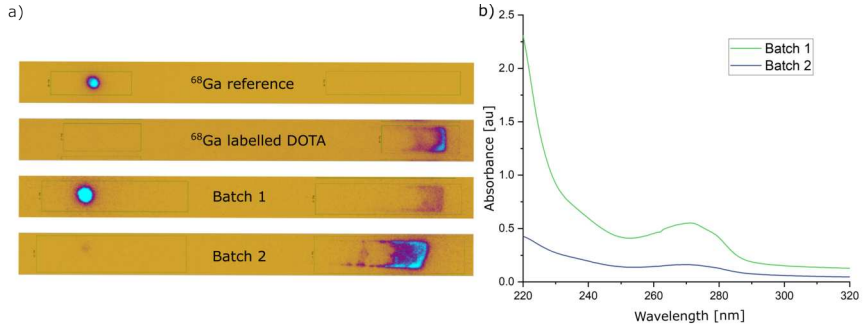

Figure 6.4: a) iTLC strips showing the effect of BPHA contamination during radiolabelling of DOTA. Labelling was executed with DOTA in the absence and presence of varying concentrations of BPHA, as shown by the UV-Vis spectra in b).

the iTLC strips and corresponding UV-Vis spectra (Fig. 6.4) indicate the correlation between differing labelling efficiencies and concentration of BPHA contamination. Cu-64 radiolabelling to DOTA also show the interference of contamination. The reference solution without DOTA but with DIZ contamination shows a labelling efficiency of 21 ± 10 %, showing that the ^{64}Cu-DIZ complex moves on the iTLC strip in the same way ^{64}Cu-DOTA does. The DOTA labelling without DIZ contamination resulted in 22.1 ± 5.5 %. When repeated with presence of DIZ contamination the LE% increased to 48 ± 13 %, which did not show an improvement of DOTA labelling, but the presence of DIZ labelled Cu-64. Since the DOTA concentration in the solution was high enough to exceed radionuclide concentrations by several orders of magnitude, metallic contaminations can not be the cause of the drop in labelling efficiencies (usually nanomolar DOTA concentrations are sufficient to account for interfering metal contaminations [22, 23]). The results during labelling in the presence of BPHA and DIZ contamination showcase the potential interference of chelator contaminations obtained after solvent extraction during radiopharmaceutical labelling.

6.3.3. Microcolumn purification

To prevent chelator contamination from interfering with radiolabelling, an additional clean-up step of the collected solution after solvent extraction is essential. For this purification a microcolumn-based clean-up method is presented that can be integrated in an automated solvent extraction procedure.

As a case study, the purification of a Ga-68 in 6 M HCl solution after solvent extraction with BPHA in chloroform is further discussed in detail. First, two different microcolumn sizes were packed with AG 1-X8 ion-exchange resin, as shown in Fig. 6.5 a). Adsorption efficiencies of over 98 % were achieved with both microcolumns using flowrates of 20 and 50 µL/min. Only at 100 µL/min a decrease in adsorption efficiency to 90.59 ± 0.48 %

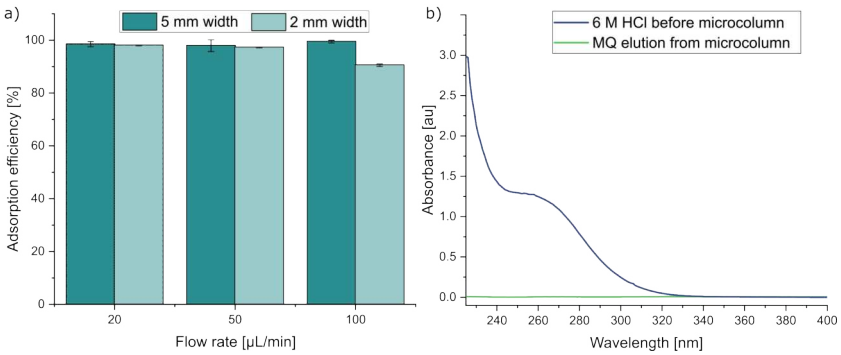

Figure 6.5: a) Adsorption efficiency of Ga-68 from 6 M HCl at varying flowrates in two different microcolumn widths. b) UV-Vis spectra of 6 M HCl solution before loading of the microcolumn and MQ elution from the microcolumn afterwards, showing no BPHA contamination.

was observed in the 2 mm wide column. Elution of Ga-68 was accomplished into MQ and elution profiles are shown in Fig. 6.6. From both microcolumns, around 98 % of Ga-68 could be eluted. However different volumes of MQ were needed, namely 90 µL and 150 µL for the 5 mm wide column and the 2 mm wide column, respectively. Fig. 6.5 b) shows the UV-Vis absorption spectra of the 6 M HCl solution before the microcolumn purification step, exhibiting a significant amount of BPHA contamination, as well as a MQ solution obtained after elution from the microcolumn, with no indication of residual BPHA contamination. These spectra indicate the ability of the microcolumn to purify solutions from chelator and chloroform contaminations.

Additionally, a significant reduction of acidity (from 6 M HCl to MQ) and volume (from 5 mL to below 150 µL) could be achieved during the microcolumn purification. This is particularly important as small volumes and specific pH are needed for radiopharmaceutical labelling. The elution in MQ allows for easy buffering to obtain the necessary pH [12].

Furthermore, the distribution of Zn, Fe and Cu contamination was measured, due to their frequent occurrence in irradiated targets [24, 25]. Of special interest was the radionuclide Cu-61, which can be co-produced during irradiation of Zn-68 for the production of Ga-68 [25]. The total recovery of Zn, Fe and Cu after adsorption and elution was found to be 97.6 ± 3.5 %, 77.9 ± 3.8 % and 5.8 ± 0.9 %, respectively, showing that especially Cu contamination (including Cu-61) can be reduced significantly by almost 95 %. Finally, a DOTA labelling experiment was repeated with the purified Ga-68, as described above, which resulted in a radiolabelling efficiency of 98.3 % ± 1.8 %. This showcases again the successful elimination of the BPHA contamination by the microcolumn purification method. After production of Ga-68 by either elution from a ^{68}Ge/^{68}Ga generator or after irradation of Zn-68 in a cyclotron with subsequent sepa-

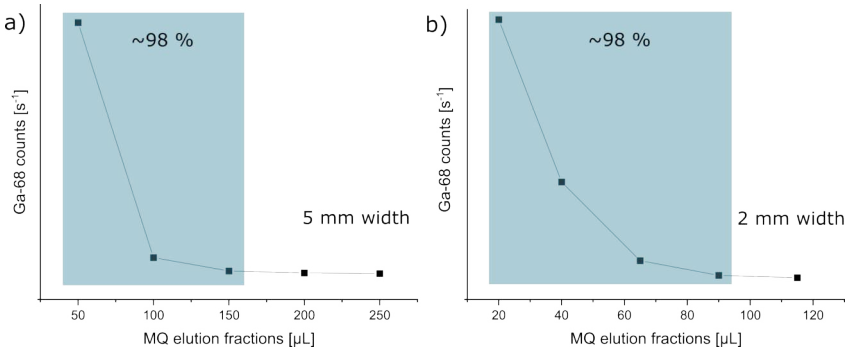

Figure 6.6: Ga-68 elution was achieved into MQ at a flowrate of 100 µL/min from a) a 5 mm wide microcolumn with 21 mg of AG 1-X8 resin and b) a 2 mm wide microcolumn with 8 mg of AG 1-X8 resin. The total eluted Ga-68 percentage was determined as the ratio of Ga-68 activity in the elution fractions vs. the total added Ga-68 activity.

ration of Ga-68 via cation-exchange, an extra purification/concentration step is often necessary, as done in this chapter. Elution from a generator usually results in volumes of 4 to 7 mL [12, 13]. The most commonly used approach for this step includes the use of cation-exchange columns with subsequent elution of Ga-68 in a solution containing high amounts of acetone [12–14, 26]. Rösch et al. obtained 97% of Ga-68 in 400 µL in a 97.6% acetone/0.05 M HCl solution [14] using a cation exchange micro-chromatography column filled with 50 mg of AG 50W-X8 resin (BioRad). Even if Ga-68 was produced via cyclotron irradiation with subsequent separation by cation exchange columns, it is often further purified and concentrated using the same method by Zhernosekov et al. [12] as described above, including the use of an acetone/HCl solution [27]. The presented microcolumn purification method therefore presents a successful alternative to existing purification/concentration methods, while avoiding the use of organic solvent for elutions and resulting in an even smaller elution volume. These results show that the method is not only useful for the integration into a solvent extraction procedure, but also as a purification step for Ga-68 solutions obtained from other production and separation routes, such as generator elutions and cation exchange after cyclotron production.

6.4. Conclusion

It was shown that solvent extraction of medical radionuclides can result in contamination of the used chelators in the collected solutions that are further to be used for radiolabeling of pharmaceuticals. Specifically the chelators BPHA and DIZ were found to cause a contamination that have shown to interfere with subsequent DOTA radiolabelling. Implementation of microcolumn purification step using the AG 1-X8 resin, the BPHA contamination was eliminated, the total acidity of the solution reduced from 6 M HCl to MQ, the volume reduced from 5 mL to less then 150 µL, and Cu contamination

reduced by almost 95 %. This microcolumn purification method is extremely promising also for other separation methods that result in high volumes or acidities, to circumvent the necessity of drying down the highly radioactive solutions.

References

[1] Qaim, S. M. & Spahn, I. Development of novel radionuclides for medical applications. *Journal of Labelled Compounds and Radiopharmaceuticals* **61**, 126–140 (2018).

[2] Qaim, S. M. The present and future of medical radionuclide production. *Radiochimica Acta* **100**, 635–651 (2012).

[3] Qaim, S. M., Spahn, I., Scholten, B., Spellerberg, S. & Neumaier, B. The role of chemistry in accelerator-based production and separation of radionuclides as basis for radiolabelled compounds for medical applications. *Radiochimica Acta* **110**, 707–724 (2022).

[4] Martini, P. *et al.* Perspectives on the use of liquid extraction for radioisotope purification. *Molecules* **24** (2019).

[5] Trapp, S. *et al.* Membrane-based microfluidic solvent extraction of Ga-68 from aqueous zn solutions: towards an automated cyclotron production loop. *EJNMMI Radiopharmacy and Chemistry* **8**, 9 (2023).

[6] Trapp, S., Lammers, T., Paulssen, E. & de Kruijff, R. Rapid, automated radionuclide separation with high yield - towards microfluidic solvent extraction for ^{61,64,67}Cu production. *European research reactor conference 2023 proceedings, Antwerp* 177–184 (2023).

[7] Chakravarty, R. *et al.* Microfluidic solvent extraction of no-carrier-added ^{64}Cu from irradiated Zn target for radiopharmaceutical preparation. *Chemical Engineering Journal Advances* **13**, 100433 (2023).

[8] International Atomic Energy Agency (Vienna). Gallium-68 Cyclotron Production. Tech. Rep., IAEA-TECDOC-1863 (2019).

[9] European Pharmacopoeia 10.0. Radiopharmaceutical preperation (2007).

[10] Dartiguelongue, A., Ramaekers, S. & Ooms, M. *Separation of Lu from Yb for medical purposes: Assessment of Triskem process.* No. ER-0986 in SCK CEN Reports (SCK CEN, Belgium, 2021). Score=1.

[11] Le, V. *et al.* Alternative chromatographic processes for no-carrier added 177lu radioisotope separation. ii. the conventional column chromatographic separation combined with hplc for high purity. *Journal of Radioanalytical and Nuclear Chemistry* **277**, 675–683 (2008).

[12] Zhernosekov, K. P. *et al.* Processing of generator-produced ^{68}Ga for medical application. *Journal of Nuclear Medicine* **48**, 1741–1748 (2007).

[13] Asti, M. *et al.* Validation of ^{68}Ge/^{68}Ga generator processing by chemical purification for routine clinical application of ^{68}Ga-DOTATOC. *Nuclear Medicine and Biology* **35**, 721–724 (2008).

[14] Rösch, F. *et al.* Processing of Ge-68/Ga-68 generator eluates for labeling of biomolecules via bifunctional chelators. *Journal of Nuclear Medicine* **47**, 162P (2006).

[15] Pedersen, K. S., Nielsen, K. M., Fonslet, J., Jensen, M. & Zhuravlev, F. Separation of radiogallium from zinc using membrane-based liquid-liquid extraction in flow: Experimental and COSMO-RS studies. *Solvent Extraction and Ion Exchange* **37**, 376–391 (2019).

[16] Baranyai, Z., Tircso, G. & Rösch, F. The use of the macrocyclic chelator dota in radiochemical separations. *European Journal of Inorganic Chemistry* **2020** (2019).

[17] Morroni, L., Secco, F., Venturini, M., Garcia, B. & Leal, J. M. Kinetics and equilibria of the interactions of hydroxamic acids with gallium(III) and indium([iii]). *Inorganic Chemistry* **43**, 3005–3012 (2004).

[18] Rauf, M., Hisaindee, S., Graham, J. & Al-Zamly, A. Effect of various solvents on the absorption spectra of dithizone and dft calculations. *Journal of Molecular Liquids* **211**, 332–337 (2015).

[19] von Eschwege, K. G., Conradie, J. & Kuhn, A. Dithizone and its oxidation products: A DFT, spectroscopic, and X-ray structural study. *The Journal of Physical Chemistry A* **115**, 14637–14646 (2011).

[20] Thiagarajan, N. & Subbaiyan, M. Stability of dithizone in chloroform-acetic acid solvent system. *Analytica Chimica Acta* **269**, 269–272 (1992).

[21] Wang, L. & Asher, S. A. Refractive-index matching avoids local field corrections and scattering bias in solid-state Na2SO4 ultraviolet raman cross-section measurements. *Applied Spectroscopy* **66**, 157–162 (2012).

[22] Breeman, W., de Jong, M., Visser, T., Erion, J. & Krenning, E. Optimising conditions for radiolabelling of DOTA-peptides with ^{90}Y, ^{111}In and ^{177}Lu at high specific activities. *Eur J Nucl Med Mol Imaging* **30**, 917–920 (2003).

[23] Mueller, D. *et al.* Radiolabeling of DOTA-like conjugated peptides with generator-produced ^{68}Ga and using NaCl-based cationic elution method. *Nature Protocols* **11**, 1057–66 (2003).

[24] Pandey, M. K., Byrne, J. F., Schlasner, K. N., Schmit, N. R. & DeGrado, T. R. Cyclotron production of ^{68}Ga in a liquid target: Effects of solution composition and irradiation parameters. *Nuclear Medicine and Biology* **74-75**, 49–55 (2019).

[25] Oehlke, E. *et al.* Production of Y-86 and other radiometals for research purposes using a solution target system. *Nuclear Medicine and Biology* **42**, 842–849 (2015).

[26] Ocak, M. *et al.* Full automation of ^{68}Ga labelling of DOTA-peptides including cation exchange prepurification. *Applied Radiation and Isotopes* **68**, 297–302 (2010).

[27] Alves, F. *et al.* Production of copper-64 and gallium-68 with a medical cyclotron using liquid targets. *Modern Physics Letters A* **32**, 1740013 (2017).

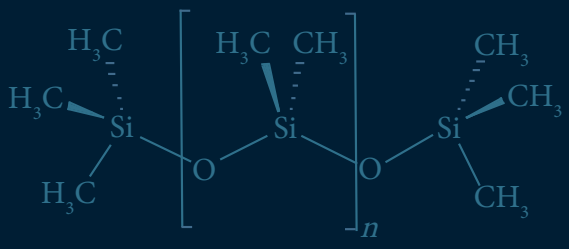

7

Chelator-impregnated PDMS beads for the separation of medical radionuclides

7

Chelator-impregnated PDMS beads for the separation of medical radionuclides

Chelator-impregnated resins have been studied earlier for the chemical separation of elements in aqueous solutions, but issues with their chemical stability have limited their use in the separation of (medical) radionuclides from their respective irradiated targets. In this study, polydimethylsiloxane (PDMS)-based chelator-impregnated beads were developed that showed a high chemical stability against leaching. Several different chelators, namely N-benzoyl-N-phenylhydroxilamine (BPHA) di-2-ethylhexylphosphoric acid (D2EHPA) and dithizone (DIZ) were tested. After impregnation of the PDMS beads with D2EHPA, an in-flow separation study with various radionuclides (Y-90, La-140, and Ac-225) was conducted. The D2EHPA-impregnated beads achieved high adsorption efficiencies of 99.89 % ± 0.14 %, 99.50 % ± 0.10 %, and 98.51 % ± 0.25 %, for Y-90, La-140, and Ac-225, respectively, while co-adsorption of minor amounts (< 3 %) of the target materials (Sr, Ba, and Ra respectively) were obtained. These results, together with the high chemical stability of the PDMS-based resin, highlight the potential of chelator-impregnated resins in the rapidly growing field of (medical) radionuclide production.

The content of this chapter has been patented in Patent Nr 2037212 and published in:

Santoso, A., Trapp, S., Blommestein, I., Saedya, S, de Kruijff, RM, van Steijn, V., van Ommen, JR., 2025. Chelator-impregnated polydimethylsiloxane beads for the separation of medically relevant radionuclides. Separation and Purification Technology 354 (3), 128865.

7.1. Introduction

In the field of nuclear medicine, antibodies, peptides, or small molecules labelled with radionuclides are used for nuclear imaging of a malignancy, or for the delivery of a therapeutic radiation dose to a specific tumor site while minimizing the dose to surrounding healthy tissue [1, 2]. For decades, just a few radionuclides have been used in clinical settings, including the positron (β^+) emitters Ga-68 and F-18 for positron emission tomography (PET) [3, 4], the gamma (γ) emitter Tc-99m for single-photon emission computed tomography (SPECT) [4], and the alpha (α) emitter Ra-223 for the treatment of bone metastases [5]. With technological advancements in targetry and irradiation facilities, increasing numbers of radionuclides are researched for their potential use in nuclear medicine to maximize worldwide capacity and availability of medical radionuclides [1, 2, 6]. Yet, few make it to clinical applications [1, 2, 6, 7].

One of the biggest challenges in realizing the full potential of these radionuclides lies in the production steps and the availability of the enriched target material needed for the production [7]. Most medical radionuclides are produced by irradiation of costly, enriched target materials, either as solid or liquid targets. After irradiation, the produced radionuclide is separated from its respective target and the target material is recovered to be re-used. This separation should be performed quickly, especially in the case of short-lived radionuclides (e.g., Ga-68 with a half-life of $t_{1/2}$ = 67.71 minutes). The separation should also result in a high chemical and radio chemical purity [8] for further use in radiopharmaceutical production. Moreover, concerns about good manufacturing practices (GMP), radiation safety, and cost necessitate a simple, automatable separation process [9, 10].

The most common method for the chemical separation of a product radionuclide from its target is ion-exchange chromatography [11]. In ion-exchange chromatography, the separation of the radionuclide from its target material is commonly done by flowing an aqueous solution containing the product radionuclide and target material through a resin-packed column. The resin consists of a solid support with covalently bound functional (charged) groups. The functional groups act as a binding site, often adsorbing both the radionuclide and the target material. Hereafter, selective elution of the radionuclide, the target, and possible contaminants from the resin is done by subsequently flowing aqueous solutions with a different pH through the column. This also necessitates multiple processing steps to recycle the expensive enriched target material [12–16].

As an alternative to traditional ion-exchange resins, chelator-impregnated resins have been studied. In this approach, a chelator or extracting agent is impregnated onto polymer-based resin beads that act as the solid support [17]. Chelators can have a high selectivity towards the product radionuclide over its target material, forming stable coordination bonds [18]. Due to this high selectivity, a lower amount of resin, and, subsequently,

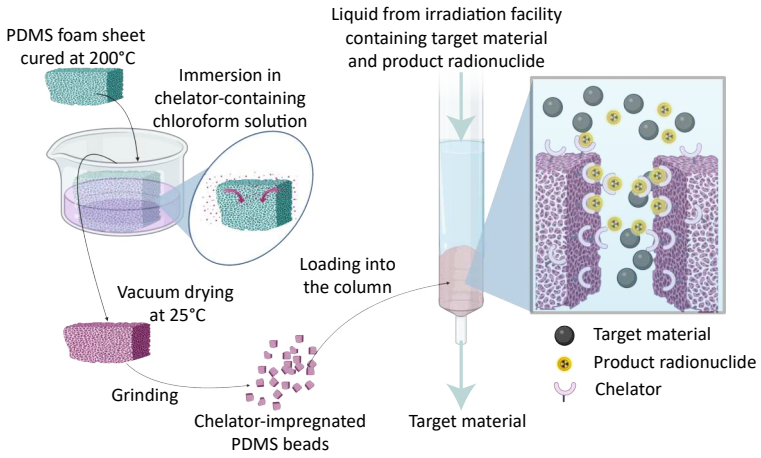

Figure 7.1: Illustration of the fabrication of chelator-impregnated PDMS beads (left) and their use in separating a product radionuclide of interest from its target material (right). Cured PDMS foam sheets are immersed in a chelator-containing chloroform solution before being vacuum-dried and mechanically ground into beads. The chelator-impregnated PDMS beads are loaded into a flow column, through which liquid containing the product radionuclide of interest and its target is flown. The radionuclide selectively binds to the chelator on the beads, resulting in a separated target solution leaving the column. The radionuclide is subsequently collected by flowing an eluting solution with a specific pH through the column.

lower volumes of chemicals are needed [19]. Additionally, chelator-impregnated resins possibly allow for direct recycling of the target when a liquid target is used [19], because the target is not adsorbed on the resin. Despite the potential advantages of chelator-impregnated resins, the chemical stability of the resins remains an issue. When in contact with acidic solutions, the chelator can be leached [20]. Consequently, the resins are no longer usable, the expensive target solution can no longer be recycled directly, and the chemical purity of the radionuclide solution decreases, posing issues with GMP production. To overcome this, a highly stable combination of support material, chelator, and impregnating method with selective adsorption towards the product radionuclide needs to be found [21].

This chapter presents the synthesis and application of chelator-impregnated polydimethylsiloxane (PDMS) beads with high selectivity towards the radionuclide of interest and a high chemical stability against leaching, for the separation of selected medical radionuclides, as illustrated in Fig. 7.1. Unique when compared with other supporting materials used for chelator-impregnated resins, PDMS has a high resistance against acids, but swells upon contact with common organic solvents in which most chelators can be dissolved [22]. This allows the incorporation of a chelator inside the PDMS, before the PDMS shrinks back upon removal of the organic solvent [23], both physically trapping the chelator and hydrophobically binding it to the surface. This improves the chemical stability of the chelator-impregnated resin and subsequently prevents leach-

ing of the chelator, a known problem in the applications of chelator-impregnated resins [21, 24]. Making use of this feature, PDMS beads were impregnated with three different chelators: di-2-ethylhexylphospho-ric acid (D2EHPA), dithizone (DTZ), and N-benzoyl-N-phenylhydroxylamine (BPHA) all dissolved in chloroform. The selection of the chelators was made due to their demonstrated applicability for the separation of the medical radionuclides Ac-225, Cu-64 [25, 26], and Ga-68 [27], respectively.

Subsequently, a case study was conducted using D2EHPA-impregnated PDMS beads for the separation of yttrium and lanthanum (both possessing medically interesting radionuclides such as the β^+ emitting Y-86 and La-132 [28, 29]) from their respective strontium and barium targets, as well as actinium from radium, motivated by the increasing attention for the use of Ac-225 in targeted alpha therapy [30, 31].

7.2. Methods and Materials

7.2.1. Fabrication of chelator-impregnated PDMS beads

PDMS beads were fabricated by suspending the PDMS elastomer (dimethylsiloxane, Sylgard 184 Elastomer Kit, Dow Corning) in water with a mass ratio of 1:5. The suspension was then mixed with a vortex mixer (Vortex Genie 2, Scientific Industries) for 10 minutes before a PDMS curing agent (methyl hydrosilane, Dow Corning) was added with a mass ratio of 1:2 to the elastomer. The mixture was then remixed with the vortex mixer for another 2 minutes before slowly being poured into a beaker containing 10 times as much water by weight at 100 °C. After pouring, an opaque solid foam-like sheet formed on the surface of the boiling water. This PDMS foam sheet was taken out and cured in an oven at 200 °C for at least 10 hours.

Impregnation of the cured PDMS foam sheet with a chelator was done by immersing the sheet in a chloroform solution containing the dissolved chelator at a concentration ranging from 0.01 M to 0.75 M, depending on the solubility of the chelator used and its common practice [32–34]. Three different chelators were studied: N-benzoyl-N-phenylhydroxylamine (BPHA, > 98%, VWR), di-2-ethylhexylphosphoric acid (D2EHPA, > 98%, Merck Sigma), and 1-anilino-3-phenyliminothiourea (dithizone, DTZ, > 98%, Merck Sigma). After immersion for 10 hours at 25 °C and atmospheric pressure in a container open to the atmosphere of a fume hood, the remaining chloroform was removed by placing the container in a vacuum desiccator (~ 10^{-2} mbar) for 30 minutes.

Chelator-impregnated PDMS beads were obtained by grinding the chelator-impregnated PDMS foam sheets in an electric coffee mill grinder (PCKSW 1021 N) for 5 minutes. Initial tests on bare PDMS beads were performed to determine the influence of the operating parameters of the grinder on the diameter of the beads (see Fig. 7.9). With the chosen operating parameters, the median diameter of the chelator-impregnated beads was 0.4 ± 0.1 mm.

7.2.2. Characterization of the PDMS beads

To characterize the diameter of the PDMS beads, brightfield images of the beads were recorded using a camera (ImagingSource DFK33UX273) mounted on an optical microscope (Oxion Inverso) through a 4x Plan Phase LWD Infinity Corrected IOS objective. The obtained images were processed using ImageJ software [35]. From the two-dimensional images, the median diameter of the beads was determined using Martin's diameter. Martin's diameter is defined as the maximum measured distance between opposite sides of the non-spherical beads and was measured transverse to the beads on a line that bisects the projected area [36]. The median diameter of the beads was obtained by measuring Martin's diameter of 100 beads. The PDMS bead diameter was used to obtain a conservative estimate of the available surface area of the PDMS beads. The impregnation of the chelators was characterized using attenuated total reflection Fourier-transform infrared spectroscopy (ATR-FTIR, Thermo Nicolet NEXUS) with a wavelength range of 4000 to 500 cm^{-1}. To observe the surface structure of the chelator-impregnated PDMS beads, field emission scanning electron microscopy was conducted (FE-SEM, Hitachi Regulus SU8230) at a beam current of 1 μA and electron energy of 3-5 keV.

To approximate the mass of the impregnated chelators in the PDMS beads, a thermogravimetric analysis (TGA, METTLER TOLEDO SF/1100) was performed by heating the beads to 800 °C at a rate of 10 °C min^{-1} under nitrogen (100 mL min^{-1}). Since PDMS starts degrading at temperature above 320 °C [37], while the chelators degrade at lower temperatures (200 °C to 300 °C for BPHA [38], 120 °C to 270 °C for D2EHPA [34, 39], and 150 °C to 250 °C for DTZ [40]), the weight difference at 310 °C was used to approximate the chelator mass [39, 41]. To gain insights on the impregnation mechanism, X-ray photoelectron spectroscopy (XPS, ThermoFisher Scientific Nexsa) was performed using an XPS spectrometer equipped with a monochromatic Al Kα radiation source and a pass energy of 30 eV for the survey scan. Since the XPS beam source and detector are placed at an angle, the XPS reading on particles with random shapes and relatively large sizes can be less reliable. Therefore, the XPS measurements were conducted on a flat layer of PDMS, spin-coated on a silicon wafer [42], and immersed in the chelator-containing chloroform solution, following the method described before. A depth profiling was then conducted by etching the surface using Ar^+ ions (2 keV with a raster size of 1 mm) while the differential charging was compensated using a flood gun. CASA-XPS software was used to post-process the XPS peak profiles, where the spectra were charge-corrected with the adventitious carbon peak at 284.8 eV.

7.2.3. Chemical stability test of chelator-impregnated PDMS beads

The stability of the impregnated beads was tested in pure Milli-Q water and the following acidic solutions: 1 M HCl, 12 M HCl (ACS reagent 37%, Merck Sigma), and 1 M HNO_3 (65%, Merck Sigma). To this end, 0.5 g of the chelator-impregnated PDMS beads were

submersed in 5 mL of the acidic solution in a 15 mL Falcon tube, which was continuously shaken (IKA Vibrax VX-2) for short (5 minutes) and long (8 hours) immersion times. The beads were subsequently washed with pure Milli-Q water before being characterized using XPS. In addition, all immersion solutions were characterized using an ultraviolet-visible spectrophotometer (UV-Vis, NanoDrop 2000/2000c) with a wide scan reading (300 - 800 nm). As a reference, the stability of chelator-impregnated silicon (IV) oxide powder (Silica, 99.5%, Millipore, 0.063 -0.200 mm) was tested as well, where the powder was impregnated with the chelators following a similar methodology to the impregnation of PDMS beads. The chelator-impregnated silica powder was subsequently immersed in the same acidic solutions. Once the powder was separated, the immersion liquid was characterized using UV-Vis. Since the concentration of the chelators leached from the silica powder was higher than the concentration from the PDMS beads, the immersion liquid was diluted 1000 times before being measured with UV-Vis. Please note that the concentration of the leached BPHA and DTZ from silica powder after dilution was within the detection limit of the UV-Vis. However, the leached D2EHPA was in the liquid phase at room temperature. Due to its relatively high concentration, the leached D2EHPA from silica powder was highly dispersed in the immersion liquid, resulting in an opaque liquid. This high opacity reduced the reliability of UV-Vis measurement, even after being diluted 10^9 times. Therefore, to quantify the leached D2EHPA from the chelator-impregnated silica powder reliably, the opaque D2EHPA immersion liquid was left in the fume hood for 24 hours to partition. After 24 hours, two liquid phases separated and a clear boundary between the two phases was observed. The top liquid was decanted and the bottom liquid was weighed, indicating the mass of the leached D2EHPA.

To evaluate the interaction between the chelator and the PDMS responsible for the chemical stability (i.e., minimal leaching), the extended Derjaguin-Landau-Verwey-Overbeek theory (EDLVO) was used [43–49]. More specifically, the Gibbs free energy was determined as an indicator of the interaction strength between the chelator and the PDMS. The details of the calculation can be found in Supplementary Information.

7.2.4. Radiotracer production and radioactivity measurements

The radiotracers Y-90, La-140, and Cu-64 were produced by neutron irradiation of Y_2O_3, La_2O_3 (Merck Sigma), and Zn-foil, respectively, at the Hoger Onderwijs Reactor (HOR) of the TU Delft Reactor Institute, the Netherlands. The Zn-foil was irradiated at a thermal neutron flux of $4.24 \cdot 10^{17}$ $m^{-2}s^{-1}$ for 6 hours, and subsequently, dissolved in 8 M nitric acid (HNO_3), slowly dried down on a heating plate, and redissolved in Milli-Q water. Y_2O_3, and La_2O_3 were irradiated at a thermal neutron flux of $4.69 \cdot 10^{16}$ $m^{-2}s^{-1}$ for 3 hours and subsequently, dissolved in 1 M HNO_3 solution, slowly dried down on a heating plate, and redissolved in Milli-Q water. The radiotracer Ga-68 was eluted from an

Eckert & Ziegler IGG100 GMP Ge-68/Ga-68 generator (generously supplied by Erasmus MC, the Netherlands) in 0.1 M HCl. The radiotracer Ac-225 was supplied by Eckert & Ziegler and Ra-223 was supplied by GE Healthcare. Radioactivity measurements of the radiotracers were performed as follows: The Wallac Wizard2 3" 2480 Automatic Gamma Counter from Perkin Elmer (Groningen, the Netherlands) was used for gamma-radiation measurements of Cu-64, Ga-68, La-140, and Ra-223, while the beta-emitting Y-90 was measured with a Liquid Scintillation Counter (tri-carb 2750TR/LL, Packard). Ac-225 was measured indirectly at equilibrium (> 30 minutes after experiments) with its γ-emitting daughter Fr-221 ($t_{1/2}$ = 4.9 minutes).

7.2.5. Separation of radionuclides with chelator-impregnated PDMS beads

Sorption capacity

To measure the sorption capacity of chelator-impregnated PDMS beads for different radionuclide-chelator combinations, 10 mg of the impregnated beads was submerged in 1 mL aqueous solutions with known concentration of Y (1 μM), La (1 μM), Cu (1 nM), or Ga (1 nM). The corresponding radioactive tracers Y-90, La-140, Cu-64, and Ga-68 were added to their respective solutions at concentrations between 1 - 10 kBq/mL. For Y and La, PDMS beads impregnated with the chelator D2EHPA were selected. For Cu and Ga, DTZ and BPHA were chosen, respectively, due to their use in prior studies on microfluidic solvent extraction of Cu-64 [25, 26] and Ga-68 [27]. The solutions containing Y and La had a pH of 6, the Cu solution had a pH of 0, and the Ga solution had a pH of 2, according to the optimal pH for the extraction with these chelators, as determined by solvent extraction experiments [25–27]. The vials containing the aqueous solutions and PDMS beads were put on a Vortex-Genie 2 (Scientific Industries, Inc) at the highest speed for 1 hour to ensure equilibrium was reached. Afterwards, the aqueous solutions were pipetted out of the vials, avoiding the PDMS beads. The concentration of Y, La, Cu, and Ga in the aqueous solutions was determined by measuring the radioactivity A of their corresponding radiotracers, which are representative of the total concentrations. The sorption capacity was calculated by subtracting the measured amount of Y-90, La-140, Cu-64, or Ga-68 after the adsorption ($n_{\text{aq, depleted}}$) from the initial amount ($n_{\text{aq, initial}}$), and dividing the adsorbed amount by the mass of the chelator-impregnated PDMS beads (m_{beads}), i.e.,

$$\text{Sorption capacity } [\frac{\text{mol}}{\text{g}}] = \frac{n_{\text{aq, initial}}\ [\text{mol}] - n_{\text{aq, depleted}}\ [\text{mol}]}{m_{\text{beads}}\ [\text{g}]}. \tag{7.1}$$

Experiments were done in triplicate and errors are given as one standard deviation of the mean.

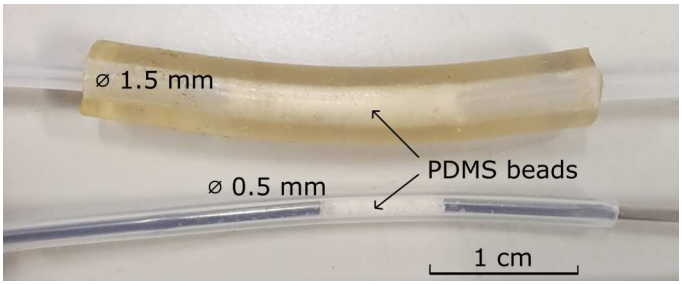

Figure 7.2: Chromatography columns with chelator-impregnated PDMS beads used for the separation of radionuclides from their target. D2EHPA-impregnated PDMS beads in a column with an inner diameter of 1.5 mm used for the in-flow separation of Y and La (top; loading 20 mg) and in a column with an inner diameter of 0.5 mm used for the in-flow separation of Ac-225 (bottom; loading 5 mg).

In-flow separation

To test the in-flow separation of Y from Sr and La from Ba, 20 mg of D2EHPA-impregnated PDMS beads were loaded into a tubing with a diameter of 1.5 mm (Fig. 7.2, top). The solutions consisted of 1 M $Sr(NO_3)_2$ with 100 μM [^{90}Y]$Y(NO_3)_2$ or 0.1 M $Ba(NO_3)_2$ with 10 μM [^{140}La]$La(NO_3)_2$, dissolved in Milli-Q water (nomenclature adapted from [50]). For the Ac-225 separation from [^{223}Ra]$Ba(NO_3)_2$, only 5 mg of D2EHPA-impregna-ted PDMS beads were loaded into a tubing with a diameter of 0.5 mm (Fig. 7.2, bottom), because of the significantly lower Ac-225 concentration in the solution (in the picomolar range, compared to the micromolar range for Y and La). The solution consisted of 0.1 M $Ba(NO_3)_2$ with 10 kBq/mL Ac-225 and 10 kBq/mL of Ra-223. These model solutions were used for the experiments to collect results, upon which future experiments with irradiated targets can be designed. The aqueous solutions containing the radionuclides were filled into syringes and pushed through the column by a syringe pump (AL-1000 Programmable Syringe pump 941-371-1003 from World Precision Instruments Inc.) at various flow rates in the range of 0.1 - 6 mL/min. The adsorption efficiency (AE) was defined as the relative difference in measured radioactivity before (A_{initial}) and after ($A_{\text{after adsorption}}$) the in-flow separation, i.e.,

$$AE\ [\%] = \left(1 - \frac{A_{\text{after adsorption}}}{A_{\text{initial}}}\right) \times 100\%. \tag{7.2}$$

After the adsorption, the radionuclide of interest needs to be eluted from the beads into another aqueous solution. Herefore, different HCl concentrations were tested, ranging from 0.1 M to 4 M HCl, to see if a difference in acidity leads to a difference in elution speed. The flow rate was kept at 0.1 mL/min. 100 µL fractions were collected consecutively and their radioactivity was measured as described above. Co-adsorption of Sr, Ba, and Ra-223, from 1 M $Sr(NO_3)_2$ for Sr, and 0.1 M $Ba(NO_3)_2$ for Ba and Ra-223, was also studied in-flow using the above procedure and the adsorption efficiency was deter-

mined according to Eq. 7.2. Of note, for Sr and Ba, instead of the ratio of the radioactivities, the ratio of the concentrations before and after the in-flow separation was used, as measured by inductively coupled plasma mass spectrometry (ICP-MS, Perkin Elmer, NexION 2000). For the separation of Ac-225 from Ra-223 a separation factor (S) was calculated additionally, for the results at the optimal flowrate of 0.3 mL/min, according to Eq 7.3, where D is defined as the ratio of the adsorbed and not adsorbed radioactivity.

$$S = \frac{D_{\mathrm{Ac}}}{D_{\mathrm{Ra}}} \tag{7.3}$$

The co-adsorption of the potential metal contaminants Ni, Fe, Cu, Zn, Pb, Al, and Ca to the D2EHPA-impregnated PDMS beads was studied as well. These contaminations are commonly found in irradiated targets [51]. They are essential to study, since one important parameter for the use of the already separated radionuclides is the specific activity, which is the radioactivity per unit mass. A solution consisting of 100 µg/L of each metal contaminant was flown through the column as described above. A flow rate of 0.3 mL/min was applied, which was identified as the optimal flow rate for Ac-225 adsorption, as explained later. The initial concentrations and concentrations after the adsorption, as well as the elution into 0.1 M HCl (in which Ac-225 is collected), were measured by ICP-MS and the *AE* was calculated as described above. The total recovery of the contaminants was calculated as

$$\text{Total recovery [\%]} = \frac{c_{\mathrm{elution}}}{c_{\mathrm{initial}}} \times 100\%, \tag{7.4}$$

where c_{elution} is the measured concentration of the contaminant in the elution and c_{initial} is the initial concentration of the contaminant in the solution during the in-flow separation. All experiments were executed in triplicate and errors are given as one standard deviation of the mean.

7.3. Result and Discussion

7.3.1. PDMS beads impregnated with three different chelators

Fig. 7.3 shows the FTIR spectra of bare PDMS beads and PDMS beads impregnated with three different chelators. These spectra confirm the presence of the chelators on the impregnated beads, evident from peaks in the spectra specific to the specific bonds in the molecular structure of the different chelators. For BPHA, its presence is confirmed by the peak on the wavelength of 1622 cm^{-1} associated with the C=O bond of BPHA and on the wavelength of 3171 cm^{-1} associated with the O-H bond [49] (see Fig. 7.3 (a)). For D2EHPA, its presence is confirmed by the peak on 1230 cm^{-1} corresponding to the P=O bond of D2EHPA and by extra stretching in the 3000 - 2900 cm^{-1} region (see Fig. 7.3 (b)). Although DTZ is harder to observe than the other two chelators as most of its

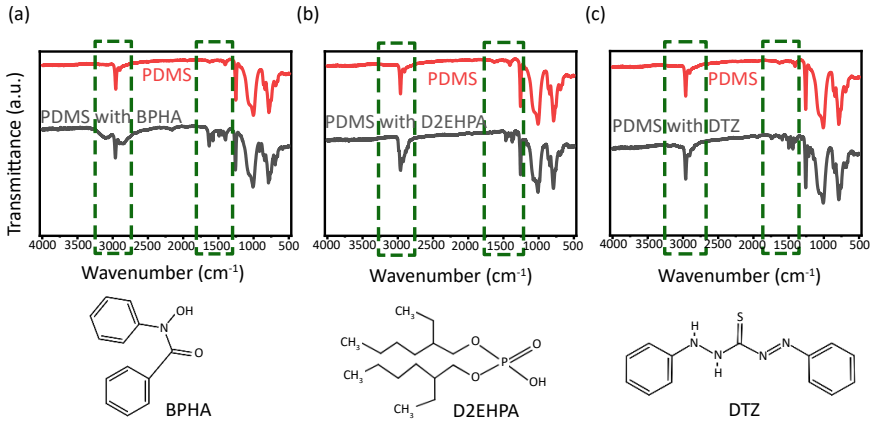

Figure 7.3: FTIR spectra of bare PDMS beads and PDMS beads impregnated with the chelators BPHA (a), D2EHPA (b), and DTZ (c), along with their corresponding chemical structure. The spectra of bare PDMS beads are in red, the spectra of the impregnated PDMS beads are in grey, and the peaks characteristic for the chelators are highlighted in the green boxes. The FTIR of the pure chelators can be found in the literature [34, 49, 52].

characteristic peaks overlap with the peaks of PDMS, the presence of DTZ was confirmed by the peaks in the 3000 - 2900 cm^{-1} region (see Fig. 7.3 (c)).

Since the final application of the chelator-impregnated PDMS beads is to adsorb radionuclides, the chelators are preferably located at the outer surface, where most of the adsorption takes place. While FTIR spectra indicate the presence of the characteristic peaks corresponding to the chemical groups of the chelators, its penetration depth is relatively high (in µm range), and it does not reveal where the chelators are present. Therefore, additional FE-SEM and XPS measurements were done, showing that the surface morphology changes with the impregnation (see Fig. 7.11). More specifically, particle-like structures can be seen on the surface of the PDMS beads impregnated with BPHA and DTZ, while a smoothening-like effect is observed on the surface of the PDMS beads impregnated with D2EHPA. This difference may arise from the fact that D2EHPA is in liquid form at room temperature, while DPHA and DTZ are in powder form, resulting in crystallites on the PDMS surface after evaporation of the chloroform. Furthermore, the XPS survey spectra show the presence of characteristic atomic peaks on the first few nanometers of the surface of the samples: a nitrogen peak on the PDMS impregnated with BPHA, a phosphorus peak on the PDMS impregnated with D2EHPA, and a nitrogen peak, and a sulfur peak on the PDMS impregnated with DTZ (see Fig. 7.10). The XPS survey scans on the surface thus agree with the visual FE-SEM inspections, which indicates that the chelators may be present on the surface of the PDMS beads. Interestingly, the depth profiling of the samples shows the characteristics peaks even after etching of 400 seconds (see Fig. 7.10). This indicates infiltration of the chelators inside the PDMS beads.

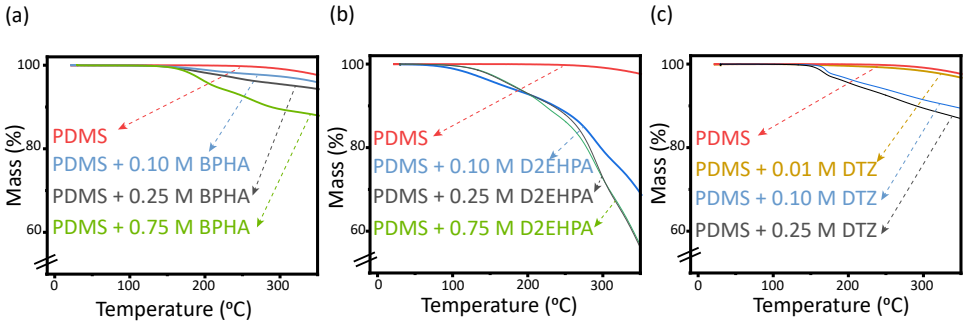

Figure 7.4: Quantification of the amount of chelator impregnated in the PDMS beads using thermogravimetry. Thermogravimetry of PDMS beads impregnated with (a) BPHA, (b) D2EHPA, and (c) DTZ at various concentrations of these chelators in chloroform.

This infiltration is explained by the entrapment of the chelators in the matrix of PDMS during the chloroform swelling process [53]. This swelling process hence is important, increasing the loading capacity of the chelators in the PDMS beads.

To investigate further whether the chelators are chemically or physically sorbed, the XPS survey scans of Si2p are resolved. The Si2p peaks are chosen as they are exclusive peaks present in PDMS beads and not in the chelators. Fig. 7.12 shows the scan of Si2p where both bare PDMS and PDMS impregnated with three different chelators have comparable peaks, indicating no chemical changes in the Si atomic bond. This result implies the absence of a chemical interaction between the chelators and the Si atoms of the PDMS beads. Additionally, XPS survey scans of C1S were conducted and resolved. In Fig. 7.12, extra peaks are visible in the C1s scans (at 288.1 eV) of the chelators-impregnated PDMS beads when compared with the C1s scans of bare PDMS beads. These peaks correspond to the presence of C-O bonds in the samples. However, this C-O bond is typically present in BPHA, D2EHPA, and DTZ. Thus, to infer the presence of chemical interaction between PDMS beads and the chelators from this bond is difficult. Furthermore, most C1s peaks (as well as the O1s peaks) also experience broadening and shifts, common occurrences in non-conductive samples such as PDMS beads. The broadening and the shifts of the peaks make the inferring of the resolve less reliable. From the resolves of Si2p, it is arguable that the impregnation process, as indicated by other works [20, 54], is a physisorption process, with a swelling-induced transport of chelators into the matrix of the PDMS beads.

Since the maximum sorption capacity is limited by the amount of chelators present, it is important to quantify the amount of impregnated chelators on the PDMS beads. This amount can be determined based on thermogravimetry. The mass of the beads was measured at temperatures increasing from 25 °C to 800 °C and the mass of the samples impregnated with the three types of chelators was calculated at various concentrations

relative to the initial mass of the samples at 100 °C. Following the common practice of assuming that the mass decline between 25 °C and 100 °C is due to sample dehydration, the mass difference between bare PDMS beads and impregnated PDMS beads at 310 °C was considered, where bare PDMS starts decreasing in mass, as an approximation of the total mass of the impregnated chelators. For BPHA-impregnated PDMS beads, the mass difference increases from 1.8 % ± 0.1 % for PDMS beads impregnated with 0.10 M BPHA in chloroform to 3.7 % ± 0.1 % and 9.7 % ± 0.2 % for PDMS beads impregnated with 0.25 M and 0.75 M BPHA in chloroform, respectively (see Fig. 7.4(a)). This indicates an increasing BPHA amount impregnated in the PDMS beads as the available BPHA in chloroform increases. Since the solubility of BPHA in chloroform is around 155 g L^{-1} (equivalent to 0.72 M [32]), it can be assumed that the impregnated BPHA amount does not increase further. This hypothesis is supported by the TGA results of DTZ-impregnated PDMS beads where the beads impregnated with 0.01 M DTZ in chloroform show a mass difference of 1.4 % ± 0.1 %, while the beads impregnated with DTZ solutions of 0.10 M and 0.25 M, above their saturation concentration (solubility of DTZ is 17 g L^{-1} or 0.075 M in chloroform [33]) show no significant difference in their mass difference (7.4 % ± 1.0 %, and 8.9 % ± 1.7 %, respectively) (see Fig. 7.4(c)). For D2EHPA, liquid at room temperature, a similar trend of increasing mass difference between PDMS beads impregnated with 0.10 M and 0.25 M D2EHPA in chloroform is observed, from 21.0 % ± 0.9 % to 30.9 % ± 1.1 % (see Fig. 7.4(b)). The difference does not significantly increase when the beads are impregnated with 0.75 M (31.3 % ± 1.2 %), indicating the maximum capacity of the PDMS matrix in accommodating D2EHPA.

To confirm this hypothesis about PDMS matrix capacity, an additional swelling test was conducted. The bare PDMS bead samples were submersed in chloroform for 10 hours, resulting in a volumetric increase of 16.0 % ± 2.2 % and a mass increase of 23.4 % ± 3.1 %. This PDMS volumetric increase due to swelling corresponds well with the mass increase, as the density of chloroform is 1.489 g mL^{-1}, indicating the filling of the PDMS matrix with chloroform. However, a similar calculation was applied to 0.25 M D2EHPA-impregnated PDMS beads samples, the expected mass increase (15.6%, the density of D2EHPA is 0.976 g mL^{-1}) due to D2EHPA impregnation is lower than the measured mass decrease by TGA (30.9 % ± 1.1 %). This difference could happen due to the adsorption of D2EHPA on the surface of the PDMS beads. To resolve this, the surface adsorption effect was reduced by immersing a PDMS block with a lower surface-to-volume ratio (1 cm x 1 cm x 1 cm) in a similar chloroform solution containing 0.25 M D2EHPA. Next, TGA measurements were conducted on the cut samples to approximate the amount of the impregnated D2EHPA. The result shows a much lower mass decrease (15.8%) compared to the bead samples. This measured mass decrease is closer to the calculated mass increase due to swelling.

From both tests, it can be assumed that the total impregnated chelator amount is the

sum of the amount of D2EHPA accommodated inside the PDMS matrix and the amount of D2EHPA located on the surface. This result also emphasizes the importance of the PDMS beads' diameter, where a smaller diameter leads to an increase in surface area and subsequently an increase in the impregnation amount. While this study focuses on a fabrication method using simple kitchen equipment, there have been many studies on increasing the surface area of PDMS beads (e.g., PDMS beads with a median diameter of 1 μm obtained using droplet microfluidics [55] or porous PDMS using template moulding [56]). Fig. 7.4 also implies that the chelator-impregnated PDMS beads are stable at temperatures below 120 °C.

7.3.2. Chemical stability of the chelator-impregnated PDMS beads

A known problem in the applications of chelator-impregnated resins is the low chemical stability, leading to leaching of the impregnated chelator over time, causing contamination during elution [21, 24]. To assess the chemical stability of the chelator-impregnated PDMS beads, the beads were immersed in three solutions of different acidity: Milli-Q water, 1 M HCl, and 12 M HCl. For D2EHPA-impregnated PDMS beads, the XPS spectra obtained after washing and drying are shown in Fig. 7.5(a). P2p peaks are observed in all samples, indicating the presence of D2EHPA in all the samples. Furthermore, the phosphorus atom remains in a phosphate form (at 134 eV) with no significant chemical state change even after washing it with 12 M HCl. The Cl2p spectra show no chlorine sorbed into the PDMS beads, reducing the possibility of contamination during the separation of the radionuclides.

Complementing the XPS results, Fig. 7.5(b) shows the UV-Vis spectra of the immersion solutions. Pure D2EHPA (100%(v/v)) shows a peak at 274 nm [57], while no peaks are observed in all liquid samples after 5 minutes of immersion, indicating at least no detectable D2EHPA. The liquids remain visibly clear and no fluid separation after 24 hours is observed. On the other hand, the immersing liquid from D2EHPA-impregnated silica powder is opaque and cloudy, indicating the presence of dispersed D2EHPA. After decanting, these impregnated silica samples show a D2EHPA release of 220 mg/g ± 13 mg/g, 45 mg/g ± 11 mg/g, and 52 mg/g ± 12 mg/g in Milli-Q water, 1 M HCl, and 12 M HCl, respectively.

When the stability of the D2EHPA-impregnated PDMS beads is challenged by immersing them in both 1 M HCl and 12 M HCl for a longer period (8 hours), as well as in a different acid (1 M HNO_3), no indication of leached D2EHPA can be found, aside from the samples immersed for 8 hours in 12 M HCl (see Fig. 7.5(b)). The stability tests were also done for BPHA-impregnated PDMS beads and DTZ-impregnated PDMS beads along with BPHA- and DTZ-impregnated silica powder. As expected, all BPHA-impregnated PDMS samples (washed and non-washed) show the presence of N1s peaks in the XPS spectra, while no BPHA-indicative peaks are found in the immersing liquids

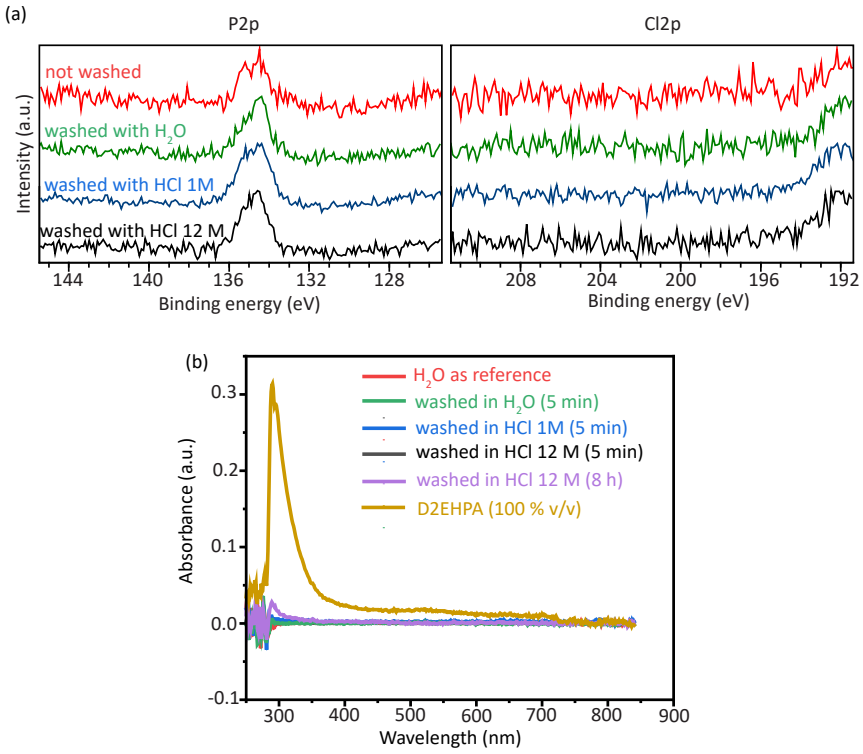

Figure 7.5: Chemical stability of D2EHPA-impregnated PDMS beads against leaching measured with XPS and UV-Vis. (a) XPS P2p scan and Cl2p scan of D2EHPA-impregnated PDMS beads before and after 5 minutes of immersion in solutions of different acidity (b) the corresponding UV-Vis spectra of the immersion solutions.

around 200 nm (indicating the N-phenylhydroxamide group [58]) in the UV-Vis spectra, (see Fig. 7.13(a) and (c), respectively). The difference in the shape of the N1s peaks in the XPS spectra of non-washed BPHA-impregnated PDMS samples is due to protonation of BPHA, as reported in previous work [59]. Similar behavior is observed for all DTZ-impregnated PDMS samples, with the presence of N1s XPS peaks for washed and non-washed beads, while no peaks are found in the immersing liquids around 450 nm and 618 nm (indicative for DTZ [60]) (see Fig. 7.13(b) and (d), respectively). In contrast, all immersion liquids of the impregnated silica powder samples show intense peaks in the UV-Vis spectra (see Fig. 7.13(e) and (f)). Please note, that in Fig. 7.13(f), the peaks shifted due to possible oxidization of DTZ [60].

To understand the reason behind the stability of the impregnated chelator on PDMS beads, the interactions between the chelator and PDMS in an aqueous medium was studied using the extended Derjaguin-Landau-Verwey-Overbeek (EDLVO) theory [46, 61]. The Gibbs free energy was determined using this theory, complemented by a series

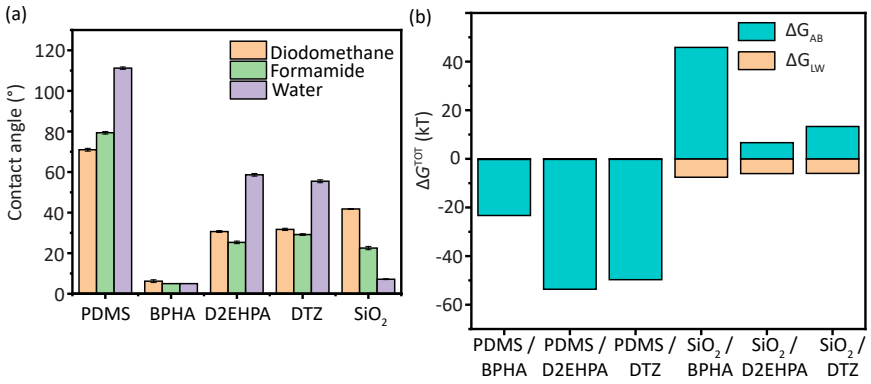

Figure 7.6: Approximation of hydrophobic interaction between PDMS beads and chelators. (a) The average measured static contact angle of non-polar liquid diiodomethane and polar liquid formamide and water on various substrates (the error bars represent 1 standard deviation from the average) and (b) Gibbs free energy calculated for estimating the interaction strength using the extended Derjaguin-Landau-Verwey-Overbeek approach.

of contact angle measurements. This indicates the presence (or absence) of hydrophobic interactions, a common interaction found in polymeric materials, where a negative Gibbs free energy indicates the presence of hydrophobic interactions [45, 47, 62]. Fig. 7.6(a) shows the measured contact angle of three different liquids on PDMS and the three different chelators. Additionally, reference measurements were performed on silica. Our reported contact angle values for PDMS and silica are comparable with previous works [63–66]. Fig. 7.6(b) shows the subsequently calculated Gibbs free energy. The interaction between PDMS and all three chelators shows a negative Gibbs free energy, indicating the presence of hydrophobic interaction. This is consistent with previous works on PDMS [67–69]. From Fig. 7.6(b), most of the negative Gibbs free energy for the PDMS-chelator combinations is contributed by the acid-base interaction (ranging from -20 kT to -60 kT), while the Lifshiftz-van der Waals interaction contributes much less (~-1 kT). This suggests that the resulting hydrophobic interaction is due to hydration repulsion towards the chelators instead of a direct attraction force of PDMS [70, 71]. Furthermore, while the interaction between PDMS and D2EHPA, and PDMS and DTZ show comparable negative values, the interaction between PDMS and BPHA shows a less negative Gibbs free energy, implying a relatively weaker hydrophobic interaction. This result is in line with the theoretical use of the octanol-water partition coefficient (K_{ow}) of the chelators to predict the sorption behavior (and sorption strength) of the chelators [72] on hydrophobic material. A positive K_{ow} indicates a partition preference of the chelators in octanol (as opposed to water), with higher K_{ow} indicating a higher octanol partition, and subsequently stronger hydrophobic interaction. Previous works indicate K_{ow} of 4 for D2EHPA [73], 3-4 for DTZ [74] and 2-3 for BPHA [75]. In sharp contrast to the

Table 7.1: Sorption capacity of PDMS beads with different chelators, specific for yttrium (Y), lanthanum (La), copper (Cu), and gallium (Ga) (n=3).

Chelator	Element	Sorption Capacity
D2EHPA	Y	2.75 ± 0.53 mg/g
D2EHPA	La	4.03 ± 0.41 mg/g
DTZ	Cu	4.0 ± 1.1 ng/g
BPHA	Ga	0.329 ± 0.092 ng/g

interaction between the chelators and PDMS, all interactions between the chelators and silica show a positive Gibbs free energy, explaining the high release of the chelators when immersed in an aqueous medium (Fig. 7.13). However, this approach neglects a plausible complementary phenomenon where the chelator molecules are physically trapped in the PDMS matrix and therefore become immobile. While this complimentary effect is not incorporated, the comparison to the silica samples already shows that chelators are more strongly bound to PDMS beads than to silica powders.

7.3.3. Sorption capacity of PDMS beads with different chelators

Table 7.1 shows the measured sorption capacity of D2EHPA-, DTZ-, and BPHA-impregnated PDMS beads, for Y, La, Cu, and Ga, respectively. The results show a much higher sorption capacity of the D2EHPA-impregnated PDMS beads over the DTZ- and BPHA-impregnated PDMS beads. More specifically, the D2EHPA-impregnated PDMS beads have a six orders of magnitude higher sorption capacity towards Y and La than the DTZ-impregnated PDMS beads have towards Cu, and a seven orders of magnitude higher sorption capacity than the BPHA-impregnated PDMS beads have towards Ga. This proves again the significantly higher integration of D2EHPA into the PDMS compared to BPHA and DTZ, with the underlying reasons discussed in the previous section.

In comparison to other commercial ion-exchange resins, the D2EHPA-impregnated beads show a lower sorption capacity. For example, the Dowex 50W-X8 resin has a sorption capacity towards rare earth elements between 191 and 294 mg/g [76], Ln resin has a sorption capacity of 30.67 mg/g for Eu [77], the Amberlite IR120H (AIR120H) resin has a sorption capacity of 8.2 mg/g for Ce [78], and HDEHP-loaded microcapsules (impregnated) have a sorption capacity of 58.07 mg/g for Eu [77]. Since the primary focus of this study is on the development of a selective and stable resin, optimizing the sorption capacity for the chelator-impregnated beads is outside the scope of the present work. It can be expected that higher sorption capacities can be obtained, for example by optimization of the diameter and the porosity of the beads for example as shown by [79] and [55].

7.3.4. In-flow separation with D2EHPA-impregnated PDMS beads

Given the high chemical stability and the higher sorption capacities of the D2EHPA-impregnated PDMS beads for Y and La, in-flow separation and elution studies were done using a chromatography column with these combinations of chelator and radionuclides. For the separation of La from its Ba target, an aqueous solution consisting of 10 μM La (and a La-140 radiotracer with 0.1 M $Ba(NO_3)_2$) was prepared and injected the mixture at various flow rates in the column to study the influence of the residence time on the adsorption efficiency. For the separation of Y from its Sr target, an aqueous solution containing 100 μM Y (and a Y-90 radiotracer) and 1 M $Sr(NO_3)_2$ was prepared, and injected in the column.

For the lowest range of flow rates studied, it can be observed that both Y and La were adsorbed to the D2EHPA-impregnated PDMS beads with an almost 100 % adsorption efficiency (see Fig. 7.7(a)). For increasing flow rates, i.e., decreasing residence times, the adsorption efficiency declines. A notable decline can be observed for flow rates above 1 mL/min and 4.5 mL/min for Y and La, respectively. Apart from this difference in onset, a clear difference in slope is visible. While the adsorption efficiency already decreases from 99.89 % ± 0.14 % at 1 mL/min to 77.5 % ± 1.8 % at 2.6 mL/min for Y, it only decreases from 99.50 % ± 0.12 % at 4.5 mL/min to 91.1 % ± 1.4 % at 6 mL/min for La. The difference in onset and slope might be explained by (I) the concentration of Y being ten times higher than the concentration of La in their respective solutions and (II) the smaller ionic radius of Y.

For the application of the chelator-impregnated PDMS beads in the field of nuclear medicine, it is not only important that the adsorption efficiency of the radionuclide of interest is close to 100 %, but also that the adsorption efficiency of the corresponding target is as low as possible. Therefore, the co-adsorption of the Ba and Sr target solutions was studied at the largest flow rates that still result in high adsorption efficiencies of La and Y. Ba co-adsorption was measured to be 1.28 % ± 0.45 % at a flow rate of 4 mL/min and Sr co-adsorption was 1.24 % ± 0.57 % at a flow rate of 1 mL/min. From these results, the co-adsorption of the corresponding target material is low, showing a promising application in the clinical field. Elution of Y and La from the D2EHPA-impregnated PDMS beads was studied for elution solutions of different acidity. The elution of Y is incomplete after 1 mL at only 65 %, while the elution of La is about 85 % in the first 1 mL (see Fig. 7.7b) and c)). This difference in behavior might be due to the higher concentration of Y, necessitating higher volumes to increase the total eluted fraction. The acidity of the solutions does not significantly influence the elution profiles. Additionally, the smaller ionic size of Y leads to a more stable complex with D2EHPA. This trend of increasing complex stability with increasing charge density (i.e., decreasing ionic radius) is often found in chelate complexation [80] and was shown before for lanthanide and actinide complexes [81], making it more difficult to fully elute in small volumes.

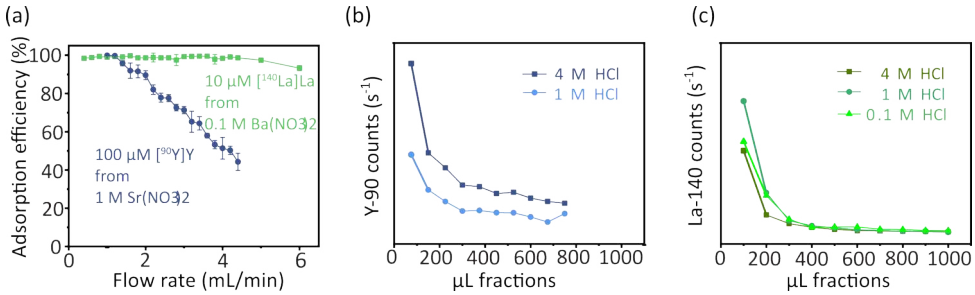

Figure 7.7: Chromatography column separation and elution with D2EHPA-impregnated PDMS beads for Y and La. (a) In-flow separation of 10 μM [^{140}La]La and 100 μM [^{90}Y]Y from their respective target solutions of 0.1 M $Ba(NO_3)_2$ and 1 M $Sr(NO_3)_2$ (n=3). (b) Elution profile of [^{90}Y]Y into 4 M and 1 M HCl at a flow rate of 0.1 mL/min (n=1). (c) Elution profile of [^{140}La]La into 4 M, 1 M and 0.1 M HCl at a flow rate of 0.1 mL/min (n=1).

A radionuclide that currently receives increasing attention for its potential in targeted alpha therapy is Ac-225. For this reason, the in-flow separation Ac-225 from its target Ra-223 was investigated with subsequent elution in a chromatography column loaded with D2EHPA-impregnated PDMS beads. Since the total concentration of Ac-225 compared to Y and La was significantly lower by nine orders of magnitude, only 5 mg of PDMS beads was used. The results again show an adsorption efficiency close to 100 % for the lower range of flow rates, with a decline in adsorption efficiency for increasing flow rate (see Fig. 7.8(a)). At a flow rate of 0.3 mL/min, the adsorption efficiency of Ac-225 is 98.51 % ± 0.25 % , while the co-adsorption of its target Ra-223 is 0.94 % ± 0.57 %.

Elution of Ac-225 was achieved with 0.1 M HCl at a flow rate of 0.1 mL/min. 80.3 % ± 0.9 % of Ac-225 was eluted in the first 1 mL and 93.2 % ± 1.7 % in the first 2 mL (see Fig. 7.8b)). The final eluted solution contains 0.053 % ± 0.014 % of the initial amount of Ra-223 in the first 1 mL and a total of 0.068 % ± 0.015 % in 2 mL, resulting in a separation factor that averages over 6000. The column was washed with Milli-Q water before the elution of Ac-225, reducing the amount of Ra-223 in the elution solution by 90.8 % ± 2.5 %. A known problem during the production of Ac-225 is the contamination of the Ac-225 solution with metal contaminants, as reported by Ramogida et al. [51]. For this reason, the in-flow separation and elution of these metals was studied as well. Table 7.2 shows the adsorption efficiency and the total recovery. From all measured metal contaminants only Zn is co-adsorbed at 15.7 % ± 7.1 % and also fully eluted in 0.1 M HCl, resulting in a total recovery of 15.1 % ± 7.1 % in the elution fraction. While Fe shows a high *AE* of 82.8 % ± 4.6 %, it is not eluted in 0.1 M HCl and only 1.38 % ± 0.24 % of the initial amount is present in the elution solution, meaning that it is also cleared from the target solution. All other tested elements are neither co-adsorbed nor eluted in significant amounts. These results indicate a high degree of decontamination during the Ac-225 separation with the presented D2EHPA-impregnated PDMS beads.

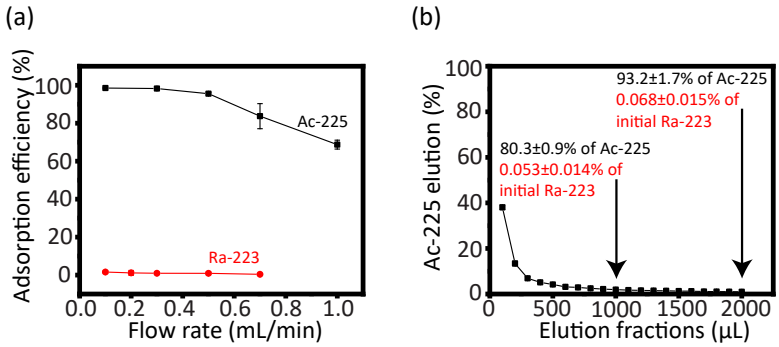

Figure 7.8: Chromatography column separation and elution with D2EHPA-impregnated PDMS beads for Ac-225. (a) In-flow separation of Ac-225 at different flow rates (n=3). b) Elution profile of Ac-225 indicated by Fr-221 in 0.1 M HCl at a flow rate of 0.1 mL/min (n=2).

Overall, the D2EHPA-impregnated PDMS beads have proved successful in the separation of Ac-225 from [^{223}Ra]Ba$(NO_3)_2$ with around 93 % of Ac-225 and below 0.1 % of Ra-223 in the first 2 mL of elution. In comparison, multiple other methods have been investigated in the literature for the separation of Ac-225 from radium targets, including ion-exchange column chromatography (using AG50×8 [82] or AG50X4 [83], Ln- [84] or DGA resin [85]), microfluidic ion-exchange [83], as well as solvent impregnated resins [86]. While all of these methods achieve a good separation of Ac-225, they all show different drawbacks, such as the need for (i) large volumes of chemicals [82, 85, 86], (ii) highly acidic solutions for elution [82, 83, 86], (iii) slow processing [83, 86], or (iv) additional clean-up steps [84]. Furthermore, it has been reported that DGA resin is highly sensitive to radiolysis and extra washing steps are needed to reduce radiolytic degradation products [85], partially due to the characteristic water loading [87].

While it remains to be shown if the presented D2EHPA-impregnated PDMS beads have a higher radiation stability, D2EHPA and PDMS separately are reportedly highly resistant against radiation [88, 89]. Thus, in comparison with existing separation methods, the presented chelator-impregnated PDMS beads are promising to separate medical radionuclides in a commercial setting.

Table 7.2: Adsorption of metal contaminants during the separation of Ac-225. Adsorption efficiency (*AE*) and total recovery of the metal contaminants in the 0.1 M HCl elution. The concentrations of the metals were 100 µg/L. Experiments were done in triplicate and errors are given as one standard deviation of the mean.

	Ni	Fe	Cu	Zn	Pb	Al	Ca
AE [%]	0.99 ± 0.86	82.8 ± 4.6	0.95 ± 0.64	15.7 ± 7.1	14.5 ± 6.6	48.1 ± 1.8	11.78 ± 0.88
Recovery [%]	0.020 ± 0.003	1.38 ± 0.24	0.92 ± 0.06	15.1 ± 7.1	4.8 ± 1.5	0.13 ± 0.08	3.81 ± 0.97

7.4. Conclusions

Chelator-impregnated PDMS beads were presented that allow the selective and efficient separation of the medically-interesting radionuclides (Y-90, La-140, and Ac-225) from their liquid target ($Sr(NO_3)_2$, $Ba(NO_3)_2$, and $[^{223}Ra]Ba(NO_3)_2$), with minimal leaching of the chelator from the beads when contacted with the acidic solutions used for adsorption and subsequent elution of the radionuclides. This minimal leaching is beneficial for the purity of the radionuclide solution and at the same time offers the possibility of direct liquid target recycling. The simple fabrication of the chelator-impregnated PDMS beads together with the ability to impregnate PDMS with different types of chelators offers a versatile approach towards increasing the applicability of chelators for the simple, automatable separation of medical radionuclides.

References

[1] Oyen, W. *et al.* Targeted therapy in nuclear medicine—current status and future prospects. *Annals of Oncology* **18**, 1782–1792 (2007).

[2] Weber, W. A. *et al.* The future of nuclear medicine, molecular imaging, and theranostics. *Journal of Nuclear Medicine* **61**, 263S–272S (2020).

[3] Sanchez-Crespo, A. Comparison of gallium-68 and fluorine-18 imaging characteristics in positron emission tomography. *Applied Radiation and Isotopes* **76**, 55–62 (2013).

[4] Crișan, G. *et al.* Radiopharmaceuticals for PET and SPECT imaging: A literature review over the last decade. *International Journal of Molecular Sciences* **23**, 5023 (2022).

[5] Deshayes, E. *et al.* Radium-223 dichloride for prostate cancer treatment. *Drug Design, Development and Therapy* **11**, 2643–2651 (2017).

[6] Eychenne, R., Chérel, M., Haddad, F., Guérard, F. & Gestin, J.-F. Overview of the most promising radionuclides for targeted alpha therapy: The “hopeful eight”. *Pharmaceutics* **13**, 906 (2021).

[7] Decristoforo, C., Neels, O. & Patt, M. Emerging radionuclides in a regulatory framework for medicinal products–how do they fit? *Frontiers in Medicine* **8**, 678452 (2021).

[8] Qaim, S. M. & Spahn, I. Development of novel radionuclides for medical applications. *Journal of Labelled Compounds and Radiopharmaceuticals* **61**, 126–140 (2018).

[9] McAlister, D. R. & Horwitz, E. P. Automated two column generator systems for medical radionuclides. *Applied Radiation and Isotopes* **67**, 1985–1991 (2009).

[10] Synowiecki, M. A., Perk, L. R. & Nijsen, J. F. W. Production of novel diagnostic radionuclides in small medical cyclotrons. *EJNMMI radiopharmacy and chemistry* **3**, 1–25 (2018).

[11] Martini, P. *et al.* Perspectives on the use of liquid extraction for radioisotope purification. *Molecules* **24**, 334 (2019).

[12] Mastren, T. *et al.* Simultaneous separation of actinium and radium isotopes from a proton irradiated thorium matrix. *Scientific Reports* **7**, 8216 (2017).

[13] Radchenko, V. *et al.* Application of ion exchange and extraction chromatography to the separation of actinium from proton-irradiated thorium metal for analytical purposes. *Journal of Chromatography A* **1380**, 55–63 (2015).

[14] Kotovskii, A. *et al.* Isolation of actinium-225 for medical purposes. *Radiochemistry* **57**, 285–291 (2015).

[15] Rébufa, C., Traboulsi, A., Labed, V., Dupuy, N. & Sergent, M. Experimental design approach for identification of the factors influencing the γ-radiolysis of ion exchange resins. *Radiation Physics and Chemistry* **106**, 223–234 (2015).

[16] Wang, P., Zu, J., Khayambashi, A., Liu, R. & Wei, Y. Gamma radiolysis of anion exchange resins based on 4-vinylpyridine in aqueous solution. *Journal of Radioanalytical and Nuclear Chemistry* **311**, 1619–1625 (2017).

[17] Aguilar, M. & Cortina, J. L. *Solvent extraction and liquid membranes: Fundamentals and applications in new materials* (CRC Press, 2008).

[18] Itabashi, H. & Nakahara, T. Chelation solvent extraction for separation of metal ions. *Comprehensive Analytical Chemistry* **41**, 459–494 (2003).

[19] Alam, M. F., Begum, Z. A., Furusho, Y., Hasegawa, H. & Rahman, I. M. Selective separation of radionuclides from environmental matrices using proprietary solid-phase extraction systems: A review. *Microchemical Journal* **181**, 107637 (2022).

[20] Kabay, N., Cortina, J. L., Trochimczuk, A. & Streat, M. Solvent-impregnated resins (SIRs)– Methods of preparation and their applications. *Reactive and Functional Polymers* **70**, 484–496 (2010).

[21] Tamang, A. M., Singh, N., Chandraker, S. K. & Ghosh, M. K. Solvent impregnated resin a potential alternative material for separation dyes, metal and phenolic compounds: A review. *Current Research in Green and Sustainable Chemistry* **5**, 100232 (2021).

[22] Lee, J. N., Park, C. & Whitesides, G. M. Solvent compatibility of poly (dimethylsiloxane)-based microfluidic devices. *Analytical Chemistry* **75**, 6544–6554 (2003).

[23] Rumens, C., Ziai, M., Belsey, K., Batchelor, J. & Holder, S. Swelling of PDMS networks in solvent vapours; applications for passive RFID wireless sensors. *Journal of Materials Chemistry C* **3**, 10091–10098 (2015).

[24] Trochimczuk, A., Kabay, N., Arda, M. & Streat, M. Stabilization of solvent impregnated resins (sirs) by coating with water soluble polymers and chemical crosslinking. *Reactive and Functional Polymers* **59**, 1–7 (2004).

[25] Trapp, S., Lammers, T., Paulssen, E. & de Kruijff, R. M. Rapid, automated radionuclide separation with high yield - towards microfluidic solvent extraction for ^{61,64,67}cu production. *European Research Reactor Conference (Antwerp)* 177–184 (2023).

[26] Chakravarty, R. *et al.* Microfluidic solvent extraction of no-carrier-added 64cu from irradiated zn target for radiopharmaceutical preparation. *Chemical Engineering Journal Advances* **13**, 100433 (2023).

[27] Trapp, S. *et al.* Membrane-based microfluidic solvent extraction of ga-68 from aqueous zn solutions: towards an automated cyclotron production loop. *EJNMMI Radiopharmacy and Chemistry* **8**, 9 (2023).

[28] Oehlke, E. *et al.* Production of Y-86 and other radiometals for research purposes using a solution target system. *Nuclear Medicine and Biology* **42**, 842–849 (2015).

[29] Chakravarty, R., Patra, S., Jagadeesan, K., Thakare, S. & Chakraborty, S. Electrochemical separation of 132/135 La theranostic pair from proton irradiated Ba target. *Separation and Purification Technology* **280**, 119908 (2022).

[30] Kratochwil, C. *et al.* ^{225}Ac-PSMA-617 for PSMA-targeted alpha-radiation therapy of metastatic castration-resistant prostate cancer. *Journal of Nuclear Medicine* **57**, 1941–1944 (2016).

[31] Engle, J. W. The production of Ac-225. *Current Radiopharmaceuticals* **11**, 173–179 (2018).

[32] Priyadarshini, U. & Tandon, S. Spectrophotometric determination of vanadium (v) with n-benzoyl-n-phenylhydroxylamine. *Analytical Chemistry* **33**, 435–438 (1961).

[33] Aguado, R. J. *et al.* Durable nanocellulose-stabilized emulsions of dithizone/chloroform in water for Hg^{2+} detection: A novel approach for a classical problem. *ACS Applied Materials & Interfaces* **15**, 12580–12589 (2023).

[34] Singh, K. K. *et al.* Study of uranium sorption using D2EHPA-impregnated polymeric beads. *Journal of Applied Polymer Science* **130**, 3355–3364 (2013).

[35] Abràmoff, M. D., Magalhães, P. J. & Ram, S. J. Image processing with ImageJ. *Biophotonics International* **11**, 36–42 (2004).

[36] Church, T. Problems associated with the use of the ratio of Martin's diameter to Feret's diameter as a profile shape factor. *Powder Technology* **2**, 27–31 (1968).

[37] Lewicki, J. P., Liggat, J. J. & Patel, M. The thermal degradation behaviour of polydimethylsiloxane/montmorillonite nanocomposites. *Polymer Degradation and Stability* **94**, 1548–1557 (2009).

[38] Meyer, R. A., Hazel, J. F. & McNabb, W. M. Thermal analysis of some metal n-benzoyl-n-phenylhydroxylamine chelates. *Analytica Chimica Acta* **31**, 419–425 (1964).

[39] Croft, C. F., Almeida, M. I. G. & Kolev, S. D. Characterisation of micro polymer inclusion beads by thermogravimetric analysis. *Polymer* **283**, 126203 (2023).

[40] Aprilita, N. H., Luqman, M. & Suratman, A. Removal of cobalt (II) by dithizone-immobilized nickel slag. *Results in Chemistry* **5**, 100698 (2023).

[41] Cai, J. *et al.* Processing thermogravimetric analysis data for isoconversional kinetic analysis of lignocellulosic biomass pyrolysis: Case study of corn stalk. *Renewable and Sustainable Energy Reviews* **82**, 2705–2715 (2018).

[42] Santoso, A., Damen, A., van Ommen, J. R. & van Steijn, V. Atmospheric pressure atomic layer deposition to increase organic solvent resistance of pdms. *Chemical Communications* **58**, 10805–10808 (2022).

[43] Zhang, Y. *et al.* Revealing the sorption mechanisms of carbamazepine on pristine and aged microplastics with extended dlvo theory. *Science of the Total Environment* **874**, 162480 (2023).

[44] Badea, S.-L., Lundstedt, S., Liljelind, P. & Tysklind, M. The influence of soil composition on the leachability of selected hydrophobic organic compounds (HOCs) from soils using a batch leaching test. *Journal of Hazardous Materials* **254**, 26–35 (2013).

[45] Suo, Y. & Ren, Y. Research on the mechanism of nanofiltration membrane fouling in zero discharge process of high salty wastewater from coal chemical industry. *Chemical Engineering Science* **245**, 116810 (2021).

[46] Israelachvili, J. N. Surface forces. In *The Handbook of Surface Imaging and Visualization*, 793–816 (CRC Press, 2022).

[47] Mishchuk, N. A. The model of hydrophobic attraction in the framework of classical DLVO forces. *Advances in Colloid and Interface Science* **168**, 149–166 (2011).

[48] Liu, X., Xu, J., Zhao, Y., Shi, H. & Huang, C.-H. Hydrophobic sorption behaviors of 17β-estradiol on environmental microplastics. *Chemosphere* **226**, 726–735 (2019).

[49] Artiushenko, O., Avila, E. P., Nazarkovsky, M. & Zaitsev, V. Reusable hydroxamate immobilized silica adsorbent for dispersive solid phase extraction and separation of rare earth metal ions. *Separation and Purification Technology* **231**, 115934 (2020).

[50] Coenen, H. H. *et al.* Consensus nomenclature rules for radiopharmaceutical chemistry — setting the record straight. *Nuclear Medicine and Biology* **55**, v–xi (2017).

[51] Ramogida, C. *et al.* Evaluation of polydentate picolinic acid chelating ligands and an α-melanocyte-stimulating hormone derivative for targeted alpha therapy using ISOL-produced ^{225}Ac. *EJNMMI Radiopharmacy and Chemistry* **4** (2019).

[52] Mudasir, M. *et al.* Simultaneous adsorption of Zn (ii) and Hg (ii) ions on selective adsorbent of dithizone-immobilized bentonite in the presence of Mg (ii) ion. *Journal of Environmental Chemical Engineering* **8**, 104002 (2020).

[53] Soltane, H. B., Roizard, D. & Favre, E. Effect of pressure on the swelling and fluxes of dense PDMS membranes in nanofiltration: An experimental study. *Journal of Membrane Science* **435**, 110–119 (2013).

[54] Batra, S., Awasthi, A., Iqbal, M. & Datta, D. Solvent impregnated resins for the treatment of aqueous solutions containing different compounds: a review. *Reviews in Chemical Engineering* **38**, 209–242 (2022).

[55] Choi, Y. H., Chung, K. H., Hong, H. B. & Lee, W. S. Production of PDMS microparticles by emulsification of two phases and their potential biological application. *International Journal of Polymeric Materials and Polymeric Biomaterials* **67**, 686–692 (2018).

[56] Dufaud, O., Favre, E. & Sadtler, V. Porous elastomeric beads from crosslinked emulsions. *Journal of Applied Polymer Science* **83**, 967–971 (2002).

[57] Zhang, G. *et al.* A novel D2EHPA-based synergistic extraction system for the recovery of chromium(III). *Chemical Engineering Journal* **302**, 233–238 (2016).

[58] Saha, B., Venkatesan, K., Natarajan, R., Antony, M. & Vasudeva Rao, P. Studies on the extraction of uranium by n-octanoyl-n-phenylhydroxamic acid. *Radiochimica Acta* **90**, 455–459 (2002).

[59] Guo, X., Hurley, B., Yang, F. & Buchheit, R. A novel organic conversion coating based on n-benzoyl-n-phenylhydroxylamine chemistry for the corrosion protection of AA2024 – T3. *Electrochimica Acta* **246**, 197–207 (2017).

[60] Tavallali, H., Deilamy-Rad, G., Parhami, A. & Kiyani, S. Dithizone as novel and efficient chromogenic probe for cyanide detection in aqueous media through nucleophilic addition into diazenylthione moiety. *Spectrochimica Acta Part A: Molecular and Biomolecular Spectroscopy* **121**, 139–146 (2014).

[61] Van Oss, C. J. *Interfacial forces in aqueous media* (CRC press, 2006).

[62] Smith, A. M., Borkovec, M. & Trefalt, G. Forces between solid surfaces in aqueous electrolyte solutions. *Advances in Colloid and Interface Science* **275**, 102078 (2020).

[63] Mustin, B. & Stoeber, B. Single layer deposition of polystyrene particles onto planar polydimethylsiloxane substrates. *Langmuir* **32**, 88–101 (2016).

[64] Bower, M. J., Bank, T. L., Giese, R. F. & van Oss, C. J. Nanoscale forces of interaction between glass in aqueous and non-aqueous media: A theoretical and empirical study. *Colloids and Surfaces A: Physicochemical and Engineering Aspects* **362**, 90–96 (2010).

[65] Fazle Rabbi, K. *et al.* Polydimethylsiloxane-silane synergy enables dropwise condensation of low surface tension liquids. *Advanced Functional Materials* **32**, 2112837 (2022).

[66] Vlassov, S. *et al.* Adhesion and mechanical properties of PDMS-based materials probed with AFM: A review. *Reviews on Advanced Materials Science* **56**, 62–78 (2018).

[67] Donaldson Jr, S. H. *et al.* Correlated diffusivities, solubilities, and hydrophobic interactions in ternary polydimethylsiloxane–water–tetrahydrofuran mixtures. *Macromolecules* **49**, 6910–6917 (2016).

[68] Donaldson Jr, S. H. *et al.* Developing a general interaction potential for hydrophobic and hydrophilic interactions. *Langmuir* **31**, 2051–2064 (2015).

[69] Chen, J., Peng, Q., Peng, X., Zhang, H. & Zeng, H. Probing and manipulating noncovalent interactions in functional polymeric systems. *Chemical Reviews* **122**, 14594–14678 (2022).

[70] Ninham, B. W. On progress in forces since the DLVO theory. *Advances in Colloid and Interface Science* **83**, 1–17 (1999).

[71] Fu, Y. *et al.* Application and mechanisms of microalgae harvesting by magnetic nanoparticles (MNPs). *Separation and Purification Technology* **265**, 118519 (2021).

[72] Xu, J., Wang, L. & Sun, H. Adsorption of neutral organic compounds on polar and nonpolar microplastics: Prediction and insight into mechanisms based on pp-LFERs. *Journal of Hazardous Materials* **408**, 124857 (2021).

[73] Bridoux, M. C., Malandain, H., Leprince, F., Progent, F. & Machuron-Mandard, X. Quantitative analysis of phosphoric acid esters in aqueous samples by isotope dilution stir-bar sorptive extraction combined with direct analysis in real time (DART)-Orbitrap mass spectrometry. *Analytica Chimica Acta* **869**, 1–10 (2015).

[74] Akaiwa, H. & Kawamoto, H. The partition of dithizone between carbon tetrachloride and aqueous sulphuric acid. *Journal of Inorganic and Nuclear Chemistry* **29**, 541–545 (1967).

[75] Alimarin, I. P., Sudakov, F. P. & Golovkin, B. Use of n-benzoyl-n-phenylhydroxylamine in analytical chemistry. *Russian Chemical Reviews* **31**, 466 (1962).

[76] Monazam, E., Siriwardane, R., Miller, D. & McIntyre, D. Rate analysis of sorption of ce3+, sm3+, and yb3+ ions from aqueous solution using dowex 50w-x8 as a sorbent in a continuous flow reactor. *Journal of Rare Earths* **36**, 648–655 (2018).

[77] Momen, M. A. & Dietz, M. L. High-capacity extraction chromatographic materials based on polysulfone microcapsules for the separation and preconcentration of lanthanides from aqueous solution. *Talanta* **197**, 612–621 (2019).

[78] El-Din, A. M. S., Rizk, H. E., Borai, E. H. & Afifi, E. S. M. E. Selective separation and purification of cerium (iii) from concentrate liquor associated with monazite processing by cationic exchange resin as adsorbent. *Chemical Papers* **77**, 2525–2538 (2023).

[79] Liu, W. *et al.* Effect of pore size distribution and amination on adsorption capacities of polymeric adsorbents. *Molecules* **26**, 5267 (2021).

[80] Chapman, D. Electronegativity and the stability of metal complexes. *Nature* **174**, 887–888 (1954).

[81] Mishustin, A. Estimate of the stability constants of trivalent actinide and lanthanide complexes with o-donor ligands in aqueous solutions. *Russ. J. Inorg. Chem.* **55**, 746–752 (2010).

[82] Fitzsimmons, J. *et al.* Optimization of cation exchange for the separation of actinium-225 from radioactive thorium, radium-223 and other metals. *Molecules* **24**, 1921 (2019).

[83] Davern, S. *et al.* Microfluidics-based separation of actinium-225 from radium-225 for medical applications. *Separation Science and Technology* **54**, 1994–2002 (2019).

[84] Robertson, A. K. H., Ramogida, C. F., Schaffer, P. & Radchenko, V. Development of Ac-225 radiopharmaceuticals: Triumf perspectives and experiences. *Current Radiopharmaceuticals* **11**, 156–172 (2018).

[85] Zielinska, B., Apostolidis, C., Bruchertseifer, F. & Morgenstern, A. An improved method for the production of Ac-225/Bi-213 from Th-229 for targeted alpha therapy. *Solvent Extraction and Ion Exchange* **25**, 339–349 (2007).

[86] Friend, M. T. *et al.* Extraction chromatography of ^{225}Ac and lanthanides on n, n-dioctyldiglycolamic acid/1-butyl-3-methylimidazolium bis (trifluoromethylsulfonyl) imide solvent impregnated resin. *Journal of Chromatography A* **1624**, 461219 (2020).

[87] Baidak, A. & LaVerne, J. A. Radiation-induced decomposition of anion exchange resins. *Journal of Nuclear Materials* **407**, 211–219 (2010).

[88] Venkateswara Rao, C., Rout, A., Mishra, S. & Venkatesan, K. Thermophysical properties of neat and radiolytically degraded acidic extractants present in room temperature ionic liquid. *Journal of Radioanalytical and Nuclear Chemistry* **321**, 907–916 (2019).

[89] Pucić, I., Cetina, I. & Šantić, A. Component compatibility influences radiation stability of low temperature cured gels based on PDMS. *Radiation Physics and Chemistry* **185**, 109493 (2021).

Supplementary Information

Bead diameters

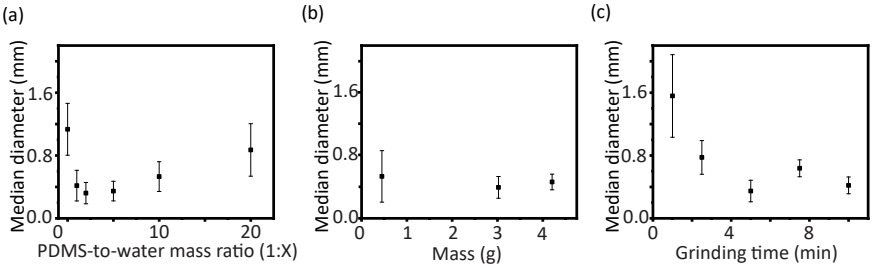

Figure 7.9: Median diameter of bare PDMS beads fabricated with (a) different PDMS-to-water ratios (with 3 g of PDMS foam sheet and 5 min of grinding time), (b) different total weight (with 1:2 PDMS to water ratio and 5 min of grinding time) and (c) different grinding times (with 1:2 PDMS to water ratio and 3 g of PDMS foam sheet. In this chapter, the beads are fabricated by grinding 3 g of PDMS foam sheet made out of 1:2 PDMS to water ratio for 5 min.

Chelator detection by XPS

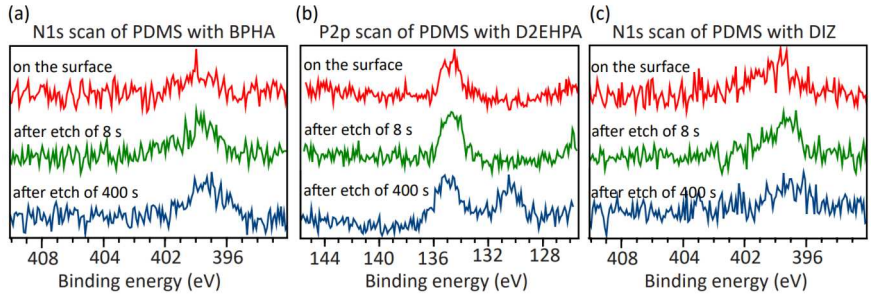

Figure 7.10: Presence of chelator on and inside the impregnated beads confirmed by XPS. Overlay of XPS survey scans of (a) the N1s peak of BPHA-impregnated, (b) the P2p peak of D2EHPA-impregnated, and (c) the N1s peak of DTZ-impregnated PDMS coated flat silicon wafer. The survey scans were conducted at the surface (without ion-etching), after etching of 8 seconds (estimated to be ~1.6 nm, representing removal of possible surface contaminant groups), and after etching of 400 seconds (estimated to be ~80 nm, representing infiltration of the chelators inside the PDMS beads). d) the N1s peak and e) P2p peak of bare (not-impregnated) PDMS coated silicon wafer. f) Comparison of N1s and P2p surface atomic percentage of bare PDMS and chelator-impregnated PDMS samples, where n.d. stands for non-detectable.

Bead morphology

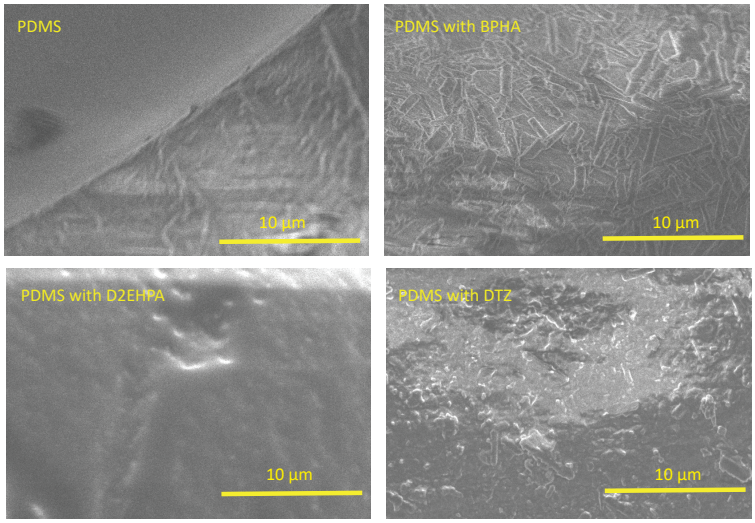

Figure 7.11: Morphology of the beads' surface. FE-SEM image of bare PDMS beads and PDMS beads impregnated with three different chelators (using chelator-containing chloroform solution, each with a concentration of 0.25 M).

Chemical interaction between chelator and PDMS

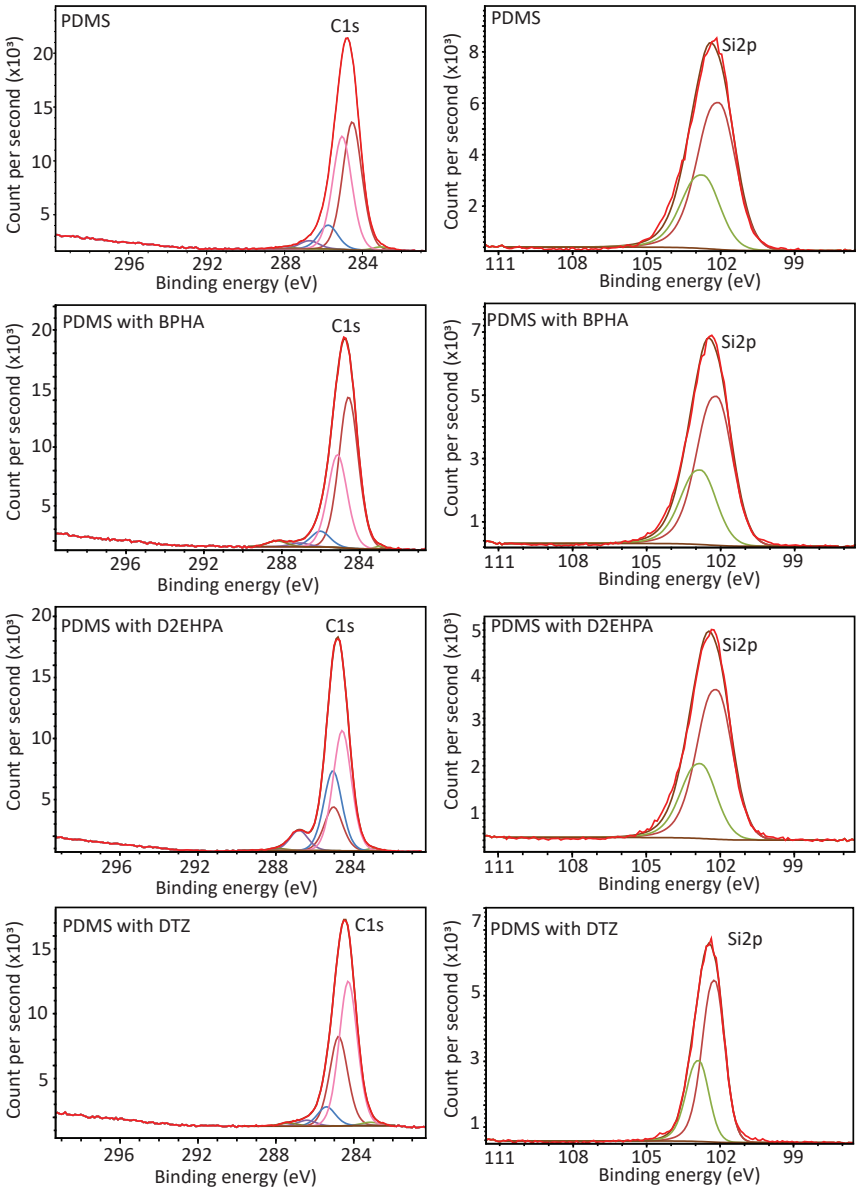

Figure 7.12: Evaluation of the presence of chemical interaction between the chelators and PDMS. XPS survey scans of C1s (left) and Si2p (right) for bare PDMS beads and chelator-impregnated PDMS beads. The lines inside the peaks are the XPS resolves.

Chemical stability

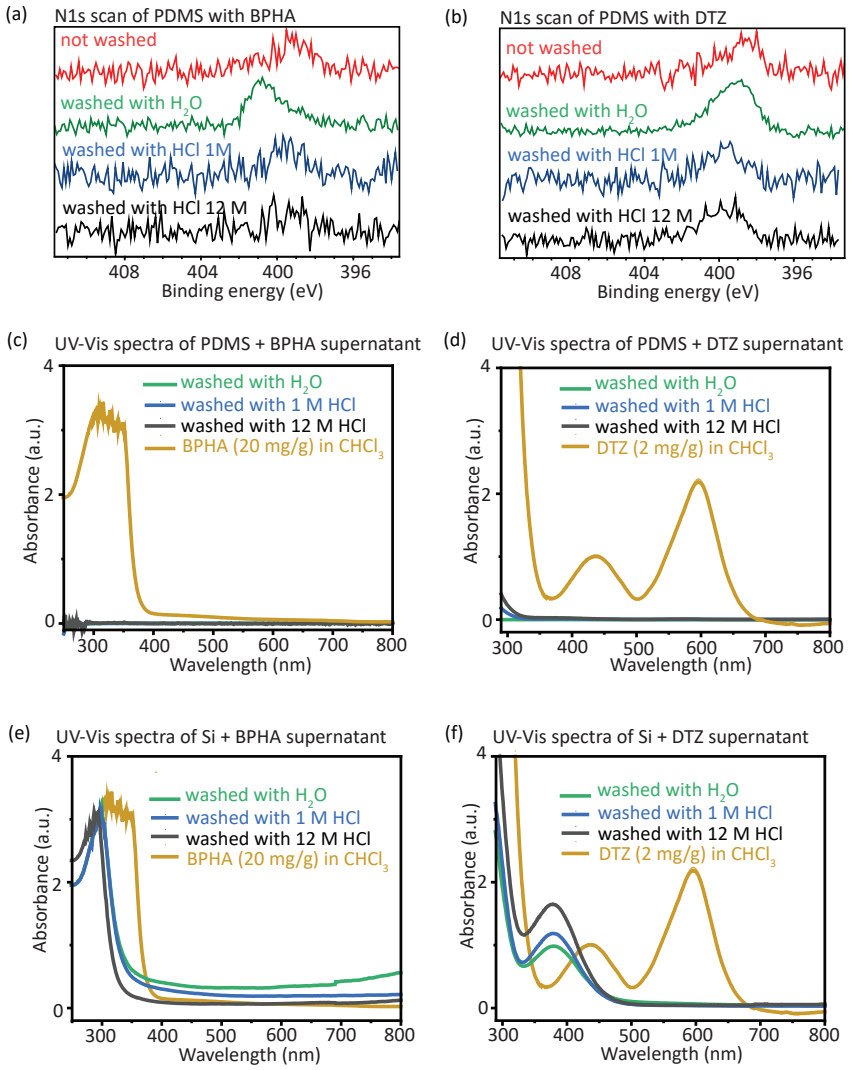

Figure 7.13: Chemical stability of BPHA- and DTZ-impregnated PDMS beads and silicon oxide powder against leaching measured with XPS and UV-Vis. (a-b) XPS N1s scan of (a) BPHA-impregnated and of (b) DTZ-impregnated PDMS beads before and after washing with the liquids for 5 minutes. (c-d) the corresponding UV-Vis spectra of their immersing liquid. (e-f) the UV-Vis spectra of immersing liquids used for washing (e) BPHA-impregnated and (f) DTZ-impregnated silicon oxide powder.

8

General Conclusions

8

General Conclusions

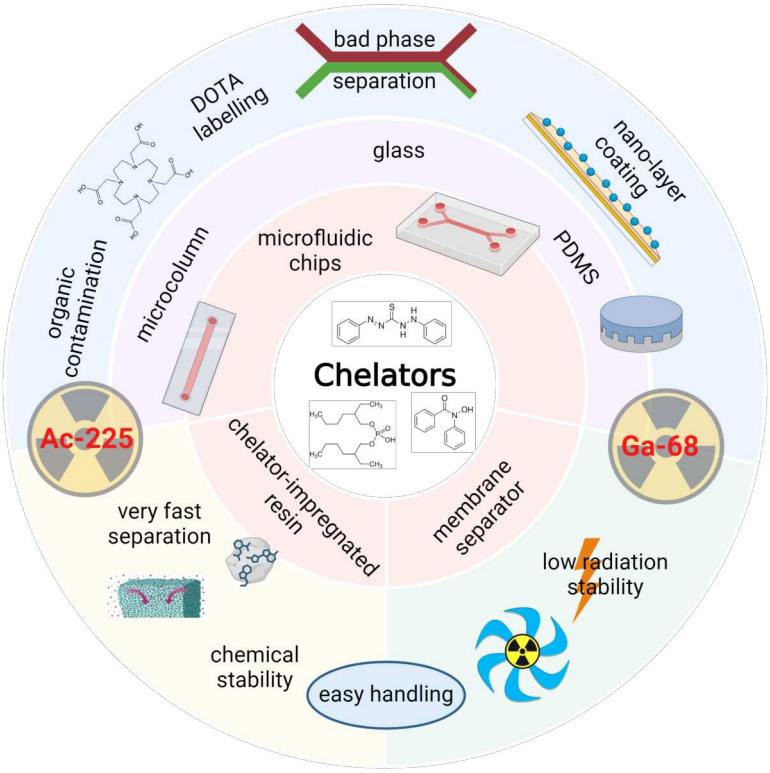

The main focus of this thesis was the development of chemical methods for the solvent extraction of medical radionuclides from irradiated targets. Microfluidic devices where tested effectively for their potential use in solvent extraction, an essential step for the automation of solvent extraction. Automation of the separation process is crucial when dealing with highly radioactive substances, to reduce the radiation dose received by personnel that handle the separation process.

In Chapter 2, a commercial microfluidic membrane separator was used for the separation of Ga-68 from $Zn(NO_3)_2$ liquid targets. Applying N-benzoyl-N-phenylhydroxilamine (BPHA) as the chelator during solvent extraction showed high potential for the extraction of Ga-68. In the batch approach, very high extraction efficiencies of up to 99.5% ± 0.6% could be achieved within 10 minutes of contact time, with only minor co-extraction of the zinc. Back-extraction of Ga-68 into 2 M HCl achieved efficiencies of up to 94.5 % ± 0.6 %. It was also found that low HNO_3 concentrations in the target solution are preferable for the extraction. A concentration of 0.01 M HNO_3 was determined as the optimal condition for the separation, as well as for the cyclotron irradiation of a $Zn(NO_3)_2$ liquid target (as described in the literature [1–3]). When the membrane separator was used for the separation process, extraction efficiencies of 99.2 % ± 0.3 % were still achievable. The back-extraction in a microfluidic device turned out to be slower. To speed up the process, back-extraction was done into 6 M HCl, resulting in an efficiency of 95.8 % ± 0.8 %. Next, the process was tested with a liquid 2 M $Zn(NO_3)_2$ target in 0.01 M HNO_3, irradiated for 30 min with a 13 MeV cyclotron at TRIUMF, Canada, resulting in a produced Ga-68 activity of 500-600 MBq. While the membrane separator was easy to operate, and comparable extraction efficiencies to the batch process could be achieved in this process, it was observed that the high activities, causing radiolysis, induce degradation of the membrane, resulting in reduced phase separation of the aqueous and organic solutions. The degradation of the membrane was later shown in SEM-images, where the brittleness of the PTFE membranes could be observed. Therefore, these membranes appear to be inadequate to be used for the continuous separation of highly radioactive nuclides and a different membrane or microfluidic device needs to be developed for the automation of solvent extraction.

In Chapter 3 solvent extraction of copper from highly acidic $Zn(NO_3)_2$ solutions was studied using a commercial YY glass microfluidic chip. We compared several extracting agents for the selective extraction of copper from $Zn(NO_3)_2$ solutions. In conventional batch extraction, using dithizone as the extracting agent, efficiencies of up to 90% ± 5% were achieved within 1 minute. To apply this method to a microfluidic chip, first, a stable, stratified flow had to be established. However, the commercial YY-junction glass chip consistently failed to achieve a perfect phase separation, as reported before in the

literature [4]. Depending on the flow rate ratios either aqueous, organic, or even simultaneous leakage was observed. Furthermore, a much lower EE(%) of Cu was found using the microfluidic chip, plateauing at approximately 40 %. Longer contact times would be needed to further increase the EE(%) in flow, which the microfluidic setup in this study did not allow for.

To address the issue of consistently low phase separation of microfluidic chips, in Chapter 4, a PDMS-based YY microfluidic chip was developed. Applying a hook design to the channel to pin the interface of the two solutions was successful in achieving a near perfect phase separation. However, PDMS is not resistant against organic solvents and swells upon contact. Therefore, a silicon oxide nano-layer was coated on the inside of the microchannel, not only increasing the resistance of the PDMS against organic solvents, but also stabilizing the flow inside of the channel due to a change in surface conditions. In a case study for the extraction of Ac-225 from Ra, a near perfect phase separation and a highly stable flow of the aqueous and organic flow could be established. Using D2EHPA as the chelator for the extraction resulted in extremely high efficiencies exceeding 98 %, not only in the batch approach but also during the microfluidic extractions within contact times of under 2 seconds. Back-extraction of Ac-225 into 0.1 M HCl was successful, but it is noteworthy that the back-extraction in a microfluidic channel was significantly slower due to the low concentrations of the Ac-225-chelator complex, while still being surrounded by a large amount of chelator. This led to a reduced diffusion-based movement of Ac-225 to the interface, resulting in lower back-extraction efficiencies. Again, the contact time would need to be increased to achieve maximum back-extraction efficiencies.

To determine necessary contact times and optimize future microfluidic solvent extraction experiments, as well as chip designs, numerical models can be developed, but these models rely on existing kinetic and diffusion data. Unfortunately, diffusion data is often lacking, partially due to the complexity of available techniques for diffusion coefficient measurements, as well as very low concentrations limiting inter-molecular interactions that drive diffusion [5]. Therefore, Chapter 5 explores the use of microfluidic chips for the determination of diffusion coefficients. It was found that while it was possible to use microfluidic chips for diffusion studies, varying flow rate can result in significant differences between the measured apparent diffusion coefficients. Best results could be obtained when the apparent diffusion coefficients were plotted against contact time, showing an exponential trend which could subsequently be fitted, resulting in the actual diffusion coefficient of the compound. By doing so, diffusion coefficients of $4.47 \pm 0.21 \cdot 10^{-10}$ m^2/s and $2.78 \pm 0.09 \cdot 10^{-10}$ m^2/s could be obtained for rhodamine-6G in water and gallium in a 2 M $Zn(NO_3)_2$ in 0.01 M HNO_3 solution, respectively. The contact

time needed to reach the plateau of the exponential fit might vary between different microfluidic chips and compounds and needs to be investigated for each individual set-up.

After the development of multiple microfluidic solvent extraction methods for different radionuclides in Chapters 2 - 4, Chapter 6 dealt with the presence of chelator contamination in the aqueous solutions after back-extraction. It was found that both BPHA and DIZ, as well as chloroform are detectable in these aqueous solutions as contaminations by UV/Vis-spectroscopy. A DOTA-labelling study was executed, showing the potential interference the contaminations can cause during radiopharmaceutical labelling. The results indicate that directly after solvent extraction, the present BPHA and DIZ contamination reduce the labelling efficiencies significantly. In a case study for the purification of Ga-68 after solvent extraction, an ion-exchange microcolumn was developed. The PDMS-based microcolumn was filled with AG 1-X8 ion-exchange resin. The Ga-68 solution was obtained from the solvent extraction experiments as described in Chapter 2, therefore consisting of 6 M HCl, Ga-68 and the BPHA contamination. Adsorption of the Ga-68 to the ion-exchange resin was successfully achieved with efficiencies over 99 % at a flow rate of 100 μL/min. Elution was done into MQ with an efficiency of approximately 98 % in a very small volume (of less than 200 µL compared to the initial 5 mL). UV/Vis measurements of the collected solution could not detect any remaining chelator contamination. This type of ion-exchange microcolumn could easily be integrated in a continuous, microfluidic solvent extraction process, increasing the purity of the obtained radionuclide-containing solutions, but could also be included in standard ion-exchange separation methods to reduce acidity and final volume of the solution.

In the final study in Chapter 7, an alternative chelator-based separation method was explored. Here, a chelator-impregnated resin was developed, using PDMS as the solid support. While chelator impregnation is a well know technique, it usually suffers from low chemical stability [6], meaning that the chelator leaches out quickly, contaminating the solutions and reducing the potential sorption efficiency. We made use of the swelling of PDMS upon contact to organic solvents, impregnating PDMS beads with chelators in the presence of chloroform. This resulted in an uptake of the chelator during the swelling and subsequent physical trapping of the chelator in the PDMS structure after drying and de-swelling. A high chemical stability and a high uptake was found, especially for the chelator D2EHPA. 5 mg of the obtained D2EHPA-impregnated PDMS beads were loaded into a tube and used in a case-study for the separation of Ac-225 from radium, as previously done in Chapter 4 by solvent extraction. This study resulted in an adsorption efficiency of 98.51 % ± 0.25 % at a flow rate of 0.3 mL/min. Subsequent elution was achieved into 0.1 M HCl at a flow rate of 0.1 mL/min, resulting in a recovery of over 90 % of Ac-255 with less than 0.07 % of initial radium in the elution. While these are only pre-

liminary results, and further studies using irradiated Ra-targets with high activities need to be conducted in the future, the results of this study show a great potential of the newly developed chelator-impregnated PDMS beads, allowing the future use in the production of medical radionuclides.

In conclusion, this thesis demonstrates multiple methods for chelator-based separation of medical radionuclides and applications of microfluidic chips. The results presented are a promising proof-of-concept that could lead to the future use of chelator-based separation methods during radiopharmaceutical production. Additionally, if optimized and applied to liquid targets, the presented microfluidic solvent extraction methods could enable the direct recycling of the costly, enriched target material, reducing the necessary chemical processing steps that are usually needed between irradiations. Future research of microfluidic solvent extraction should include testing the radiation stability of the presented materials as well as the translation into a GMP production of radiopharmaceuticals. A major challenge for the use of microfluidic chips for continuous solvent extraction will be to incorporate all necessary steps including extraction, back-extraction and purification into one device that is still able to create a reproducible stable flow of the solutions. However, work has already been done in the development of microfluidic modules, showing the possibilities of microfluidic technologies [7, 8]. Because of the increasing success of microfluidic- and lab-on-a-chip technologies in other fields [9–12], a future high demand for the developed microfluidic chip, not only for the separation of medical radionuclides, but also for other hydro-metallurgical or separation applications can be expected.

References

[1] Oehlke, E. *et al.* Production of Y-86 and other radiometals for research purposes using a solution target system. *Nuclear Medicine and Biology* **42**, 842–849 (2015).

[2] Alves, F. *et al.* Cyclotron production of Ga-68 for human use from liquid targets: From theory to practice. *AIP Conference Proceedings* **1845** (2017).

[3] Pandey, M. K., Byrne, J. F., Schlasner, K. N., Schmit, N. R. & DeGrado, T. R. Cyclotron production of ^{68}Ga in a liquid target: Effects of solution composition and irradiation parameters. *Nuclear Medicine and Biology* **74-75**, 49–55 (2019).

[4] Dalmázio, I. & Oehlke, E. Cyclohexanone microfluidic extraction of radioactive perrhenate from acid solutions. *International Nuclear Atlantic Conference, Belo Horizonte, Brazil* (2017).

[5] Mueller, C. B. *et al.* Precise measurement of diffusion by multi-color dual-focus fluorescence correlation spectroscopy. *Europhysics Letters* **83**, 46001 (2008). Available at `https://dx.doi.org/10.1209/0295-5075/83/46001`.

[6] Kabay, N., Cortina, J. L., Trochimczuk, A. & Streat, M. Solvent-impregnated resins (SIRs)– Methods of preparation and their applications. *Reactive and Functional Polymers* **70**, 484–496 (2010).

[7] Lai, X., Yang, M., Wu, H. & Li, D. Modular microfluidics: Current status and future prospects. *Micromachines* **13** (2022).

[8] Wu, J., Fang, H., Zhang, J. & Yan, S. Modular microfluidics for life sciences. *Journal of Nanobiotechnology* **21** (2023).

[9] Niculescu, A. G., Chircov, C., Bîrcă, A. C. & Grumezescu, A. M. Fabrication and applications of microfluidic devices: A review. *International Journal of Molecular Sciences* **22**, 1–26 (2021).

[10] Azizipour, N., Avazpour, R., Rosenzweig, D. H., Sawan, M. & Ajji, A. Evolution of biochip technology: A review from lab-on-a-chip to organ-on-a-chip. *Micromachines* **11**, 1–15 (2020).

[11] Gharib, G. *et al.* Biomedical applications of microfluidic devices: A review. *Biosensors* **12** (2022).

[12] Pattanayak, P. *et al.* Microfluidic chips: recent advances, critical strategies in design, applications and future perspectives. *Microfluidics and Nanofluidics* **25** (2021).

Acknowledgements
List of Publications
PhD Portfolio
Curriculum Vitae

Acknowledgements

First and foremost, I want to thank my amazing supervisors for everything. Robin and Elisabeth, thank you for the opportunity to do my PhD thesis with you! You made this journey much easier and I could never imagine having better supervisors. I learned so much from the both of you, you really made me a researcher! Robin specifically, you have not only been an amazing daily supervisor, but also a very good friend. You were always there for me, I could let out all my frustrations and concerns to you, and you would always find a way to build me up again and show me that it's all not too bad. You went above and beyond to help me in every imaginable situation, no matter how busy you were. Thank you for your never-ending enthusiasm, support, motivation, and knowledge! I couldn't have done this without you. And I am sure your future students will be very lucky to have you as a supervisor!

I furthermore would like to thank Antonia for being my promotor. Thank you for your insightful tips and knowledge and your continuous support for my PhD work, even though it wasn't your project originally. You make the ARI group a very welcoming place!

To my two partners in crime and fellow sufferers, Anand Sudha and Albert Santoso, it was amazing to have you with me in the project. We did it!! Albert, I cannot thank you enough for everything you have done for me, from preparing an incredible amount of chips, for directly telling me when my ideas will not work out, for listening to my complaints, for giving me private tutoring on engineering topics, for fun beer evenings, and most of all, for being my friend!

Of course, more people were involved in this project and contributed to the outcome of my thesis. I regularly received great feedback from Volkert van Steijn and Ruud van Ommen, not only during the monthly project meetings but also when Albert and I aimed to write a paper together. We ended up writing two papers plus one patent together, all of which went through the review process with little dispute, thanks to your rigorous corrections and improvements of our work. I greatly appreciate the time you put into this!

Next, I would like to appreciate Martin Rhode. As the PI of our entire project, you were always approachable, always helpful, always exceptionally nice to everyone, and always open to everything we had to say. You really kept the project going and I am very

grateful to have been surrounded by such an amazing group of people in the project!!

I also wish to acknowledge the sponsors and user committee of my PhD project, the Dutch research council (NWO) for financing this project, Urenco, NRG, umcg, and Fluidomica. Specifically, I want to acknowledge our collaborators from TRIUMF. Conny, thank you for inviting me and giving me the opportunity to experiment at TRIUMF and even going to a conference in Whistler! Canada has always been on my bucket list and you made it possible, Conny! While talking about TRIUMF, I would also like to thank everyone involved who made my time in Vancouver unforgettable! Gokce Engudar, thank you for your help in the Lab, Chelsey Currie, thank you for the wonderful evenings we had and for showing me around! And to everyone else I met in Vancouver, thank you for making this a special time!

I would also like to acknowledge all the technicians at the ARI group. Baukje, Astrid, Folkert, Eline, thank you so much for all your help in and out of the lab, whether it was helping me with irradiations, the broken ICP, my inability to deal with technology and my never ending stream of questions. You patiently answered all of them and helped me without hesitation! Throughout these past four years I have learned a lot from you all, without your invaluable help this thesis would not have been possible.

To all my fellow PhD students and Post-Docs in the group, Rogier, Robin, Chao, Huanhuan, Retna, Jacky, Bing, Gauri, Esther, thank you for making my time at ARI unforgettable. I have been very lucky to be part of this awesome group. Alexandra, it has been my pleasure to share an office with you and a big thank you for always having an open ear and the opportunity to vent in our outside breaks (let's call'em that :D). We shared many frustrations, thank you for helping me through! You continued to be there for me even after you left the country and had way more fun things to do than listen to my complaints. Thank you for being such a good friend! I really hope this friendship will continue, no matter where we end up in life!

A big thank you goes out to all of my colleagues and fellow PhD candidates at the Reactor Institute outside of ARI. Members of the PhD Council, the SBD, the barkeepers in 't Koepeltje, the NCSV, INAA, you all made this journey a lot more interesting and also bearable with a lot of Friday afternoon beers. Who doesn't enjoy alcohol below a nuclear reactor!

Furthermore, I would like to thank my bachelor and master students that I had the pleasure to supervise during my PhD. You greatly contributed to the outcome of my thesis and I hope you all have great careers ahead of you! Tom, Bart, Isabelle, Emma, Esmee,

Brenda, Lywke, Jessey, Maud, Cees, Marc - thank you all for your trust in me and for lots of fun times, in and out of the lab!

To all my friends back home, thanks for staying with me and never losing touch, even though my communication skills suffered greatly under all the work a PhD brings with it. Your understanding, the possibility to always 'go back home', and also tons of zoom nights during Covid19 lock-downs were a great emotional help, that is greatly appreciated!

I also wish to thank my family, my mother and brother for their continuous support throughout my entire educational journey and my life! To my late father, thank you for inspiring me to thrive, even though you are not here to witness it. This thesis is dedicated to you!

And finally, I want to acknowledge my amazing husband! Gerrit, you are not only the best man I could have married, but also the greatest support, the most detailed dictionary, the absolute best private tutor, and the most brilliant mind I know! Without you and your never ending support, even when I let out all of my frustration on you, I would not even have had the courage to start this project, let alone finish it. I owe this dissertation to you!

Thank you!

List of Publications

Journal articles

Trapp, S. Santoso, A., van Ommen, R., van Steijn, V., Paulssen, E., de Kruijff, R.M., 2024. Solvent extraction of Ac-225 in nano-layer coated solvent-resistant PDMS microfluidic chips. Scientific Reports 14, 29988. https://doi.org/10.1038/s41598-024-81177-5

Santoso, A.,**Trapp, S.**, Blommestein, I., Saedy, S., de Kruijff, R.M., van Steijn, V., van Ommen, R., 2025. Chelator-impregnated polydimethylsiloxane beads for separation of medical radionuclides. Separation and Purification Technology, 54(3), 128865. https://doi:10.1016/j.seppur.2024.128865

Trapp, S., Lammers, T., Engudar, G., Hoehr, C., Denkova, A.G., Paulssen, E., de Kruijff, R.M., 2023. Membrane-based microfluidic solvent extraction of Ga-68 from aqueous Zn solutions: towards an automated cyclotron production loop. EJNMMI Radiopharmacy and Chemistry 8(9). https://doi:10.1186/s41181-023-00195-2.

Trapp, S., Janák, M., Fassmer, K., Froitzheim, N., Münker, C., Georgiev, N., 2020. Variscan ultra-high-pressure eclogite in the Upper Allochthon of the Rhodope Metamorphic Complex (Bulgaria). Terra Nova 33(2), 174–183. https://doi.org/10.1111/ter.12503

Conference Proceedings

Trapp, S., Lammers, T., Paulssen, E., de Kruijff, R.M. Rapid, automated radionuclide separation with high yield - towards microfluidic solvent extraction for ^{61,64,67}Cu production. European research reactor conference 2023 proceedings. Antwerp; 2023. p. 177–184

Patents

Santoso, A., **Trapp, S.**, van Ommen, R., van Steijn, V., de Kruijff, R.M. Method for preparing polydimethylsiloxane beads loaded with chelating agent for separation of radioisotopes. Patent number 2037212.

Conference Abstracts

Trapp, S., Santoso, A., van Ommen, R., van Steijn, V.Hoehr, C., Denkova, A.G., Paulssen, E., de Kruijff, R.M.. Chelator-impregnated polydimethylsiloxane beads for Ac-225 separation. Workshop on Targetry and Target Chemistry, Heidelberg, Germany, 2024.

Santoso, A., **Trapp, S.**, de Kruijff, R.M., Paulssen, E., van Steijn, V., van Ommen, J.R.. Liquid-liquid extraction of medical radioisotopes in microfluidic channels treated by atomic layer deposition. Netherlands Process Technology Symposium 18, Enschede, The Netherlands, 2023.

de Kruijff, R.M., **Trapp, S.**, Lammers, T., Paulssen, E.. Rapid, automated radionuclide separation

with high yield - towards microfluidic solvent extraction for ^{64,67}Cu and ^{68}Ga production. European Research Reactor Conference, Antwerp, The Netherlands, 2023.

Santoso, A., **Trapp, S.**, Paulssen, E., de Kruijff, R.M., van Ommen, R., van Steijn, V. Extraction of medical radioisotopes from cylotron liquid target using atomic layer deposited microfluidics. International Syposium on Radiopharmaceutical Sciences, Honululu, Hawaii, The United States of America, 2023.

de Kruijff, R.M., **Trapp, S.** Medical Radioisotope Production Research at The Reactor Institute Delft, The Netherlands. The Fifth International Conference on Application of Radiotracers and Energetic Beams in Sciences, ARCEBS-2023, Purilia, India, 2023.

Trapp, S., Denkova, A.G., Paulssen, E., de Kruijff, R.M. Microfluidic solvent extraction of ^{68}Ga from zinc nitrate liquid targets. Nederlandse Klinische Radiochemie Vereniging, Amsterdam, The Netherlands, 2023.

Trapp, S., Paulssen, E., de Kruijff, R.M. Mikrofluidische Flüssig-Flüssig-Extraktion von ^{68}Ga. Jahrestagung Nuklearchemie, Bergisch Gladbach, Germany, 2022.

Trapp, S., Paulssen, E., de Kruijff, R.M.Microfluidic solvent extraction from cylotron liquid targets. Workshop on Targetry and Target Chemistry, Whistler, Canada, 2022.

Trapp, S., Paulssen, E., de Kruijff, R.M. Microfluidic solvent extraction for an automated ^{68}Ga cyclotron production loop. 19th RadChem, Marianske Lazne, Czech Republic, 2022.

Trapp, S., Paulssen, E., de Kruijff, R.M. Microfluidic solvent extraction of cyclotron produced ^{68}Ga from zinc nitrate solutions. Miller Online Workshop on Radiation Chemistry, 2022.

PhD Portfolio

Name of PhD candidate:	Svenja Trapp
Department:	Radiation Science and Technology
Research group:	Applied Radiation and Isotopes
Research school:	TU Delft graduate school
PhD period:	November 2020 - November 2024
Promotor:	Dr. ir. Antonia G. Denkova
Co-promotor:	Dr. ir. Robin M. de Kruijff
Co-promotor:	Prof. Dr. rer. nat. Elisabeth Paulßen

PhD Training

Transferable Skill Courses, TU Delft Graduate School

PhD start-up	2021
Resilience and Me	2021
Dutch for foreigners	2021
Data visualisation	2021
Research data management 101	2021
Effective Management of your PhD Research	2021
Designing Scientific Posters and Covers for Theses with Adobe InDesign	2022
Career Development - Exploring a career outside academia	2022
Project Management for PhD Candidates	2022
Career Development - Marketing Tools to Position Yourself in the Job Market	2023
Career Development - Job Interview Preparation	2024
Effective Negotation	2024

Scientific Courses

RPO Dispersible Radioactive Material level-D - *TU Delft Stralingsonderwijs*	2020
Nuclear Chemistry - *TU Delft, ARI*	2021
Nano- and Microfluidics - *TU Eindhoven, Microsystems*	2021
Nuclear Medicine - *TU Delft, ARI*	2022
Summer school on Targetry and Target chemistry - *TRIUMF, Vancouver*	2022
WMD Non-Proliferation and Disarmament Pathways - *SIPRI, EU Non-Proliferation and Disarmament Consortium*	2023

Conferences

Miller Online Workshop on Radiation Chemistry	2022
Nuklearchemie Jahrestagung, - *Bergisch Gladbach, Germany*	2022
19th RadChem conference - *Marianske Lazne, Czech Republic*	2022
18th Targetry and Target Chemistry Workshop - *Whistler, Canada*	2022
NKRV Workshop - *Amsterdam, the Netherlands*	2023
19th Targetry and Target Chemistry Workshop - *Heidelberg, Germany*	2024

Other

PhD Council member - *Department of Radiation Science and Technology*	2023-2024

Supervision

Martijn Meijer	Leren onderzoeken 2 (LO2)	2022
Shamim Ferdos	Leren onderzoeken 2 (LO2)	2022
Isabelle van Veen	Bachelor student Molecular Science and Technology	2021
Emma Kersten	Bachelor student Applied Physics	2021
Lywke Zwetsloot	Bachelor student Molecular Science and Technology	2022
Esmee Spuijbroek	Bachelor student Molecular Science and Technology	2022
Brenda Giling	Bachelor student Molecular Science and Technology	2022
Tom Lammers	Master student Chemical Engineering	2021
Bart Bekkema	Master student Applied Physics	2022
Cees Breevart	Master student Chemical Engineering	2023
Marc Scholtens	Master student Applied Physics	2023

Curriculum Vitæ

Hi, I'm Svenja Trapp, a geologist and nuclear chemist. I was born and raised in Mönchengladbach, Germany, where I received my lower education.

In 2013, I moved to Bonn where I started studying Geosciences at the University of Bonn, originally because I was a fan of the Jurassic Park movies since I was a child, and wanted to learn more about dinosaurs, which is part of the Geosciences bachelor program in Bonn. But after starting my Bachelor, my interest quickly moved towards structural geology and geochemistry. I proceeded to write my Bachelor thesis about the geology of the Saxonian Granulite Mountains in the Structural Geology group and received my Bachelor of Science degree in 2016. I continued to do my Master in Geosciences as well, specifically in the Geochemistry track. I was working as a teaching assistant in the Structural Geology group, where I later also did my Master thesis, which included $^{176}Lu/^{176}Hf$ radiodating for the purpose of geological reconstruction of the continent-continent collision that formed the Variscan Orogen 330 million years ago. During this time, I gained a lot of experience in Lab work, specifically working in the HF Lab of the Geochemistry and Cosmochemistry group at the University of Cologne.

After successfully finishing my Master of Science in 2019, I decided that I wanted to continue in research by starting a PhD project. However, I also wanted to expand my knowledge to new areas. I was lucky enough to be able to start my PhD in Nuclear Chemistry at the Applied Radiation and Isotopes (ARI) group of the Delft University of Technology under the supervision of Dr. ir. Robin M. de Kruijff, Prof. Dr. rer. nat. Elisabeth Paulßen and Dr. ir. Antonia G. Denkova. I am very grateful for their trust in my ability to accomplish the rather dramatic change in research fields. I started this PhD during the height of the corona pandemic in 2020, which, together with multiple long shutdowns of the reactor at the TU Delft, complicated the start of my research. Nonetheless, I submitted my PhD thesis entitled "Microfluidic solvent extraction of medical radionuclides" in 2024 without delay.